Radioactive Materials Management

Deep Geologic Repository Conceptual Design

Annex 2

Finite Element Analysis

December 2002

NOTICE to the Reader

"This document has been prepared by CTECH Radioactive Materials Management, a joint venture of Canatom NPM Inc. and RWE Nukem Ltd. ("Consultant"), to update the conceptual design and cost estimate for a deep geologic repository (DGR) for long term disposal of used nuclear fuel. The scope is more fully described in the body of the document. The Consultant has used its professional judgment and exercised due care, pursuant to a purchase order dated October 2001. (the "Agreement") with Ontario Power Generation Inc. acting on behalf of the Canadian nuclear fuel owners ("the Client"), and has followed generally accepted methodology and procedures in updating the design and estimate. It is therefore the Consultant's professional opinion that the design and estimate represent a viable concept consistent with the intended level of accuracy appropriate to a conceptual design, and that, subject to the assumptions and qualifications set out in this document, there is a high probability that actual costs related to the implementation of the proposed design concept will fall within the specified error margin.

This document is meant to be read as a whole, and sections or parts thereof should not be read or relied upon out of context. In addition, the report contains assumptions, data, and information from a number of sources and, unless expressly stated otherwise in the document, the Consultant did not verify those items independently. Notwithstanding this qualification, the Consultant is satisfied that the updated conceptual design and cost estimate was carried out in accordance with generally accepted practices in a professional manner .

This document is written solely for the benefit of the Client, for the purpose stated in the Agreement, and the Consultant's liabilities are limited to those set out in the Agreement."

Contents

List of Tables.

List of Figures

1 Introduction

A design concept for deep geologic emplacement of used CANDU fuel was first developed by Atomic Energy of Canada Ltd (AECL) during the period 1978-1996, under the Canadian Nuclear Fuel Waste Management Program. Following an extensive review under the federal Environmental Assessment and Review Process, a number of changes were recommended to address comments from a broad range of stakeholders, including the public. Since then, the four owners of used nuclear fuel in Canada [Ontario Power Generation (OPG), Hydro-Québec (HQ), New Brunswick Power (NBP) and Atomic Energy of Canada Ltd (AECL)] have continued, jointly, to develop the deep geologic repository (DGR) concept for the long-term safe management of the used fuel.

This has led to the work currently being undertaken by CTECH, to update the conceptual design for a deep geologic repository facility, and to prepare a corresponding cost estimate for designing, building and operating a DGR for the long-term storage of used nuclear fuel from all Canadian reactors. As a part of this work, a number of finite element analyses have been carried out in order to provide confidence in the feasibility of the proposed concept to provide a safe long-term solution. This report summarises the results of these investigations.

2 Description of Proposed DGR

The design concept developed as a part of this contract is appropriate for a hypothetical site with geologic and hydro-geologic conditions similar to those of the sparsely fractured rock of the Whiteshell Research Area. The emplacement room is designed to be located at a depth of 1000m, in relatively impermeable, sparsely fractured granite pluton. A complete design description for the proposed used-fuel emplacement facility has been presented in Reference 1 however this section of this report gives a brief outline of the proposed design.

The used fuel will be placed in a used fuel container (UFC), which will accommodate 324 fuel bundles. The proposed UFC has an overall diameter of 1168 mm and overall length of 3867 mm. Remaining key dimensions of the UFC are shown in Figure 1, and are consistent with those quoted by OPG in Reference 2.

The UFC design consists of an outer copper corrosion-barrier vessel and an inner, carbon steel load-bearing component. The selected material for construction of the outer corrosion barrier is the reference material developed by the Swedish nuclear fuel waste management programme. It is a high purity, oxygen-free copper with a low phosphorus content of 40 to 60 ppm (OFP copper), specifically chosen to give the copper matrix the required ductility to meet the DGR performance demands. The inner load-bearing component is in the form of a carbon steel inner vessel capable of withstanding all external pressure loads expected in a hypothetical geologic repository. It has been designed such that it will not be subjected to yielding or creep failure during the UFC design lifetime.

The UFCs are protected with a bentonite jacket, and placed in the DGR emplacement room. The emplacement room comprises three main components; the opening excavated within the rock mass, the permanent furnishings required to conduct emplacement operations, and the sealing materials. The arrangement of the various room components is shown in Figure 2.

Following work by Baumgartner *et al* [3], the profile of the emplacement room was specified as having an elliptical cross-section with the major axis in the horizontal plane and an aspect ratio of approximately 1.7. The emplacement-room should be oriented such that the room axis is parallel to the maximum principal stress direction, and the major axis of elliptical cross section is parallel to the intermediate principal stress direction. In comparison with other room shapes and orientations, this design minimises the tangential stress concentrations around the room perimeter. For ease of UFC and sealing material emplacement, a minimum centreline room height of 4.2 m was established, and consequently, a centreline room width of 7.14 m.

Low-heat, high-performance concrete is used for the construction of a uniform platform on the floor of the room to facilitate fuel emplacement. Although the rails and other temporary furnishings are removed as the room is filled, the concrete floor remains as a permanent structure. The voids around the UFC are filled with clay-based sealing materials of various densities.

The DGR arrangement for in-room emplacement of nuclear fuel waste is a system of access tunnels and emplacement rooms arranged into four distinct sections (Figure 3). Each section consists of a number of emplacement rooms, with 2 UFCs placed across the width of the room. The proposed design has a maximum total DGR capacity of 11,232 UFCs or 3,639,168 fuel bundles. In order to maintain rock formation stability, a minimum pillar width between adjacent emplacement rooms of three times the emplacement room width was specified. However, in practice a greater spacing was required to maintain DGR temperatures within the specified limits. Assuming an ideal site, with no faults or stress anomalies, the minimum overall dimensions of the UFC emplacement area are approximately 1.4 km by 1.4 km. These dimensions do not account for any adaptations that may be required at an actual site because of local conditions (e.g. specific rock structures, faults and stress anomalies).

3 Design Specification

A complete design specification for the DGR and associated UFC are given in References 4 and 5. For the purposes of the thermo-mechanical design assessments carried out as a part of the current work package, the key aspects of the specification are as follows:

- The UFC shall be designed with sufficient mechanical stability and strength to provide containment of the used fuel from the time of loading through handling, transportation, emplacement and potential retrieval operations and for its specified functional design life of not less than 1,000,000 years in the DGR.

- After emplacement in the emplacement room, the surface temperature of a UFC shall not exceed 100°C. This UFC surface temperature limit will avoid undesirable phase transformation of a bentonite based buffer, which may have an adverse effect on the

swelling and self sealing properties of the buffer material [References 6, 7 and 8]. This temperature limit will also avoid boiling of groundwater that comes into contact with the UFC surface.

- The UFC shall withstand 15 MPa of external pressure loading with the usual safety margin that is employed in the ASME Boiler and Pressure Vessel Code, Section III (i.e. $2/3\sigma_{yield}$). This external load accounts for up to 1000 m of hydrostatic pressure (10 MPa) and a maximum buffer swelling pressure of up to 5 MPa.

- In addition to the normal external pressure loads prior to glaciation, the UFC shall withstand an increase in hydrostatic pressure of 30 MPa due to glaciation (i.e. corresponding to an additional hydraulic head due to the presence of a 3000 m thick ice cap). Therefore, the UFC shall withstand a maximum external pressure loading of 45 MPa (30 MPa from glacial loading and 15 MPa as described above) for the duration of the glacial episode. The glacial load is regarded as an extreme case for which no extra safety margin is required.

- An intact UFC shall withstand an internal pressure rise that may occur from gas production due to the corrosion of the UFC internal components, release of fission gas products from the used fuel, helium build-up from alpha decay of radionuclides in the used fuel, and radiolysis of any water remaining in the UFC on sealing. The effect of temperature rise on the contained gases and water shall be included.

- The UFC shall withstand the static and dynamic loads associated with used fuel loading, handling in the packaging plant, transportation to the DGR, movements within the UFC cask, emplacement and potential retrieval operations in the DGR. For structural analysis of a UFC for the static and dynamic loads, analyses shall be performed at the appropriate temperatures.

- Total acceptable strain in the UFC - The total elastic and plastic strain developed in any part of the UFC shall not exceed the creep-rupture strain of the material over the design life of the UFC. The creep-rupture strain of the material(s) shall be determined for the as-fabricated condition of the material(s) and shall account for variations due to welding and other fabrication and heat treatment processes.

- The UFC geometry shall be such that the loading pressure imposed by the UFC on the buffer does not exceed the load bearing capacity of the buffer material supporting the UFC for the UFC design lifetime.

4 Material Properties

4.1 USED FUEL PROPERTIES

The DGR design is based on the reference CANDU fuel bundle, containing 19.25 kg of elemental uranium when initially inserted into the reactor. Each fuel bundle consists of 37 fuel elements and is 495 mm long and 102 mm in diameter. For the design scoping assessments

carried out as a part of this programme of work, only the heat output from the waste fuel is required. It is assumed that neither the fuel, nor the fuel bundle contributes to the strength of the proposed design. The fuel decay has been calculated, Reference 9, from which heat output as a function of time has been derived (Table 1). It has been assumed that all fuel will undergo an initial cooling period of 30 years in surface facilities prior to emplacement within the repository.

4.2 ROCK MASS PROPERTIES

A volume of sparsely fractured granite was selected as the host medium for the waste emplacement area of the DGR. The rock mass material properties and the derived strength limits used in the design analyses are largely, based on measurements taken in the Underground Research Laboratory for Lac du Bonnet granite [Reference 10]. The sparsely fractured rock mass is assumed to be linearly elastic, isotropic and homogeneous. The assumed elastic constants and thermal properties for the rock mass are shown in Table 2.

The geothermal gradient is assumed to be 0.012°C/m of depth, with the average surface temperature of a site on the Canadian Shield being 5°C [References 11 and 12]. At the nominal DGR depth of 1000m, this gives an ambient temperature of 17°C.

The ambient principal in-situ stresses assumed for the in-room emplacement repository can be defined by the following functions, originally presented in Appendix B of Reference 3.

$$\sigma_1 = 0.1345MPa/m_{depth} + 18.5MPa \quad \text{< 300m} \quad (1a)$$

$$\sigma_1 = 0.00866MPa/m_{depth} + 56.3MPa \quad \text{from 300 to 1400 m} \quad (1b)$$

$$\sigma_1 = 0.0403MPa/m_{depth} + 12.1MPa \quad \text{> 1400 m} \quad (1c)$$

$$\sigma_2 = 0.1112MPa/m_{depth} + 9.9MPa \quad \text{< 300 m} \quad (2a)$$

$$\sigma_2 = 0.00866MPa/m_{depth} + 40.7MPa \quad \text{from 300 to 1660 m} \quad (2b)$$

$$\sigma_2 = 0.0293MPa/m_{depth} + 6.4MPa \quad \text{> 1660m} \quad (2c)$$

$$\sigma_3 = \sigma_v = 0.0260MPa/m_{depth} \quad (3)$$

where σ_v = vertical stress; and σ_1 σ_2, σ_3 are the major, intermediate and minor principal stresses respectively.

The assessment of thermo-mechanical stability is made by calculating a factor of safety based on the Hoek and Brown empirical failure criterion model [Reference 13], defined as follows:

$$\sigma_{1f} = \sigma_{3f} + \left(m \cdot \sigma_c \cdot \sigma_{3f} + s \cdot \sigma_c^2\right)^{1/2} \quad (4)$$

where σ_{1f} = major principal stress at failure,
σ_{3f} = minor principal stress at failure,

σ_c = uniaxial compressive strength, and
m, s = empirical strength parameters.

Under uniaxial conditions, for this granite, the onset of stable crack initiation (σ_{ci}) is about 70 to 75 MPa. In comparison, the stress for the onset of unconfined unstable crack growth (σ_c) is about 150 MPa, and the peak unconfined compressive strength (σ_f) is about 210 MPa (i.e., the conventional value from laboratory testing) [Reference 10]. For the purposes of the current work, the peak strength and associated empirical strength parameters used in the failure model are σ_c = 100 MPa, m = 16.6, s = 1 following excavation, rising to σ_c = 150 MPa, m = 25, s = 1 after the sealing materials have been placed. Note that the later values equate to an intact rock tensile strength of 6 MPa, which is below the average observed value of 10.4 MPa for wet Lac du Bonnet granite at the Underground Research Laboratory (Reference 14).

A criterion is also set for the structural performance of the geosphere near the ground surface. The uplift of the geosphere immediately surrounding the DGR, caused by thermal expansion from heat from the disposed waste, may open or extend near-surface, subvertical fractures and, thus, enhance groundwater flow. This, near-surface extension zone (also called the perturbed fracture or perturbed fissure zone) is defined as the volume of rock overlying the DGR that could experience loss of horizontal confining stresses; i.e. horizontal stress greater than or equal to zero for a “no-tension” analysis [Reference 15] and potential opening or extension of subvertical fractures. For the purposes of this assessment, the maximum depth of the near-surface extension zone, measured from ground surface, is set at 100 m, as in previous studies [Reference 10]

4.3 SEALING MATERIAL PROPERTIES

Following extensive research [Reference 16], three bentonite clay-based sealing materials have been specified for the in-room emplacement design: buffer material, dense backfill and light backfill. Bentonite clays are particularly attractive as sealing materials because of their swelling, and plasticity properties as well as their very low hydraulic conductivity. In addition, bentonite clay has the ability to sorb and retain cations.

The buffer [Reference 17] is a mixture of sodium-bentonite clay (a montmorillonite-rich clay found in commercial quantities in the central plains of North America) and well-graded silica sand mixed in a 1:1 dry mass ratio, giving a minimum dry bulk density of 1.67 Mg/m^3 and an optimum gravimetric moisture content of 17-19 wt%. For the in-room emplacement method, the buffer is placed around the UFC in the form of close-fitting, pre-compacted blocks.

The dense backfill material is a variant of the reference sealing material proposed for the reference borehole emplacement method [Reference 18]. It is a mixture of glacial lake clay (an illite-rich lake clay deposited in glaciated regions of North America), sodium-bentonite clay and crushed granite mixed in a proportion of 25/5/70% by dry weight, with a dry bulk density of about 2.1 Mg/m^3 and an optimum gravimetric moisture content of 8%. Like the buffer material, the dense backfill is placed as close-fitting blocks of highly pre-compacted sealing material [10].

In order to fill the upper perimeter of the emplacement room, a light backfill material, which can be blown into position is specified. The light backfill has a composition of 50% sodium-bentonite clay and 50% crushed granite, by dry weight. Based on the minimum dry density of this mix and the minimum clay dry density, it is judged that this material will yield about the same hydraulic conductivity as the dense backfill.

A mixture of dry granular bentonite and rounded sand is used to fill the gap between the buffer and the UFC's bentonite jacket, to provide for conductive heat transfer and to maintain the density of the clay-based sealing system. Rounded silica sand and granular bentonite, screened to specific sizes (i.e., fractionated) and dried, have good flow properties to fill the gap. Bentonite has been introduced to reduce the diffusion-controlled mass transport rate within the annulus around a defected UFC.

In addition to the bentonite clay based materials, low heat, high performance concrete is used for supporting rails and equipment and for placing and aligning pre-compacted dense backfill and buffer blocks, as well as the construction of bulkheads at the emplacement room entrances, in tunnels and in shafts. Cement based grouts may be used to control groundwater movement into the excavation and around seals. Recent test information suggests that these high-performance cements and concretes would have very low porosity, reduced pH and extremely low hydraulic conductivities. Microcracks generated in the high-performance materials would tend to self-seal [Reference 19].

The specifications for the basic physical properties of clay-based sealing materials are presented in Table 2. In practice, the thermal conductivity of the bentonite jacket material is dependent on the moisture content of the material, which in turn varies with distance from the surface of the UFC. Values for thermal conductivity of the jacket material have been derived, as a function of distance from the UFC, from References 20 and 21. The sealing materials are all assumed to have uniform, linear elastic, isotropic properties.

For the assessment of the structural integrity of the sealing material blocks prior to emplacement of the lower support blocks, but after positioning of the UFC, estimates of the mechanical strength of the sealing materials were required. These have been obtained from Reference 22. For the purposes of this assessment, a tensile strength of 250 kPa, and an unconfined compressive strength of 0.9 MPa for the bentonite jacket has been assumed. The relationship between compressive and shear strength is derived from the von-Mises yield criterion, which states that plastic flow occurs when the shear strain energy reaches a critical value.

$$(\sigma_1 - \sigma_2)^2 + (\sigma_2 - \sigma_3)^2 + (\sigma_3 - \sigma_1)^2 = const \quad (5)$$

In uniaxial compression, yield occurs when $\sigma_1 = Y$, $\sigma_2 = 0$, $\sigma_3 = 0$, thus

$$(\sigma_1 - \sigma_2)^2 + (\sigma_2 - \sigma_3)^2 + (\sigma_3 - \sigma_1)^2 = 2 \cdot Y^2 \quad (6)$$

At yield in pure shear, $\sigma_1 = -\sigma_2 = \tau_{xy}$, $= k$ and $\sigma_3 = 0$ thus the von-Mises criterion becomes:

$$(\sigma_1 - \sigma_2)^2 + (\sigma_2 - \sigma_3)^2 + (\sigma_3 - \sigma_1)^2 = k^2 + k^2 + 4k^2 \quad (7)$$

The constant must have the same value under any stress condition, thus

$$6k^2 = 2 \cdot Y^2 \qquad \text{or} \quad k = \frac{1}{\sqrt{3}} Y \quad (8)$$

A maximum shear strength of 250 kPa for the bentonite jacket has therefore been assumed.

The strength properties for the buffer material (a 50% silica sand and 50% bentonite mix) have been based on a “rule of mixtures” approach. It is assumed that the sand has no tensile strength and therefore the buffer material tensile strength is reduced by 50% compared to bentonite alone. A similar approach has been adopted in determining the shear strength. i.e. tensile strength = 125 kPa , and shear strength = 260 kPa.

In the absence of more detailed information at this stage, the tensile, compressive and shear strengths for the dense backfill have been assumed to be the same as for the buffer material.

Clearly the backfill material structural behaviour is highly dependent on the shear softening and strain hardening properties of the clay based materials, for which suitable material properties are not currently available. Once these properties are established for the anticipated DGR conditions, the stability analysis should be reviewed.

4.4 UFC PROPERTIES

4.4.1 Copper Properties

The outer corrosion barrier of the UFC is assumed to be OFP copper for which the material properties (Table 3) are taken from Reference 23:

Post yield properties for the copper will be modelled using a stress-strain curve defined from the true stress/ strain data shown in Table 3b. Once the final plasticity data point on the stress strain curve is reached, subsequent loading will assume perfectly plastic behaviour. The visco-plastic nature of copper on the long time-scales being considered will mean that the stresses in the UFC are over estimated.

The creep behaviour of the copper container will be assessed using the following empirical creep function for copper [Reference 24]:

$$\dot{\varepsilon} = 1.58 \cdot 10^{-17} \cdot \sigma_j^{3.4} \qquad \text{for } \sigma_j < 130 \text{ MPa.} \quad (9)$$

Where σ_j is the von Mises stress in MPa and

$\dot{\varepsilon}$ is the strain rate (1/s)

4.4.2 Carbon Steel Properties

The inner carbon steel vessel is constructed from carbon steel to SA516-70, whilst the ends are constructed using steel to SA105. Properties for this grade of steel are shown in Table 4. Post yield properties for the steel will be modelled using a stress strain curve defined by the true stress strain data shown in Table 4b.

In comparison to the copper, creep of the steel at the anticipated peak DGR temperatures is negligible, and will not be taken into consideration.

5 Initial Emplacement Room Analysis

5.1 AIM

The aim of the initial emplacement room analysis was to provide confidence that the proposed DGR design would meet the thermal design requirements, before a more detailed analysis of the DGR was carried out. In addition, the model was used to determine the sensitivity of the repository temperature to room and UFC spacing, in order to assist with the development of the final proposed repository layout.

5.2 MODEL

For the initial assessments, a 2D cross-section through the emplacement room and UFC was considered. In common with all of the finite element analyses carried out as a part of this programme, the models were constructed using PATRAN, whilst the analyses themselves were carried out using ABAQUS/Standard (version 6.2) developed by Hibbitt, Karlsson & Sorensen Inc [Reference 25]. The emplacement room layout considered was broadly similar to that considered in Reference 26, modified to accommodate the larger current design of UFC. Details of the cross-section considered are shown in Figure 5. Following an initial investigation, it was concluded that assuming the copper outer container is in intimate contact with the steel inner vessel provides a worst case for the predicted copper temperature. It is anticipated that this would, in any case, ultimately be the case, following creep of the copper due to the application of water pressure, and the effects of the sealing materials swelling. The computer model therefore ignored the small gap between the inner and outer containers. The model geosphere was bounded on top by the Earth's surface and at the bottom by a plane 2000 m below the repository horizon; on the opposing sides by the vertical mid-plane along the longitudinal axis of the emplacement room and by the vertical mid-plane along the longitudinal axis of the inter-room pillar.

The ground surface temperature was modelled as an isothermal boundary condition, with a temperature of +5°C representing the average Canadian Shield surface temperature. After 10,000 years, the assumed surface temperature was reduced to 0°C, in order to account for a period of glaciation. The lower boundary was also modelled as isothermal, at a plane 2000 m below the repository horizon, such that a geothermal gradient of +0.012°C/m of depth was achieved. This results in an initial rock formation temperature at the DGR depth of 17°C. The

vertical boundaries were modelled as adiabatic planes of symmetry to reflect the heat generated in the cell, Figure 6. In effect, therefore, the model replicates an infinite array of infinitely long parallel emplacement rooms. The condition modelled was thus representative of a UFC located in the centre of the DGR. The approach adopted is inherently conservative, in that the model considers a situation where all of the fuel is placed in the repository instantaneously, and that the decay heat from all UFCs is the same. In practice, the fuel will have spent varying lengths of time out of the reactor before emplacement, in some cases much more than 30 years, and emplacement is scheduled to take place over approximately 30 years. A further inherent conservatism of the modelling approach adopted is that the heat lost from the ends of the UFCs was not considered; the model results therefore over predict the temperature profile.

The initial analysis only considered the thermal performance of the repository. The heat flux due to the radio-active decay of the fuel was applied to the inner surface of the steel inner container. This assumes perfect heat transfer out of the fuel bundles and within the UFC, thus presenting a worst case, as far as the UFC temperature history is concerned. All voids were assumed to be filled with sealing materials and the DGR was considered to remain dry during the initial stages. As the thermal conductivity of the dry material is lower than that of partially saturated materials, this provides a conservative analysis. Furthermore, in the absence of water-flow, conduction was considered to be the dominant heat transfer mechanism, and radiation and convection heat transfer mechanisms were not considered, again yielding a conservative assessment.

5.3 INITIAL ANALYSIS RESULTS

The analysis predicted a peak copper temperature of 122.7°C, 26 years after emplacement, based on a UFC heat output of 1138.6 W at the point of emplacement, and a emplacement room separation of 45 m. The full temperature history is shown in Figure 7, for three locations within the emplacement room; the hottest point on the outer surface of the copper container, the uppermost point of the emplacement room (crown), and the horizontal extremity of the room (springline), at the granite surface, Figure 8. The thermal profile within the DGR geosphere at twenty years from emplacement is shown in Figure 9.

The results of the sensitivity analysis are summarised in Table 5. For these analyses, an earlier UFC heat loading of 993 W per UFC was used as a base case, with a emplacement room separation of 28.6 m. For this base case, the local heat flux at the surface of the UFC was used, with no attempt to account for the UFC axial spacing; this is the total heat load per UFC (993 W) divided by its internal surface area. This provides an upper bound to the predicted temperature. A lower bound value was obtained by using a reduced heat flux obtained by dividing the UFC heat load by the internal surface area of the UFC plus that of the end plug. In addition, a number of further analyses were carried out to determine the system's sensitivity to the assumed heat flux.

Subsequent analyses were used to determine the system sensitivity to the layout of the emplacement room. These considered a range of UFC separations, starting from the base case separation of 2.52 m (between centres), as well as a range of emplacement room separations.

Finally, analyses were carried out to determine the dependence on the sealing material properties. A range of light backfill thermal conductivity values were considered. The base case assessment used a light backfill conductivity of 0.7 W/m°C.

6 Near-field Analysis

6.1 AIM

The near-field analysis provides a more detailed assessment of the thermal and stress conditions in the material surrounding the emplaced UFC than that provided by the initial 2D assessment. The use of a 3D model allows the UFC longitudinal spacing to be more accurately taken into account. The results of this analysis will be used primarily to provide confidence that the proposed DGR design will meet the thermal design requirements; That is that the external surface temperature of the copper corrosion barrier will not exceed 100°C during the life of the DGR.

6.2 MODEL

The model used for this assessment considered a “unit cell” of the repository. The “cell” consisted of a hexahedral portion of the repository and geosphere, bounded on the upper side by the Earth’s surface and at the bottom by a plane 10,000 m below the repository horizon; on one set of opposing sides by the vertical mid-plane along the longitudinal axis of the emplacement room and by the vertical mid-plane along the longitudinal axis of the inter-room pillar; and on the second set of opposing sides by the vertical mid-plane between the two sets of UFCs and by the vertical mid-plane passing through the UFC. Subsequent to the initial analysis work described in the previous section, the design of the emplacement room layout was reviewed in order to improve performance and operability. This resulted in several changes to the disposition of the various sealing materials. Details of the revised dimensions assumed for the near-field analysis are given in Figure 2, and the finite element model shown in Figure 10. The longitudinal spacing between UFCs was assumed to be 1.25 m (less than 1 m required for shielding purposes), and the room spacing 45 m between room centres. By considering the minimum spacing between UFCs in this way, the assessment will provide a conservative assessment of temperatures and stresses.

For the thermal portion of the analyses, the top boundary condition (representing ground surface) was modeled as a constant temperature (i.e. isothermal) boundary set at 5°C, to represent the average Canadian Shield surface temperature. After 10,000 years, the surface temperature is assumed to reduce to 0°C, in order to account for a period of glaciation. The bottom boundary condition was also modeled as an isothermal boundary set to the ambient temperature at the bottom of the model, assuming a geothermal vertical gradient of 0.012°C/m). All four vertical boundaries were modeled as adiabatic planes of mirror symmetry to reflect the heat generated within the cell (Figure 6). This mirror symmetry mimics the thermal contribution from all the surrounding "unit" cells, in effect replicating an infinite tabular array of infinitely long parallel emplacement rooms. As such, it is representative of the conditions likely to be encountered in the middle of the DGR. As with the previous analysis,

conduction was considered to be the dominant heat transfer mechanism, and therefore the effects of radiative and convective heat transfer were not considered. This is a conservative assumption.

For the structural analyses the boundary conditions are as follows. The top boundary is free to displace vertically, and the perimeter is rigidly constrained laterally. The bottom boundary is rigidly fixed against displacement, both vertically and laterally. The four vertical boundaries are fixed against out-of-plane lateral displacement and are attached to the top and bottom boundaries to maintain the appropriate continuity (Figure 6). This also constrains the "unit" cell to displace consistently with the surrounding "unit" cells and to allow the build-up of horizontal stress caused by thermal expansion.

The model has not claimed any potential benefit due to ground support from the swelling of the sealing materials, in view of the uncertainty and time dependence of this effect. Also, the stiffness of the sealing materials has been assumed to be very low (E=0.1 GPa) therefore the reactive ground support effect is minimised. This is considered to result in a conservative assessment.

6.3 NEAR-FIELD ANALYSIS RESULTS

The results of the near-field thermal analysis are shown in Figures 11 to 15. The temperature history plots (Figures 11a) shows results at the same three locations used previously (Figure 8). The results indicate a rapid increase in the UFC temperature over the first decade, reaching a peak temperature of 97°C after 16 years for a UFC located at the center of the DGR, and given an ambient temperature of 17°C at the repository depth of 1000m. Thereafter, the temperature falls to around 75°C, until 1000 years after emplacement, when the model predicts a further rise in the UFC temperature to 95°C 6000 years after fuel emplacement. The rock temperature rises from 17°C, at the time of emplacement to 73°C after 50 years. The model then predicts a reduction in the rock temperature to 68°C, followed by a secondary rise to a temperature of 93°C 6000 years after fuel emplacement.

As a consequence of the thermal diffusivity ($\alpha = k/\rho Cp$) of the rock, combined with the rate of change of the waste radioactive decay heat, steady state thermal conditions are not achieved until late in the life of the repository. Prior to the time at which the temperature begins to rise for the second time, the thermal energy from the used fuel is dissipated by heating up an expanding volume of rock (Figure 11b). Subsequent to this, however, the volume of rock being heated remains constant, because of the increasing ambient rock temperature with depth and steady state conditions being achieved for heat flow in the repository to surface direction. Because the heat required to increase the volume of rock affected is greater than the heat lost to the atmosphere, this results in the secondary rise in temperature. Since the near field model does not allow heat to be lost at the sides of the model, it will tend to over estimate the magnitude of this effect.

The stress analysis results are shown as plots of Factor of Safety using the Hoek and Brown failure criterion described previously, for two orientations of the emplacement room, and at two

times, immediately following excavation and the time of peak stress. Figures 13a and 13b show results with the room principal axis perpendicular to the major horizontal in-situ stress component (worst case), whilst Figures 13 c and 13 d show results when the room principal axis is parallel to the major horizontal in-situ stress component. The stress analysis results are shown for 100 years after waste emplacement, this corresponding to the time of peak stress at the DGR. The time of peak stress corresponds to the time of peak rock temperature (ignoring the secondary peak effect, which as discussed above is over estimated by the current analysis).

For the worst case orientation (major horizontal stress perpendicular to the room principal axis), the factor of safety values are generally well above 2.0 at all times, beyond a perimeter annulus of about 750 mm thick or less, depending on the location around the room perimeter, and approaching 1.0 at the periphery of the room. After excavation, the factor of safety remains in excess of 1.2 in all locations, whereas at the time of peak stress, the factor of safety drops below 1.0 at the crown and floor of the emplacement room over a length of around 1 m either side of the room principal axis, and at the junction between the concrete floor and the room wall. The minimum value is 0.78, located at the crown of the emplacement room. In all cases, the region in which the failure criterion is not satisfied extends to a depth of less than 300 mm. The maximum principal compressive stress is 204 MPa, Figure 14. Therefore some localised rock damage is anticipated at the crown and base of the emplacement room. However, because the damage will not initiate until after the sealing material has been placed, and the limited extent of the damage zone, this is not considered to adversely affect the long term safety of the DGR. It will however, need to be considered should waste retrieval ever become necessary.

When the room is oriented more favourably with respect to the rock in-situ stress profile (i.e. with the maximum horizontal stress parallel to the principal axis of the emplacement room), the minimum factor of safety increases to 1.70 after excavation and 0.91 after 100 years, Figures 13c and d respectively. In this case, only a very small region in the vicinity of the junction between concrete floor and the emplacement room wall exceeds the failure criterion. The minimum principal stress (compression) is 180 MPa, Figure 15, thus the compressive strength capacity of the granite is not exceeded at any time.

Figure 16 shows the displacement of the emplacement room at various times. Excavation-induced displacements at the room perimeter are directed inward (i.e., convergence), and are of the order of 6 mm. Thermal loading causes a further convergence of about 4 mm in the walls of the room, and an expansion of about 5 mm in the roof and floor at 100 years.

Although the analysis predicts localised cracking at the crown and base of the emplacement room, in-service the rock is constrained by the sealing materials and collapse of the room is therefore not anticipated. Should a UFC need to be retrieved, however, additional precautions should be taken to ensure the safety of mining personnel against the fall of loose material.

High stresses may influence the detailed design of the emplacement room access roadways immediately prior to the bulkhead seals; an area of the DGR design not addressed by the current programme. In the event that these thermally induced stresses affect this area, a number of design solutions could be put in place to ameliorate the situation such as, increasing the spacing between the last emplaced UFCs and the emplacement room bulkhead, and/or increasing the separation between adjacent emplacement room entrances. Both these design

alterations would have the effect of reducing the rock temperatures in the emplacement room access roadways thereby reducing the thermally induced stress levels. However, these design changes would increase the area of the repository, potentially resulting in an increase in its construction costs.

7 Far-field Analysis

7.1 AIM

The far-field analysis provides an assessment of the thermal and stress conditions in the granite some distance away from the DGR. This assessment will confirm that the repository depth is adequate to prevent cracking of the surrounding rock formation due to the thermal expansion of the formation local to the repository. In addition, the assessment will enable a judgement to be made on the likely influence of the stresses on groundwater flow in the vicinity of the DGR.

7.2 MODEL

The model used a simplified representation of a quarter section of the repository, the extent of which was sufficient such that the temperature of the rock at the boundaries remained unaffected by the presence of the repository. The model was bounded on the upper side by the Earth's surface and at the bottom by a plane 10,000 m below the repository horizon. The DGR was represented by a plane of material providing the required heat loading, although details of the emplacement rooms were not included. Details of the dimensions assumed for the analysis are given in Figure 17. It has conservatively been assumed that the DGR will be configured as tightly as possible, thus maximising the temperatures and stresses at the centre of the repository. In practice, the DGR is likely to be more spread out due to local features within the rock formation, and temperatures will be reduced. The heating from the radioactive decay of the fuel was averaged over the volume of the repository, based on an assumption of a full repository containing 3.6M fuel bundles. This approach tends to under estimate temperatures locally in the DGR during the early stages. However, it gives a better indication of temperatures and stresses in the rock formation away from the emplacement rooms than the near-field models as the repository edge effects are explicitly considered. As discussed for the near-field assessment, in order to provide a conservative assessment of the peak temperature reached in the surrounding rock formation it was assumed that the DGR remains dry throughout the life of the repository, and heat transfer as a consequence of groundwater flow is not considered.

As with the previous models, the upper surface boundary condition was modelled as an isothermal boundary, with a temperature of +5°C, representing the average Canadian Shield surface temperature, reducing to 0°C after 10,000 years to account for a period of glaciation. The lower boundary was also modelled as an isothermal boundary, such that a geothermal gradient of +0.012°C/m of depth is achieved. The vertical boundaries were modelled as adiabatic planes of symmetry. The vertical planes of the model were constrained not to move, as was the lower horizontal plane. The upper horizontal plane, the earth's surface, was free to move. A summary of the boundary conditions used is shown in Figure 18. The model is thus representative of a repository positioned in an infinite extent of granite.

Stress analyses were performed at key stages in the DGR life (namely 100, 1,000, 10,000 and 100,000 years, using temperature fields appropriate to the assessment time as calculated in the thermal analysis. It has conservatively been assumed that the DGR emplacement rooms are oriented with the room's longitudinal axis perpendicular to the highest principal stress. Between 10,000 and 100,000 years, an additional load due to 3000 metres of ice spread uniformly on the surface was included. For the purposes of these assessments, it has been assumed that the effects of additional loads attributable to changes in the geologic stress field, such as the formation of local fault lines through an emplacement room, will be adequately buffered by the clay based sealing materials materials, and therefore do not need to be explicitly considered at this stage of the DGR design process.

7.3 FAR-FIELD ANALYSIS RESULTS

Figure 19 shows the thermal history for three locations within the DGR, the repository centre (equivalent to the previous near-field case), at the mid point along one edge of the repository, and at a corner location. In addition, Figure 20 shows how the temperature distribution in the surrounding geosphere varies with time. The temperatures predicted by the analysis drop significantly with distance away from the center of the repository, with the peak rock temperature at a corner of the repository being only 33°C, compared with a peak temperature at center of the repository of 69.5°C. The far-field analysis predicts that the peak temperature will be developed at around 4000 years from waste emplacement, and it would take over 100,000 years to return to the initial ambient temperature,

Also shown in Figure 19 is the temperature history at the crown of a emplacement room at the center of the repository, as predicted by the near-field analysis. As anticipated, the peak temperatures generated by the far-field model are less than those generated by the near-field model. For the initial period, approximately 100 years, this can be attributed to the heat generated by the individual UFCs in the plane of the repository being averaged over the entire waste emplacement area, as defined by the initial gross thermal load. Between 100 years and 2000 years after emplacement, there is a good correlation between the two models. Thereafter the models diverge again as the near-field model under estimates the cooling influence of the DGR periphery.

Generally, the far-field model is accurate for periods beyond 2000 years in the immediate plane of the repository and earlier in time as the distance from the plane of the repository increases (i.e. the localized heating effects are "smeared" out). It is therefore considered that the DGR will initially reach a temperature of 70°C some 100 years after fuel emplacement. The rock temperature will then remain more or less constant for some 4000 years, after which the temperature will steadily decline, returning to the initial ambient conditions around 100,000 years from emplacement.

The stress analysis predicts a maximum tensile stress (at surface) of 1.27 MPa after 10,000 years, Figure 21. This is significantly below the quoted tensile strength for the homogeneous isotropic rock considered of 6 MPa, and indicates that new fracture zones will not be initiated as a result of the DRG. The region over which the stress remains tensile, thus the region in which some limited opening or extension of subvertical fractures could occur is less than 9 metres vertically, in the vicinity directly above the DGR. This is significantly less than the specified

depth of 100m, and negligible impact on groundwater flow is anticipated. The maximum uplift is about 247 mm on the ground surface above the centre of the DGR at about 10,000 years after waste emplacement, Figure 23.

It is considered that the above results confirm that the proposed DGR design will meet the design specification. It should also be borne in mind that the above results are based on worst-case conditions, and actual figures are likely to be less onerous in practice.

In order to determine the ventilation requirements to enable operators to comfortably carry out their work within the repository, it is important to determine the likely temperature in an emplacement room adjacent to an already filled room. In order to do this the temperature profile at the edge of the far-field model has been used. This can be considered a worst case, being analogous to the condition when filling the last emplacement room, with the adjacent room having been one of the first rooms to be filled. Figure 24 shows how temperature varies with distance from the edge of the repository, thirty years after emplacement. The temperature of the rock formation in the vicinity of an adjacent emplacement room is predicted to be no higher than 21°C.

8 Pressure Analysis

8.1 AIM

One of the key requirements of the UFC is to withstand the pressure loading applied through a combination of sealing materials swelling and hydrostatic water pressure. Under normal conditions, the maximum isostatic pressure loading will be 15 MPa (5 MPa due to buffer swelling, and 10 MPa hydrostatic pressure – equivalent to the water head at 1000m). During periods of glaciation, it is assumed that the UFC will be subjected to an increase in pressure loading of 30 MPa (i.e. 45 MPa total loading) due to the additional pressure created by a 3000 m thick ice layer. The UFC design specification requires the stresses in the UFC to remain within ASME III design limits for Level A loading under normal conditions, and within ASME III design limits for Level D loading during periods of glaciation.

8.2 MODEL

An axisymmetric finite element model of the copper outer and carbon steel inner containers was created (Figure 25). The 1 mm fitting gap between the two components was explicitly modelled, with a contact surface, to allow collapse of the copper corrosion barrier to be accurately taken into account. For the purposes of the current work, assessment of the creep behaviour of the copper container has not been included in the finite element analysis model.

8.3 RESULTS

8.3.1 External Pressure Cases

The maximum (local) von Mises stress in the steel inner component under normal conditions is predicted to be 131 MPa, rising to 226 MPa as the pressure loading is increased from 15 MPa to 45 MPa (Figure 26). The corresponding Tresca stress is 151 MPa, for a uniform pressure distribution of 15 MPa, rising to 258 MPa for a pressure distribution of 45 MPa. It should be noted that these are peak stresses. For carbon steel SA516-70 / SA105, the minimum specified tensile strength is 485 MPA, and the minimum specified yield strength is 260 MPa. This gives a design stress intensity of 161.7 MPa for Level A loading, in accordance with the criteria of ASME III Article III 2000, and 260 MPa for periods of glaciation (σ_{yield}). The proposed design for the carbon steel inner container is therefore considered satisfactory.

The copper corrosion barrier is designed to collapse onto the steel inner container, and is thereafter supported by it. Following the collapse of the copper container onto the load bearing steel inner container, the maximum tensile stress in the copper, under external isotropic pressure loading of 15 MPa prior to glaciation, is 68.4 MPa (Figure 27). The creep rate at this stress level is typically less than $8x10^{-4}$ $year^{-1}$. The application of additional loading due to glaciation results in further localised collapse of the copper at the corners of the container, and a reduced residual stress of 46.7 MPa. This can be compared with an ultimate tensile strength for the copper of 200 MPa.

Under normal conditions, the maximum (localised) plastic strain in the copper outer barrier following its collapse against the steel liner is 6.6%, this rises to a strain of 9.5% at a pressure loading of 45 MPa following a period of glaciation, Figure 28. This compares with a plastic strain to failure of around 29% based on short term tensile testing [Reference 23]. Although the strain to failure in creep is generally lower than the tensile strain to failure, the results indicate that pressure deformation effects will dominate. In any case, the support offered by the steel container will mean that although there is a possibility that some creep damage may occur, it would be limited to the inner surface of the copper container. It is therefore concluded that failure of the copper corrosion barrier is unlikely. It is however recommended that a detailed creep analysis of the container be carried out once information is available on the rate of swelling of the sealing materials materials.

8.3.2 Internal Pressure Case

In addition to the external pressure cases, due to formation pressure, the intact UFC is required to withstand an internal pressure rise that may occur from gas production due to the corrosion of the UFC internal components, release of fission gas products from the used fuel, helium build-up from alpha decay of radionuclides in the used fuel, and radiolysis of any water remaining in the UFC on sealing. The analysis has determined the maximum theoretical internal pressure that can be retained by an unsupported copper container (i.e. assuming no support from the sealing materials). The absence of support from the sealing materials has been assumed because of the variation of sealing materials pressure with time, the fact that support in the region of the lifting feature is unlikely, and to cover the situation where a UFC is subsequently retrieved. The analysis indicates that initial yield occurs when the pressure reaches 0.6 MPa,

with local yielding occurring in the UFC lid (Figure 29). Ultimate failure of the copper container is predicted at a pressure of approximately 2.3 MPa (Figure 30), when global yielding of the UFC lid occurs.

According to the reaction for anaerobic corrosion, [Reference 27] 1 mole of water gives rise to 1 mole of hydrogen. Using Boyle's law, the total volume of (liquid) water required to generate an internal pressure of 0.6 MPa is therefore 67 cc. With a long-term hydrogen production rate of 1 dm^3 per year at 1 standard atmosphere, this volume of water would be consumed in approximately of 2.8 years, this defining the rate of pressure build-up in the UFC under these circumstances. This therefore provides a specification for the maximum moisture content acceptable at the time of closing the UFC. In practice, because the void space between the outer copper and the inner steel containers will be evacuated in the electron beam welding cell, and will therefore not contain a significant volume of water vapor, the actual internal pressure is likely to be very much lower than 0.6 MPa.

9 Handling Load Analyses

9.1 AIM

It is required to demonstrate that the proposed design of UFC is sufficiently robust to withstand the anticipated handling loads. In order to achieve this, a three dimensional model of the UFC was developed, incorporating details of the lifting feature. The model was subjected to two loading configurations, deemed to be typical of those likely to be encountered.

9.2 TWO-POINT LIFT

It is assumed that the UFC copper shell and it's steel inner container will be manufactured off-site and delivered to the DGR facility pre-assembled in the horizontal attitude. This empty UFC will be handled using slings with appropriate protection to ensure no damage to the copper outer surface.

This condition was replicated in the model by locally restraining the model from downward vertical movement over the lower half of the UFC at a distance of 0.5 m from each end. To account for dynamic effects, the analysis considered a maximum vertical acceleration of 5g, this being the maximum credible value for normal operation on rail or road transport [Reference 28]. Further conservatism was introduced by assuming a fully loaded UFC (25 tonne), thus ensuring that the case analysed was bounding for all similar loading conditions.

The analysis predicts a maximum von Mises stress in the copper corrosion barrier of 47 MPa (c.f. yield at 60 MPa), and 21 MPa in the steel inner container (c.f. yield at 260 MPa), Figures 31 and 32 of Annex 2 respectively. The maximum predicted deflection will be 0.16mm, Figure 33. Because the model accurately represents the post yield properties of the copper shell, and the contact between the inner and outer containers, the results predict the actual contact stress distribution, resulting in the two geometrically separate stress peaks shown in the steel shell stress profile, Figure 32.

9.3 VERTICAL LIFT

When fully loaded the UFC, with its inventory of three baskets containing spent CANDU fuel and with the inner vessel lid bolted and the copper container lid welded to the body, will be lifted using a grapple connected to the UFC lid-lifting feature. The grapple engages with the UFC lid in three locations around the circumference, each "finger" being 150 mm wide.

The half model of the UFC was used with appropriate boundary conditions to emulate this loading configuration. To account for dynamic loading, a load factor of 1.5 was applied, based on typical values used in the design of lifting equipment [Reference 29].

The analysis predicts a maximum von Mises stress of 63.3 MPa in the copper, and a corresponding maximum deflection of 0.4 mm, Figures 34 and 35. ASME III Fig NB-3221-1 places a limit of 1.5x design allowable stress (giving a limit of 60 MPa for this copper) for the sum of primary membrane plus bending stress (but excluding all secondary and peak stresses due to discontinuities). Although this peak stress is marginally above this limit, it is a self-equilibrating stress at the discontinuity and thus this limit does not strictly apply. The main issue with stress concentrations at a discontinuity is their propensity to initiate a fatigue crack. In this case, the anticipated number of loading cycles is only one or two. Fatigue data for oxygen free high purity copper [Reference 30] indicates a life in excess of 300×10^6 cycles for a stress range of 117 MPa. It is therefore considered that the proposed UFC lid lifting feature design is satisfactory. Although the proposed grapple design is also adequate, the anticipated stresses in the UFC lid could be reduced following changes to the grapple design during the detailed design stage.

In addition to the normal operation condition considered above, the analysis was extended to determine the maximum load that could be applied to the lid lifting feature before failure of the copper shell would occur. This was achieved by determining the load required to develop a plastic strain of 29%, the failure strain for the copper. The maximum load that can safely be applied to the UFC lifting feature is 75 tonnes, at which point the whole of the container wall has begun to yield, Figure 36. Changes in the design of the grapple will not result in an increase in the maximum load that can be applied to the UFC lid.

10 Emplacement Condition Analysis

To establish the integrity of the chosen emplacement room emplacement sealing materials structure during the placement of the bentonite sleeved UFCs, a 2-D mechanical analysis of the emplacement room, prior to the emplacement of the lower cavity infill blocks, was carried out using a two dimensional model.

The analysis was carried out in two stages, the first without the UFC and bentonite jacket being in place; and secondly, with the UFC and jacket in-situ. The interface between the jacket and the buffer blocks was modelled as a low friction contact surface. The purpose of the assessment was to demonstrate that the proposed emplacement procedure was feasible in principle. For simplicity, it was assumed that the various types of backfill act homogeneously. However, in practice, this will not necessarily be the case depending on the nature of the

interfaces between the individual blocks of material. Once visco-plastic properties are available for the sealing materials, and details of individual blocks and any mechanical interlocking features are designed, a more detailed analysis will be required to confirm the viability of the final design.

Before the UFC and jacket are placed in the emplacement room, the maximum displacement of the room is 1.46 mm, Figure 37. It should be noted that these results do not take into account any time dependent visco-plastic deformation of the clay, and thus if there is a significant time delay between placing the emplacement room sealing material blocks, and placing the UFC the actual deflections may be larger. Figures 38 to 40 show maximum and minimum principal stress and maximum shear stress respectively in the dense backfill and buffer material prior to positioning of the UFC and jacket. Maximum stress values are summarised, by material in Table 6, which also shows the relevant design allowable for each material. In all cases, the predicted stress is below the design allowable, and therefore it is considered that the proposed emplacement methodology is practical.

With the emplacement room in place, and the sealing materials in position, the maximum deformation is 1.27 mm, Figure 41. Figures 42 to 44 show maximum and minimum principal stress and maximum shear stress respectively in the dense backfill buffer and jacket materials after positioning of the UFC, but before placement of the lower slot infill blocks to support the UFC. As previously, maximum stress values are summarised, by material in Table 6, and once again, in all cases the predicted stress is below the design allowable, and therefore it is considered that the proposed emplacement methodology is practical.

Clearly the backfill material structural behaviour is highly dependent on the shear softening and strain hardening properties of the clay based materials, for which suitable material properties are not currently available. Once these properties are established for the anticipated DGR conditions, the stability analysis should be reviewed.

11 Conclusions

A number of finite element analyses have been carried out by AEA Technology, in support of a programme of work being undertaken by CTECH to update the conceptual design for a DGR for the long-term storage of used nuclear fuel from all Canadian reactors. These analyses have established that the proposed design for the Canadian used nuclear fuel deep geological repository can meet the design specification.

The outer surface of the UFC will reach a maximum temperature of 97.2°C, 16 years after emplacement. The surrounding granite formation will reach a maximum temperature of 72.6°C after 57 years, that will then remain nearly constant for around 10,000 years, after which the temperature will gradually decay, until after 100,000 years, the temperature in the vicinity of the DGR will have returned to near ambient temperature.

The UFC design has been shown to be able to satisfactorily withstand the design loading following saturation of the DGR, as well as any build-up of pressure within the UFC. Under normal conditions, the UFC stresses remain below the ASME III service level A design stress limit for the material, whilst during a period of severe glaciation, the stresses in the steel container remain below the materials specified minimum yield stress.

It has been shown that the UFC can withstand all credible normal handling loads. Stresses remain within acceptable limits during lifting operations using the UFC lid lifting feature, although the actual stress level will be dependent on the detailed design of the grapple used. The feature can be used to apply a maximum pull of 75 tonnes (3x the self weight of a loaded UFC), in the event of needing to retrieve a UFC at a later date. Based on IAEA acceleration profiles for road and rail transport, the UFC design will not sustain damage during transportation in a fully loaded condition.

Analyses have been carried out to demonstrate the stability of the sealing material blocks at all times during the emplacement operation. Assessments were carried out both prior to UFC placement, and also after placement, but prior to placement of the lower slot infill blocks. In both cases, deformation of the sealing material blocks was negligible, <1.5 mm. Stresses in the sealing material blocks were also low and remained within the assumed allowable limits for the various sealing materials. It was therefore concluded that the proposed emplacement methodology would be feasible.

Stress analysis of the surrounding rock formation has shown that the emplacement room excavations are stable prior to the emplacement of the UFCs. Thereafter, stresses in small regions at the top and bottom of the emplacement room exceed the Hoek and Brown failure criterion used to determine rock stability. This is limited to a region extending less than 300 mm into the rock formation, and only occurs after the decay heat has built-up after the sealing materials have been placed. In practice, therefore, this is not considered to present a threat to the safety of the emplacement room. However, should a UFC require retrieval some years after emplacement, some additional roof support may be necessary.

The analyses carried out as a part of this programme of work have all confirmed that the proposed DGR and associated UFC design and the emplacement methodology, can meet the current design specification requirements. Clearly, more detailed analysis will be required during the detailed design stage, using more site-specific thermo-mechanical material properties and details of the in-situ rock formation stress state. Also, further work will be required to demonstrate the integrity of the DGR barriers under less favourable conditions, i.e. during periods of seismic activity.

12 References

1 CTECH. 2002. Deep Geologic Repository Design Update, Report 1106/MD18085/REP/01.

2 Maak P, Simmons G R. May 2001. Summary Report: A Screening Study of Used-Fuel Container Geometric Designs and Emplacement Methods for a Deep Geologic Repository. Ontario Power Generation, Nuclear Waste Management Division, Report 06819-REP-01200-10065-R00. Toronto, Ontario.

3 P Baumgartner *et al*, "The In-room Emplacement Method for a Used Fuel Disposal Facility – Preliminary Design Considerations", AECL Technical Record, TR-655, COG-94-533, 1995.

4 2001. Technical Specification for Updating the Conceptual Design and Cost Estimate for a DGR for Used Nuclear Fuel. Ontario Power Generation, Nuclear Waste Management Division, Document No 06819-UFM-03789-0001-R00, Rev 0. Toronto, Ontario.

5 P Maak. 2001. Used Fuel Container Requirements. OPG Document number 06819-PDR-01110-1000 R01.

6 LH Johnson, DM LeNeveu, DW Shoesmith, DW Oscarson, MN Gray, RJ Lemire and N Garisto. 1994. The Disposal of Canada's Nuclear Fuel Waste: The Vault Model for Post-closure Assessment. Atomic Energy of Canada Ltd Report AECL-10714, COG-93-4.

7 R Pusch, "Chemical Processes Causing Cementation in Heat Affected Smectite – the Kinnekulle bentonite", SKB report TR98-25, 1998

8 R Pusch. 1999. Is Montmorillonite-rich Clay of MX80 type the Ideal Buffer for Isolation of HLW. SKB report TR99-33.

9 Tait J.C., Roman H, and Morrison C. April 2000.Characteristics and Radionuclide Inventories of Used fuel from OPG Nuclear Generating Stations'. Ontario Power Generation, Nuclear Waste Management Division, Report No 06819-REP 01200-10029, Volumes 1, 2 and 3. Toronto, Ontario.

10 P. Baumgartner, D.M. Bilinsky, Y. Ates, R.S. Read, J.L. Crosssthwaite, D.A.Dixon. 1996. Engineering for a Disposal Facility Using the In-Room Emplacement Method. AECL Report-11595, COG-96-223. Toronto, Ontario.

11 M. Drury and T. Lewis. 1983. Water Movement in Lac du Bonnet Batholith as Revealed by Detailed Thermal Studies of Three Closely Spaced Boreholes. Tectonophysics 95, 337-351, Elsevier, Amsterdam.

12 A.Jessop and T. Lewis. 1978. Heat low and Generation in the Superior Province of the Canadian Shield. Tectonophysics 50, 55 – 77. Elsevier.

13 E Hoek and E Brown. 1980. Underground Excavations in Rock. The Institution of Mining and Metallurgy.

14 C Martin. 1993. The Strength of Massive Lac du Bonnet Granite around Underground Openings. PhD thesis, Department of Civil Engineering, University of Manitoba, Winnipeg Manitoba.

15 O Zienkiewicz *et al*. 1968. Stress Analysis of Rock as a No-tension Material. Geotechnique 18, 55-66.

16 L.H. Johnson, D.M. LeNeveu, F. King, D.W. Shoesmith, M. Kolar, D.W. Oscarson, S. Sunder, C. Onofrei, J.L. Crosthwaite. June 1996. The Disposal of Canada's Nuclear Fuel Waste: A Study of Postclosure Safety of In-Room Emplacement of Used CANDU Fuel in Copper Containers in Permeable Plutonic Rock, Volume 2: Vault Model. Atomic Energy of Canada Limited Report AECL-11494-2, COG-95-552-2, Toronto, Canada.

17 D Dixon and M Gray. 1985. The Engineering Properties of Buffer Material – Research at Whiteshell Nuclear Research Establishment. Proceedings of 19th Information Meeting of the Nuclear Fuel Waste Management Program, Volume 3, 513-530, AECL Technical record TR-350.

18 Simmons G.R., and Baumgartner P. 1994. The Disposal of Canada's Nuclear Fuel Waste: Engineering for a Disposal Facility. AECL Report-10715. Toronto, Ontario.

19 Onofrei M., Pusch R., Gray M. N., Borgesson L., Karnland O., Shenton B. & Walker B. 1992. Sealing Properties of cement-based grout materials'. Swedish Nuclear Fuel and Waste Management Company, Stockholm. Stripa Project Report TR-92-28.

20 Ageskog and Jansson. 1999. Heat Propagation in and around the Deep Repository. Swedish Nuclear Fuel and Waste Management Company Technical Report TR-99-02. Stockholm, Sweden.

21 Dixon. 2000. Porewater Salinity and the Development of Swelling Pressure in Bentonite Based Buffer and Backfill Materials. Posiva Report 2000-04.

22 Tang, G.X., 1999. Suction characteristics and elastic-plastic modelling of unsaturated sand-bentonite mixture. PhD Thesis, Dept of Civil Engineering, University of Manitoba.

23 A Bond *et al.* May 1997. Assessment of a Spent Fuel Disposal Container; Assessment Studies for a Copper Canister with Cast Steel Inner Component. Swedish Nuclear Fuel and Waste Management Company Technical Report Technical Report TR-97-19. Stockholm, Sweden.

24 L Börgesson. July 1992. Interaction Between Rock, Bentonite Buffer and Canister. FEM Calculations of Some Mechanical Effects on the Canister in Different Disposal Concepts. Swedish Nuclear Fuel and Waste Management Company Technical Report TR-92-30. Stockholm, Sweden.

25 Karlsson and Sorenson Inc. 2001. “ABAQUS – Standard ver. 6.2 User’s Manual” Hibbitt,

26 P. Baumgartner, D.M. Bilinsky, Y. Ates, R.S. Read, J.L. Crosssthwaite, D.A.Dixon. 1996. Engineering for a Disposal Facility Using the In-Room Emplacement Method. AECL Report-11595, COG-96-223. Toronto, Ontario.

27 N.R. Smart, D.J. Blackwood and L. Werme. 2002. Anaerobic Corrosion of Carbon Steel and Cast Iron in Artificial Groundwaters: Part 2-Gas Generation, Corrosion, 58(8), 627.

28 Atomic Energy Code of Practice, AECP 1006. 1986. The Securing / Retention of Radioactive Packages on Conveyances. Atomic Energy Code of Practice, AECP 1006.

29 British Standards Institute, BS 2573 Part 1. 1983. Rules for the Design of Cranes.

30 E Brandes and G Brook. 1992. Smithells Metals Reference Book. Seventh edition, Butterworth Heineman.

The fuel decay has been calculated[1], from which the following heat outputs as a function of time have been derived for the reference CANDU fuel bundle

Time out of reactor (years)	**Container heat output (W)** 324 bundles per container
30	1138.61
40	961.40
50	821.06
60	708.48
75	580.06
100	440.84
150	310.88
200	258.73
300	221.19
500	180.99
1,000	125.27
10,000	44.48
100,000	2.55
1,000,000	0.92
10,000,000	0.62

Table 1. Used Fuel Heat Output.

1 JC Tait *et al*, "Characteristics and Radionuclide Inventories of Used Fuel from OPG Nuclear Generating Stations – Volume 3", 06819-REP-01200-10029-R00 Volume 3

Property	Lac du Bonnet Granite [1]	Low heat high performance concrete	Fractionated silica sand	Buffer	Bentonite jacket	Dense backfill
Thermal conductivity (W/m°C)	3.00	1.80	1.0 [2]	1.70	0.90 0-100mm 1.05 100 –200mm 1.15 200-250mm [3]	2.00
Specific heat (kJ/kg°C)	0.845	0.9	0.82	1.38	1.38	1.19
Density (kg/m^3)	2650	2430	1450	1970	1600	2270
Young's modulus (GPa)	60	50	0.10	0.10	0.10	0.20
Poisson's ratio	0.25	0.10	0.10	0.10	0.10	0.10
Coefficient of thermal expansion (10^{-6}/°C)	10	10	N/A	N/A	N/A	N/A
Swelling pressure (kPa)	0	0	0	800-2000	800-2000	<50

Table 2. Granite and Sealing Material Thermo-mechanical Properties.

1 P.Baumgartner *et al* "Engineering for a Disposal Facility Using the In-room Emplacement Method", AECL-11595, COG-96-223, June 1996

2 P Gierszewski, Memorandum to Sean Russel, "Thermal conductivity estimates for vault sealing materials"

3 Ageskog and Jansson "Heat Propagation in and Around the Deep Repository" SKB report TR-99-02 Stockholm 1999.

Property[1]	
Thermal conductivity (W/m°C)	380
Specific heat (kJ/kg°C)	0.390
Density (kg/m^3)	8930
Young's modulus (GPa)	117
Poisson's ratio	0.3
Coefficient of thermal expansion (10^{-6}/°C)	16
Strain to failure	29%

Table 3a. Thermo-mechanical Properties for Copper

True stress (MPa)	True plastic strain
60	0.000
80	0.015
130	0.065
180	0.154
200	0.288

Table 3b. Post-Yield Copper Properties

1 AE Bond *et al* "Assessment of a Spent Fuel Disposal Container; Assessment Studies for a Copper Canister with Cast Steel Inner Component", SKB Technical report 97-19, May 1997.

Property	
Thermal conductivity (W/m°C)	59
Specific heat (kJ/kg°C)	0.460
Density (kg/m^3)	7800
Young's modulus (GPa)	200
Poisson's ratio	0.30
Coefficient of thermal expansion (10^{-6}/°C)	12
Yield Strength (MPa)	260
Tensile Strength (MPa)	485

Table 4a. Thermo-mechanical Properties for SA516-70 and SA105 Steels

Service Level	Design Stress Intensity
ASME III Service level A	161.7 MPa
Glaciation loading	260.0 MPa

Table 4b. Design Stress Intensity

Description	Max. Temperature (°C)
Base case (ignoring axial spacing, room spacing 28.6 m, 993 W per container).	115.7
As base case, but reduced heating to allow for axial spacing.	87.5
As base case, but with 875 W per container.	104.5
As base case, but with 1138.61 W per container	145.8
As base case, but increase spacing between containers by 500 mm	114.7
As base case, but increase spacing between containers by 2 metres.	106.7
As base case, but increase spacing between containers by 4 metres.	101.0
As base case, but with room spacing increased by 14.3 metres.	94.3
As base case, but with light backfill conductivity = 1.7 W/m K.	110.9
As base case, but with light backfill conductivity = 3.0 W/m K.	109.2
1138.61 W per container, 45 metres between room centres	122.7

Table 5. Summary of Sensitivity Study Results.

Material	Maximum principal stress (Tensile)	Maximum principal stress (Compressive)	Maximum shear stress
Jacket			
After UFC placement	**0.19 MPa**	**0.28 MPa**	**0.14 MPa**
Allowable	**250 kPa**	**0.9 MPa**	**520 kPa**
Buffer			
Prior to UFC placement	**0.023 MPa**	**0.127 MPa**	**0.064 MPa**
After UFC placement	**0.032 MPa**	**0.225 MPa**	**0.118 MPa**
Allowable	**125 kPa**	**0.4 MPa**	**260 kPa**
Dense Backfill			
Prior to UFC placement	**0.017 MPa**	**0.164 MPa**	**0.084 MPa**
After UFC placement	**0.009 MPa**	**0.0243 MPa**	**0.0123 MPa**
Allowable	**125 kPa**	**0.4 MPa**	**260 kPa**

Table 6. Summary of Emplacement Analysis Results.

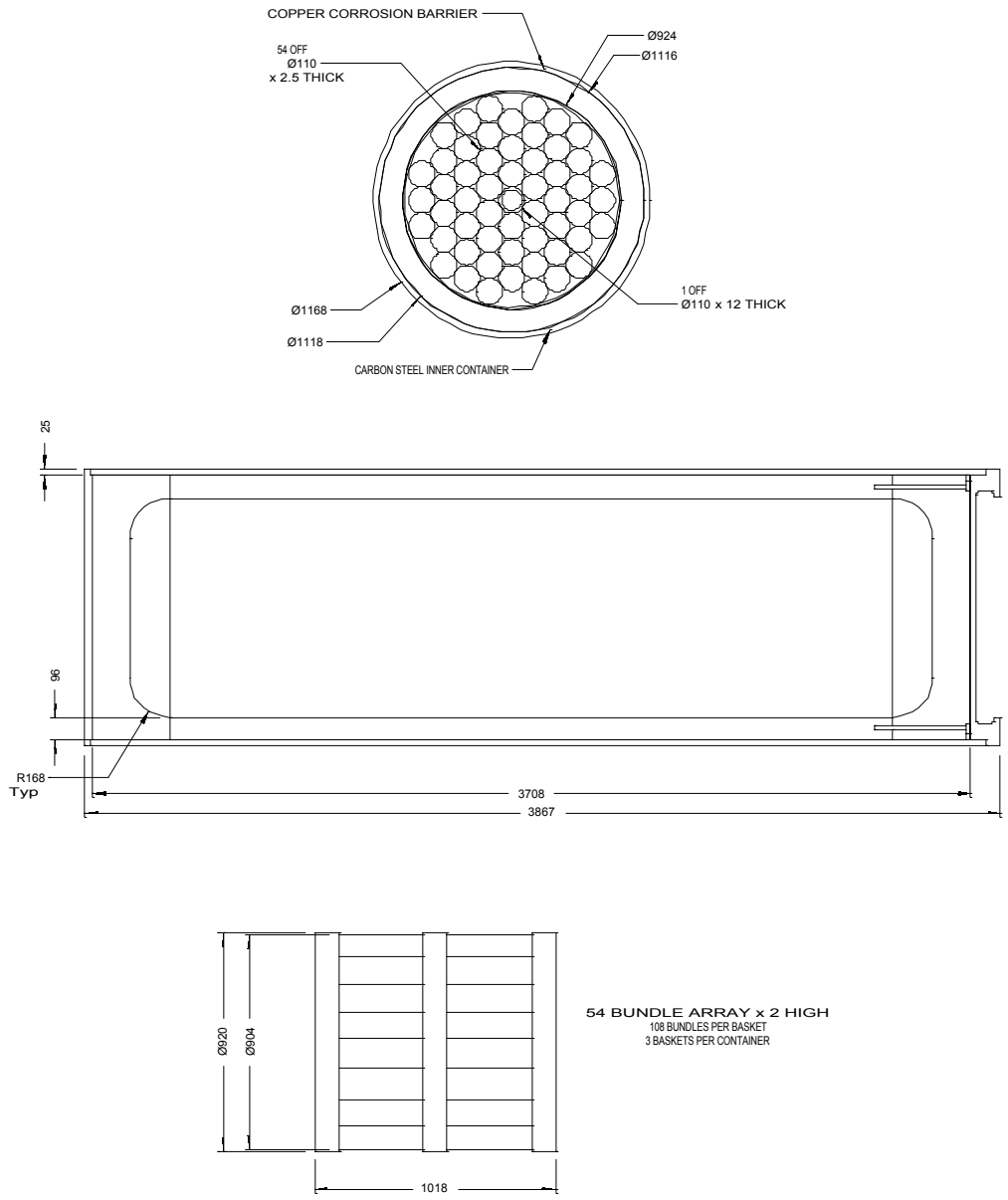

Figure 1 Used Fuel Container Design

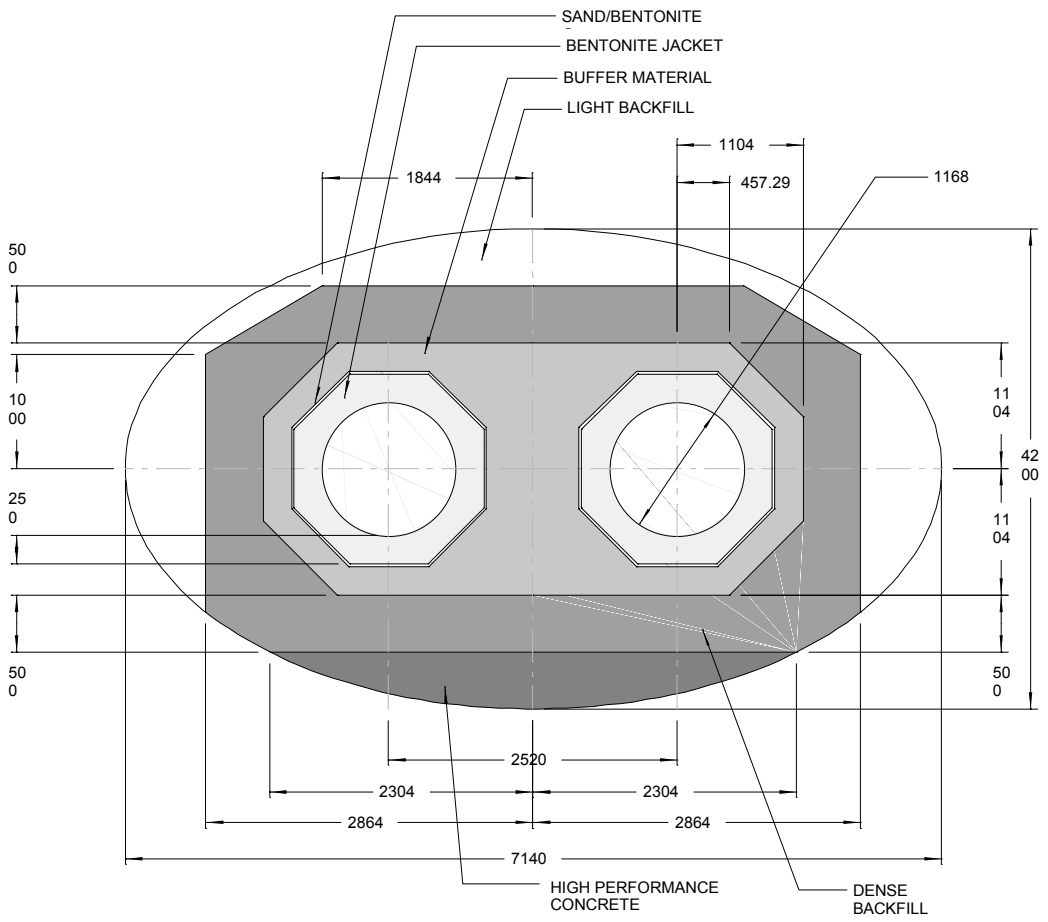

Figure 2. Sectional View of Emplacement Room (Revised Design).

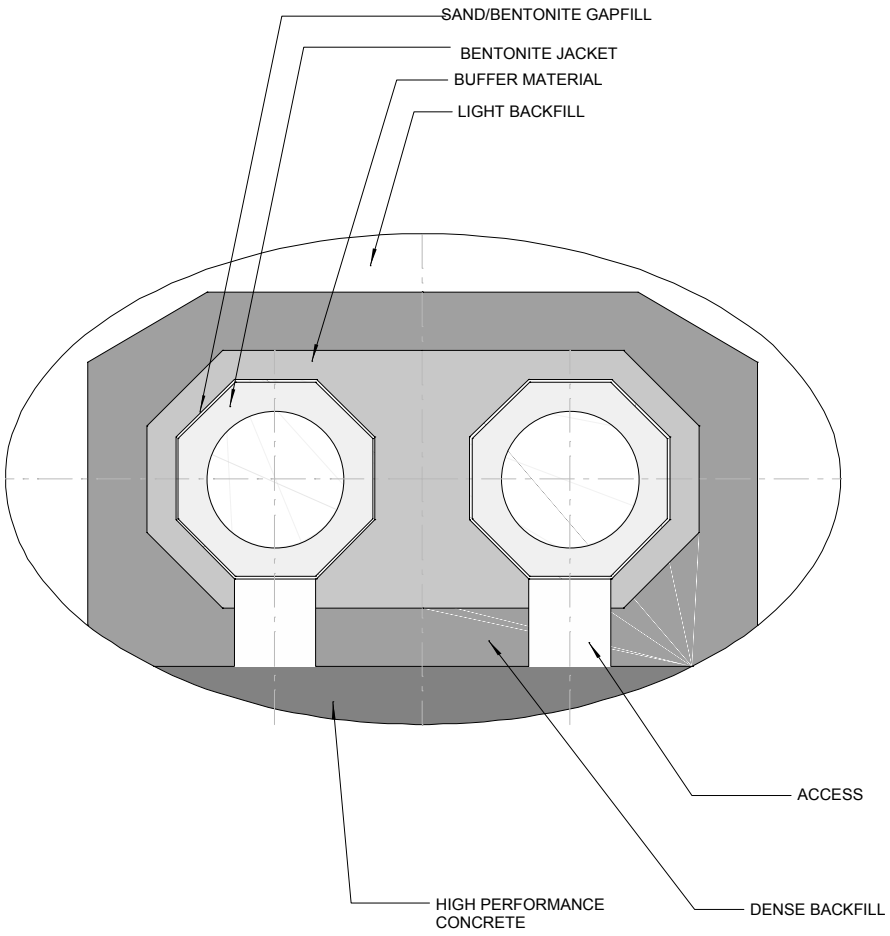

Figure 4. Sectional View of Emplacement Room (prior to UFC emplacement).

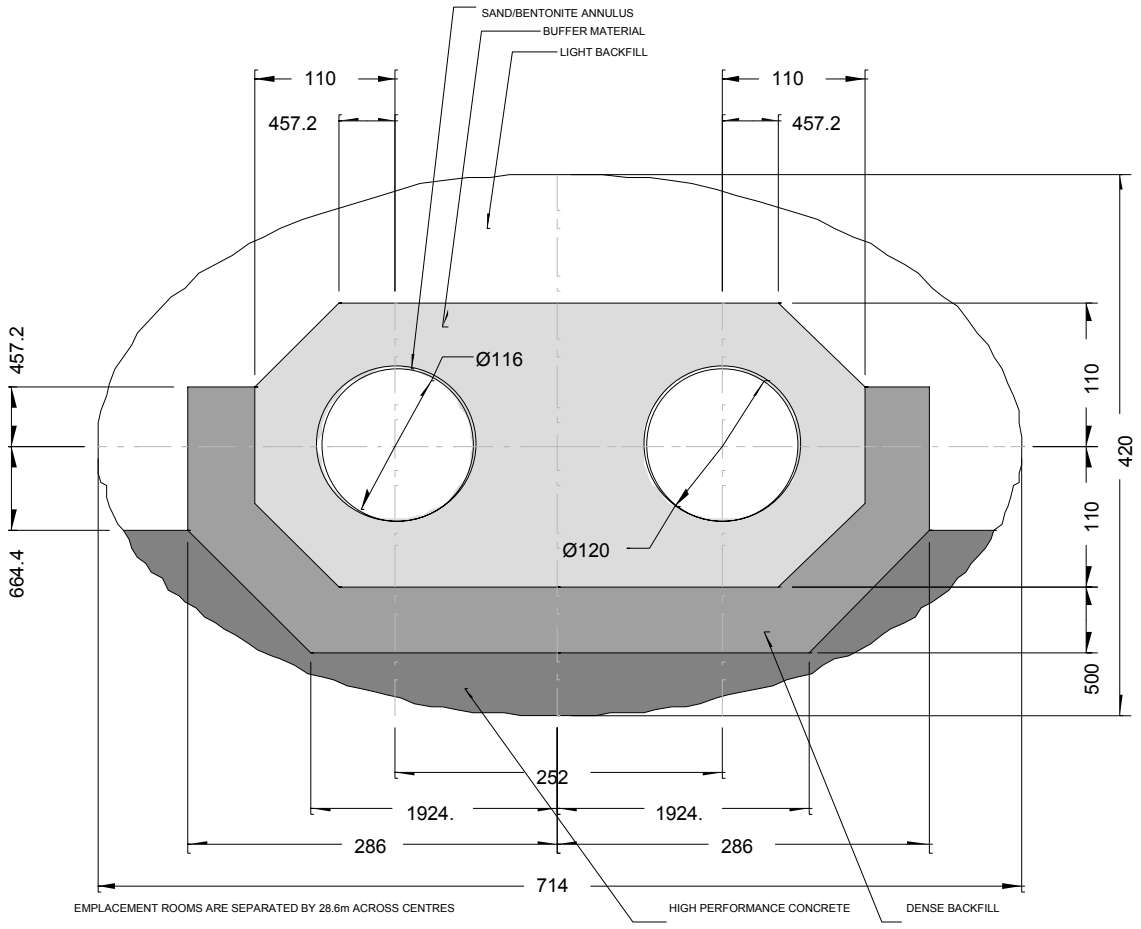

Figure 5. Sectional View of Emplacement Room (Initial design).

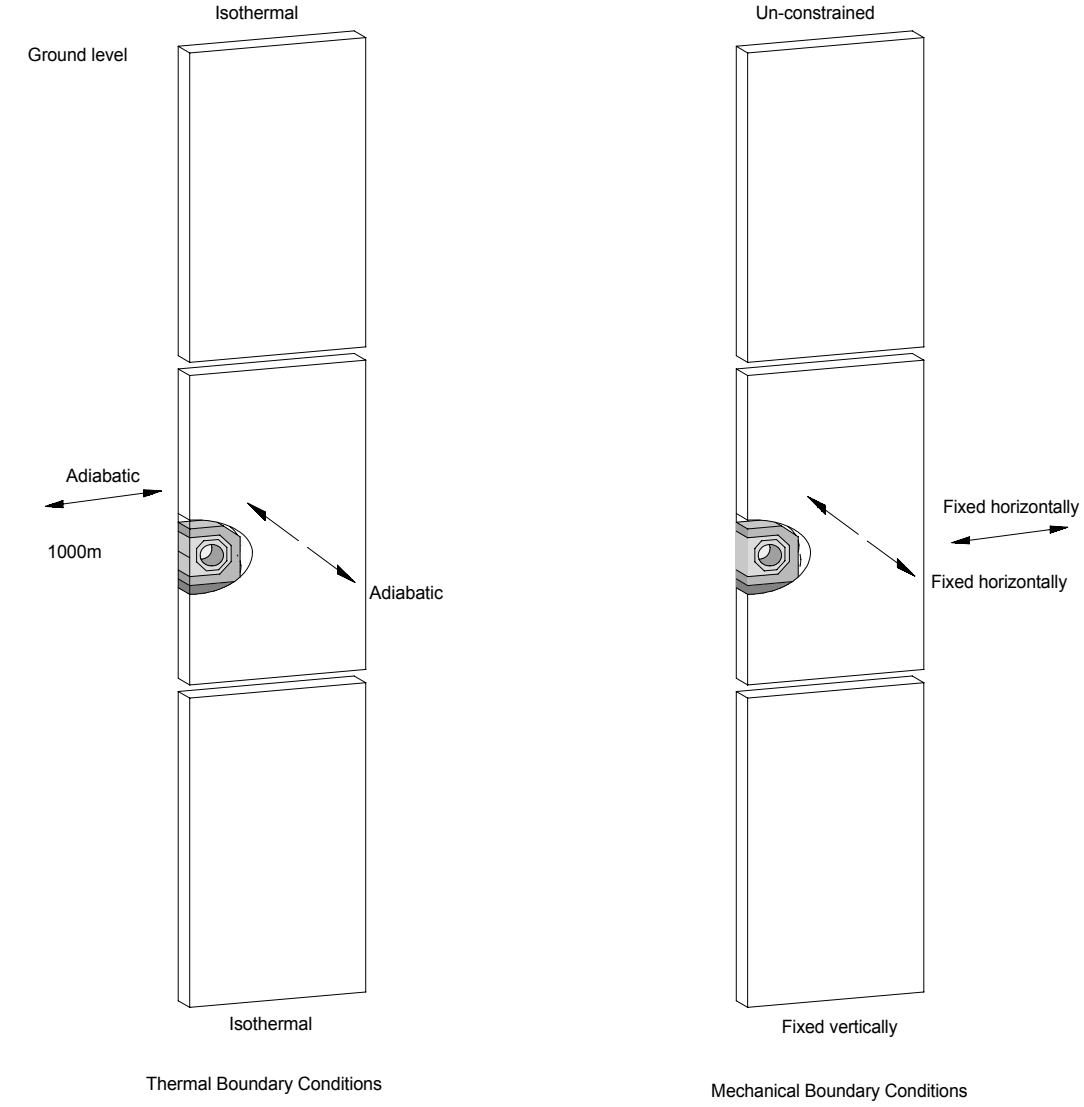

Figure 6. Thermal and Mechanical Boundary Conditions.

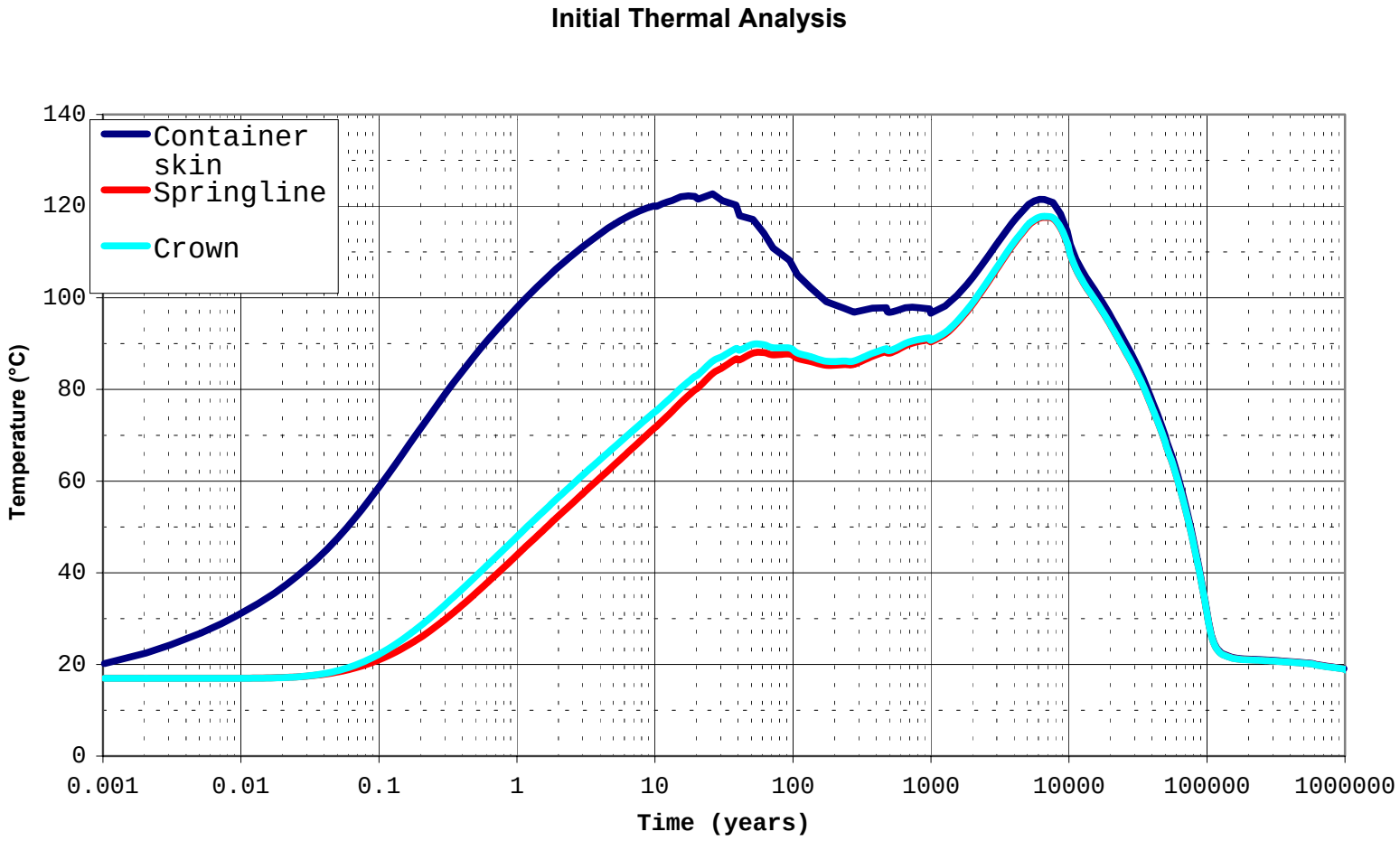

Figure 7 Temperature History.

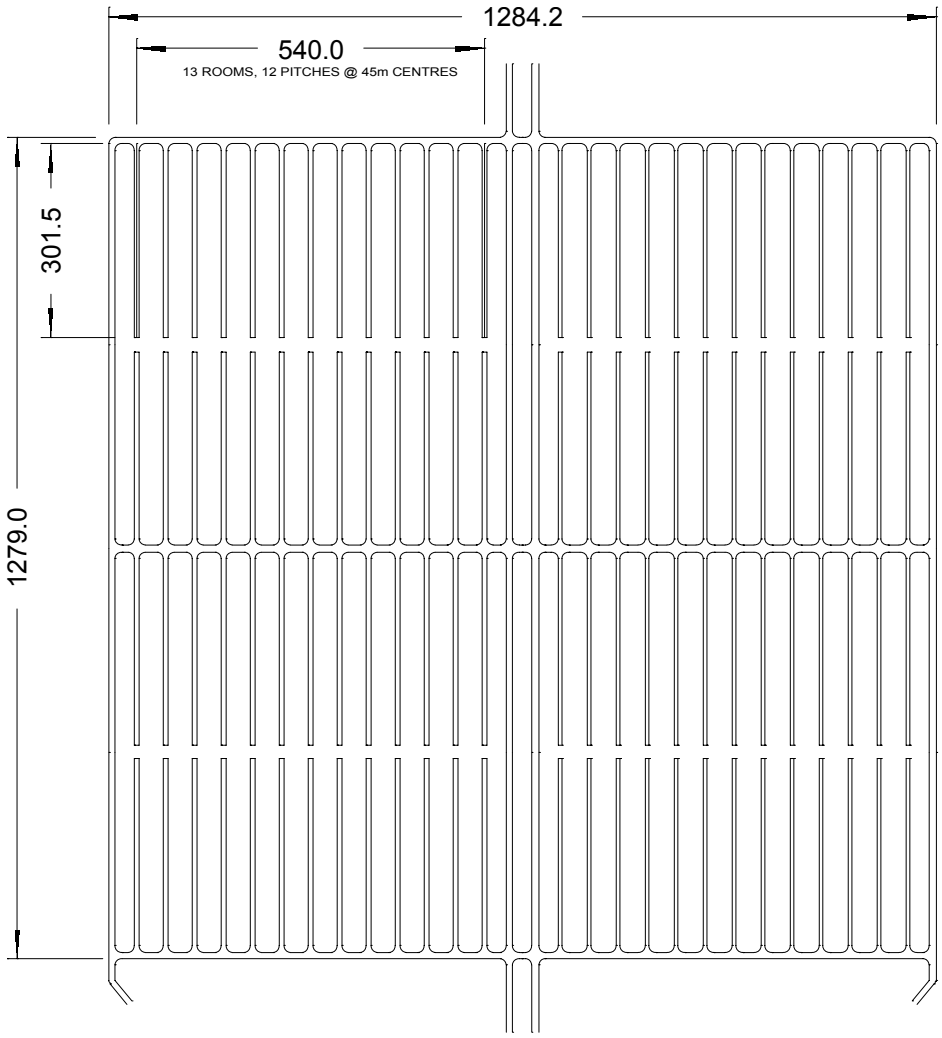

Figure 3. Proposed Plan of DGR.

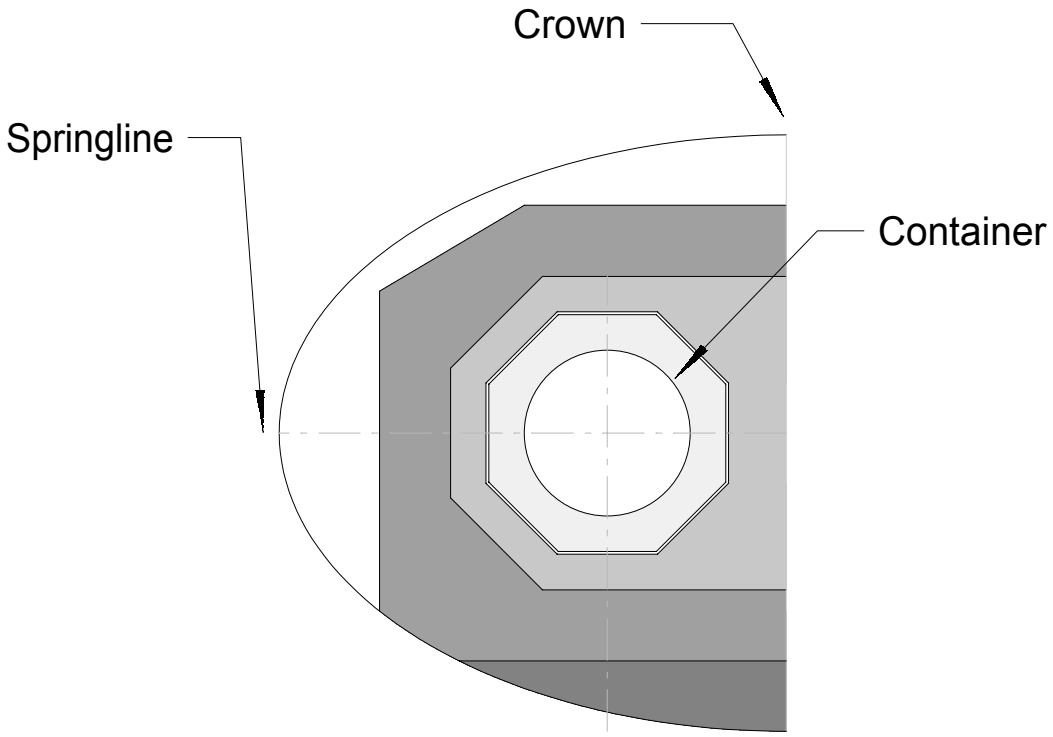

Figure 8. Monitoring Points for Temperature History Plots.

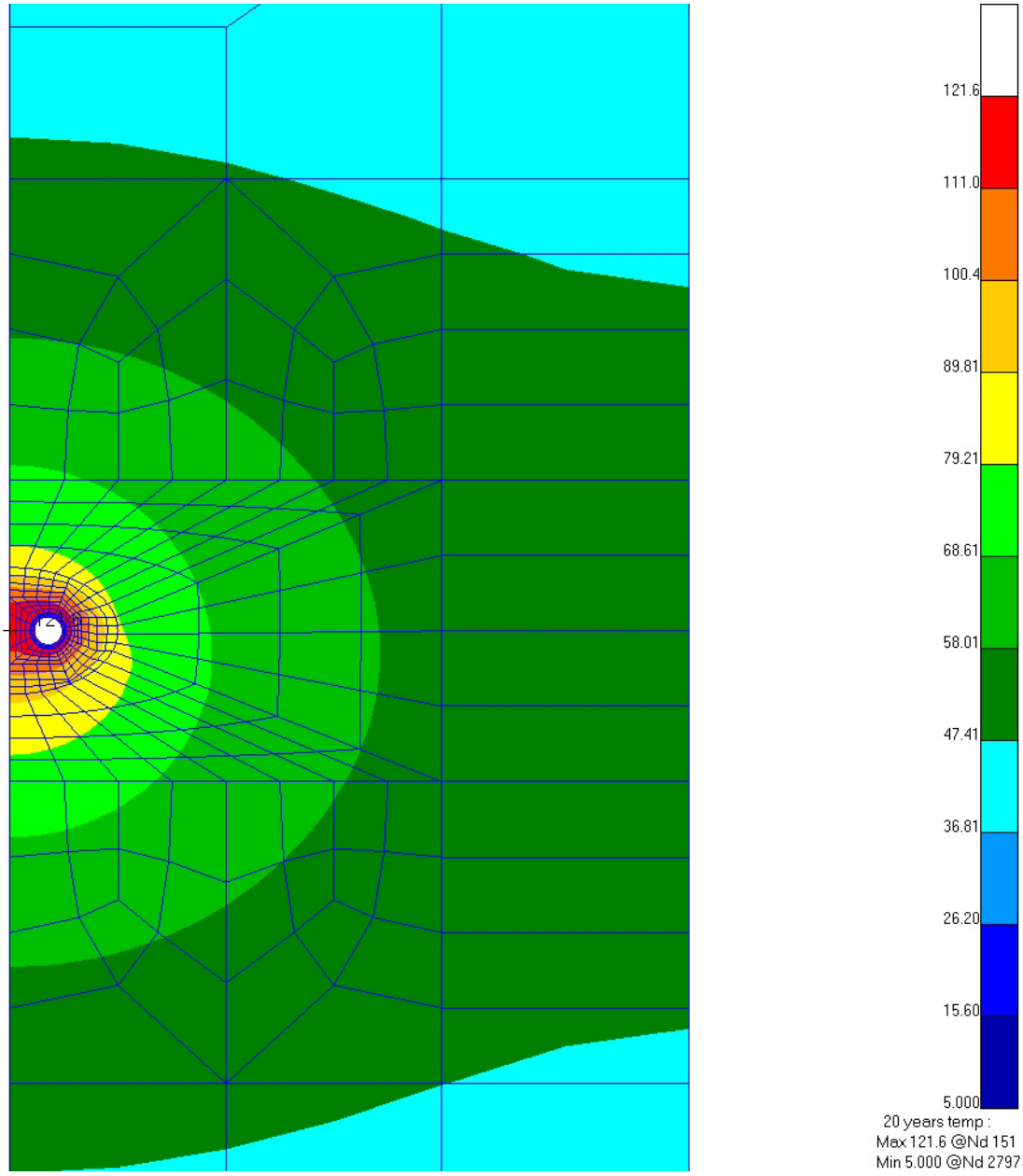

Figure 9. Temperature Profile 20 Years After Emplacement.

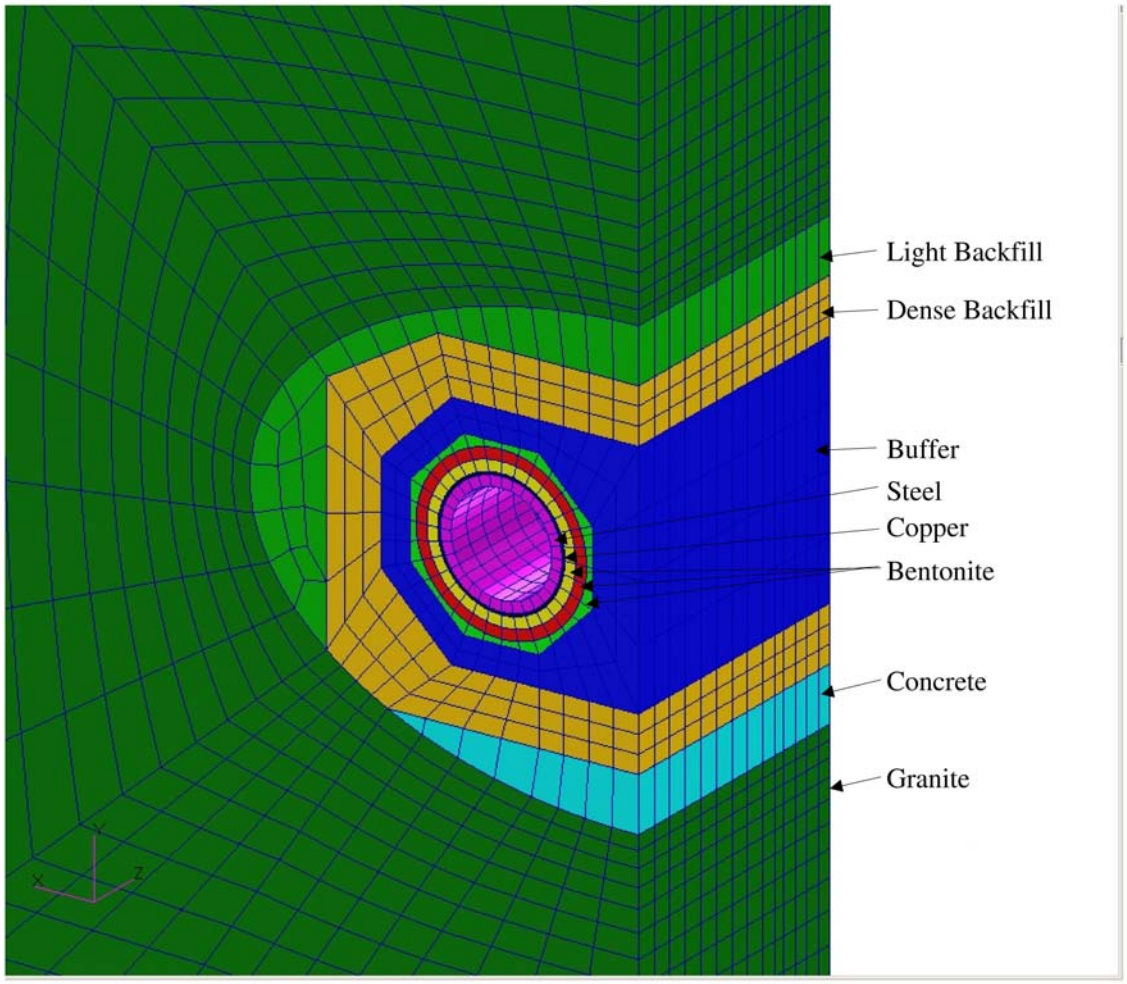

Figure 10. Finite Element Model of Emplacement Room (Revised design).

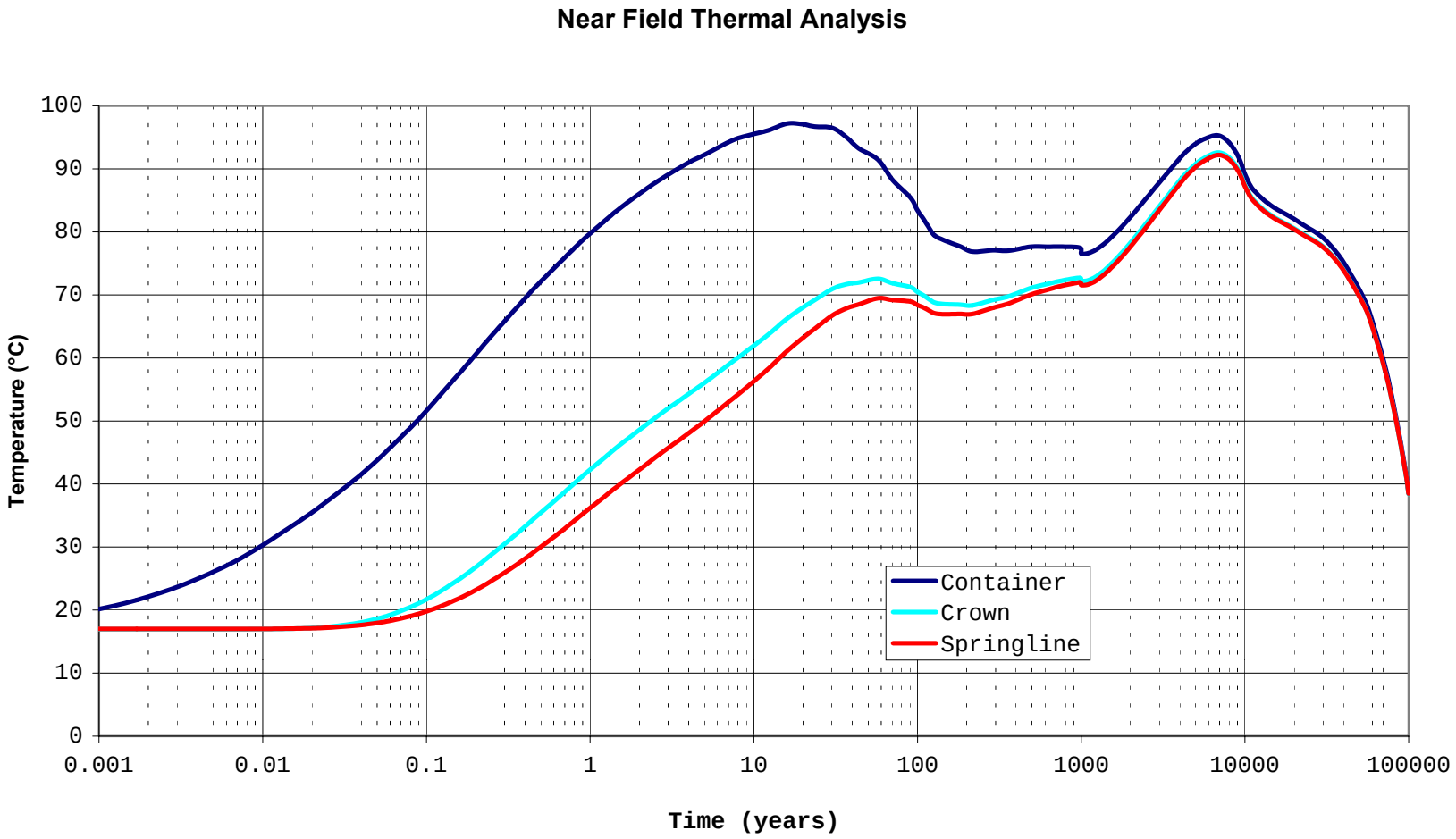

Figure 11a Temperature History.

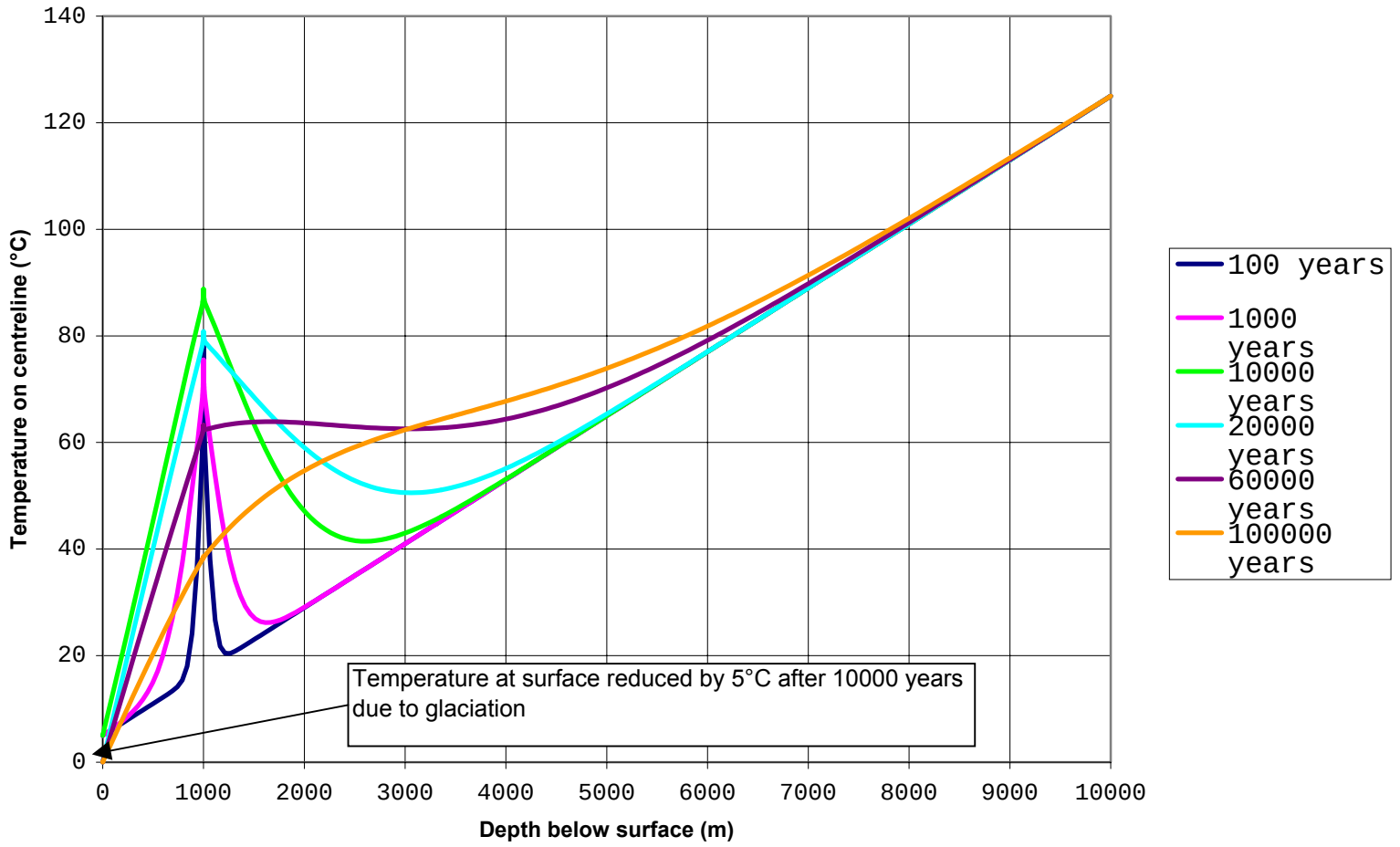

Figure 11b Temperature History.

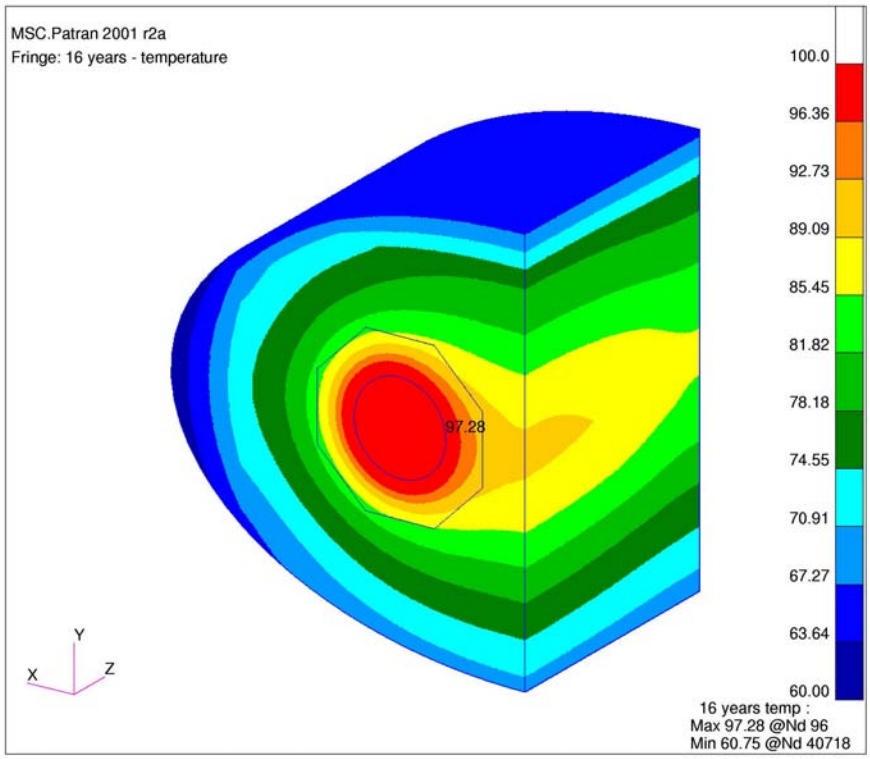

Figure 12a Temperature Profile – 16 Years (Peak container temperature).

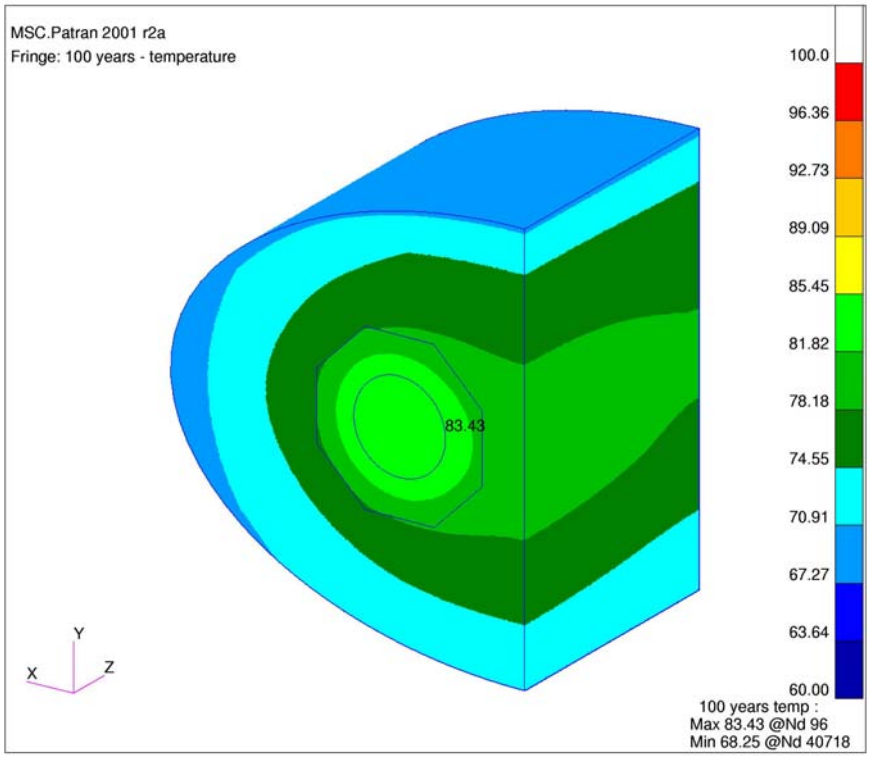

Figure 12b Temperature Profile – 100 Years

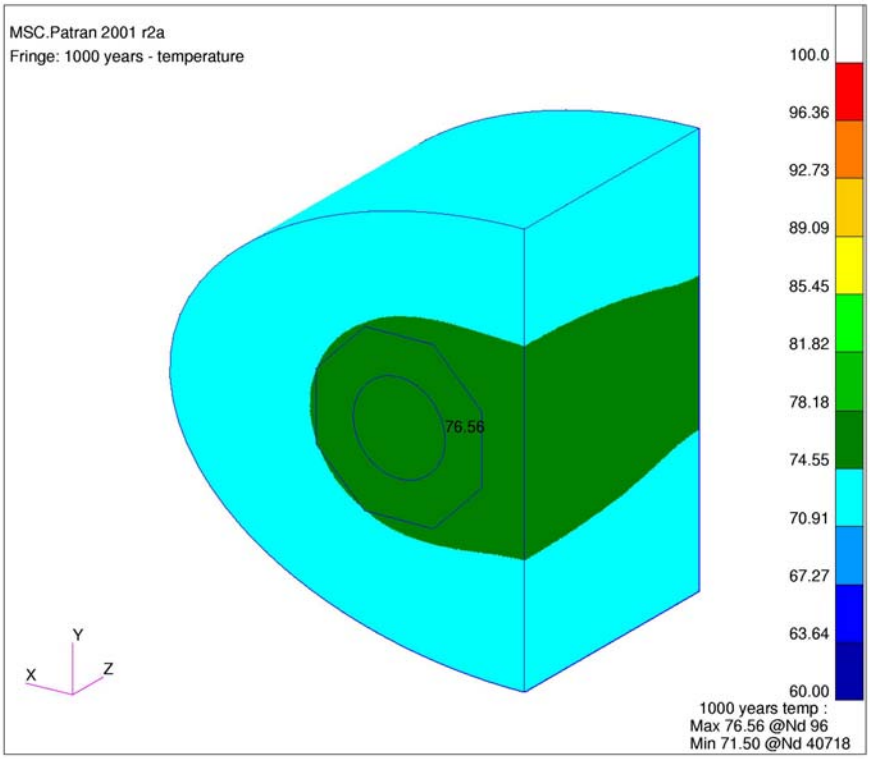

Figure 12c Temperature Profile – 1000 Years

Figure 12d Temperature Profile – 10,000 Years

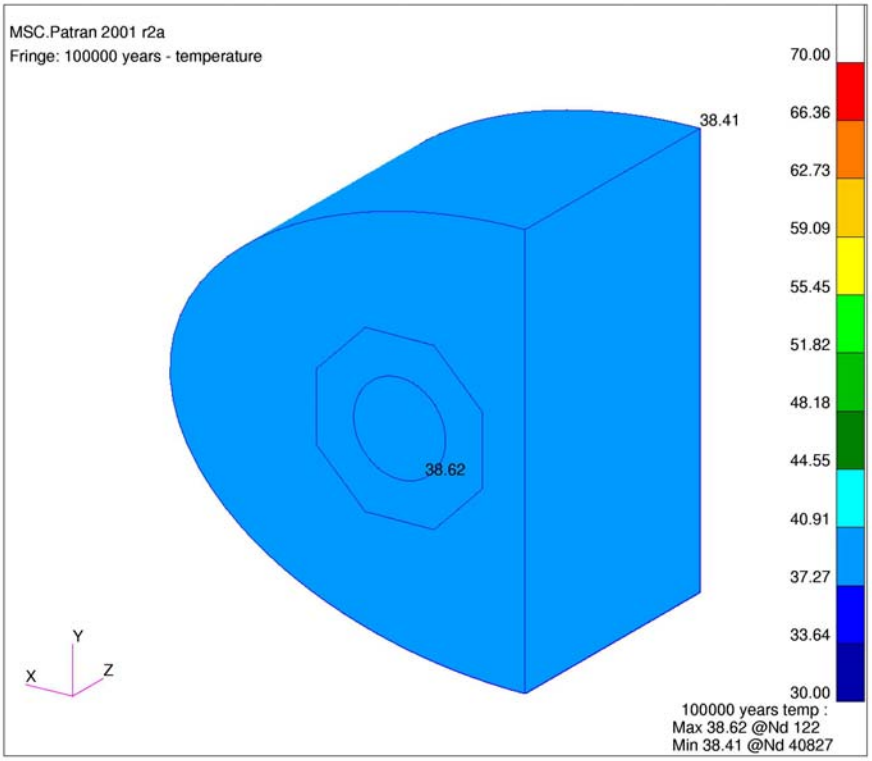

Figure 12e Temperature Profile – 100,000 Years

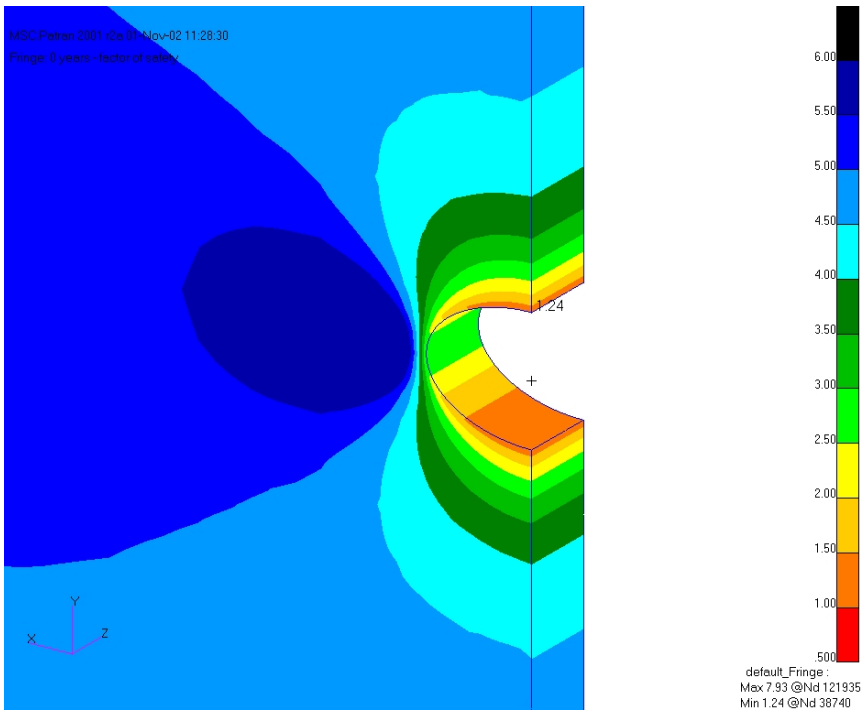

Figure 13a Emplacement Room Stability – worst case orientation/ post excavation

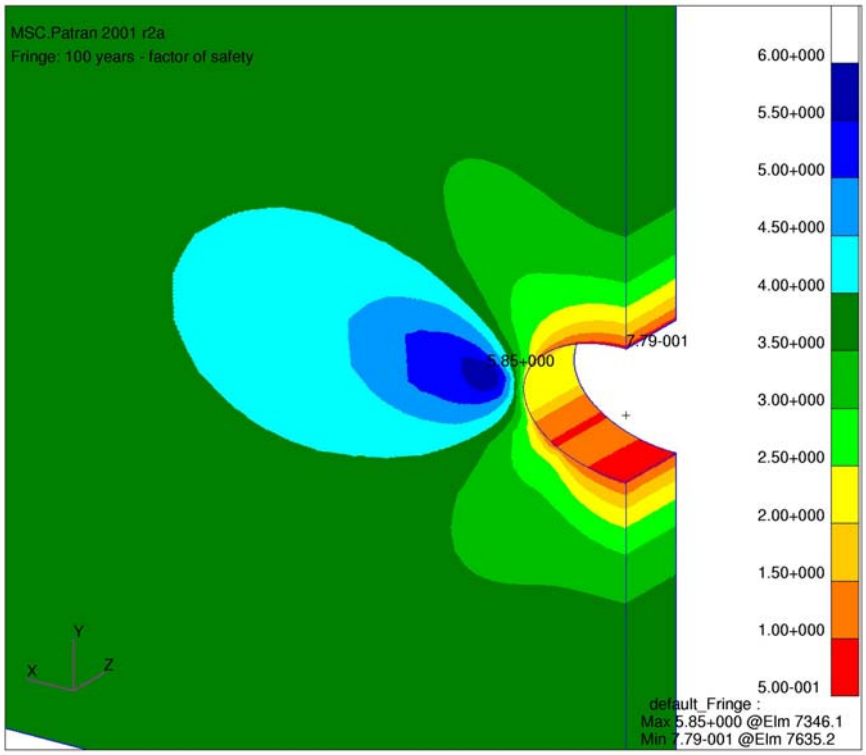

Figure 13b Emplacement Room Stability – worst case orientation/ 100 years

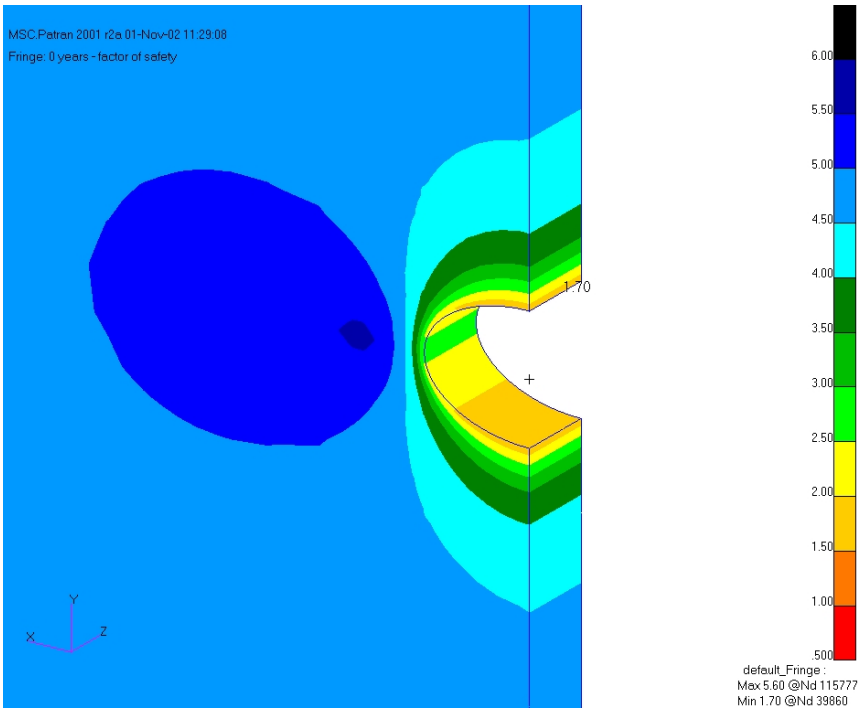

Figure 13c Emplacement Room Stability – preferred orientation/ post excavation

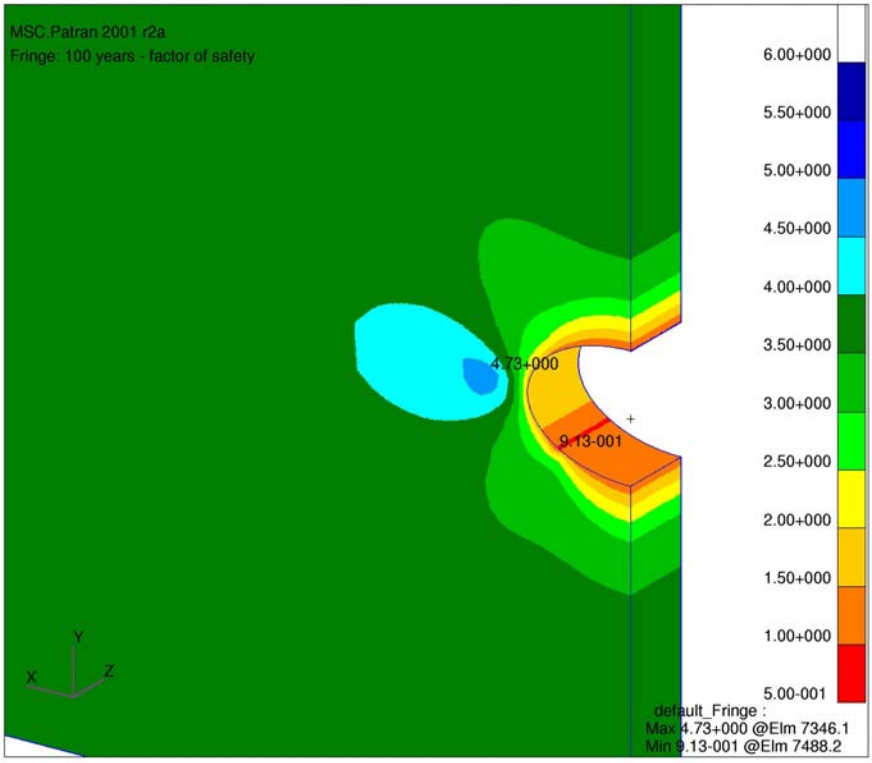

Figure 13d Emplacement Room Stability – preferred orientation/ 100 years

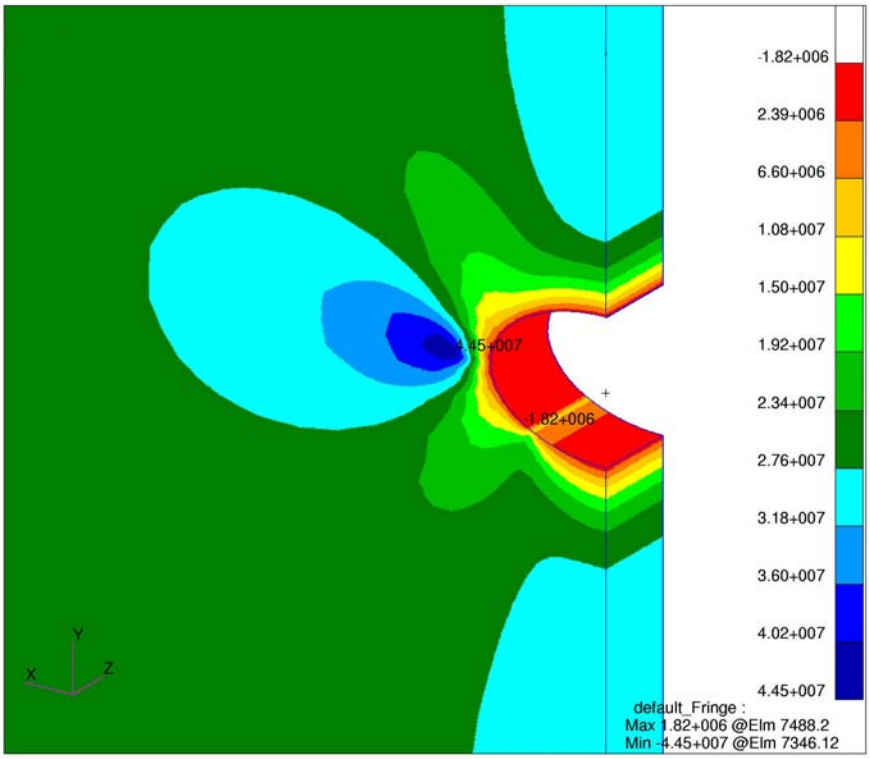

Figure 14a Maximum Tensile Principal Stress – 100 Years

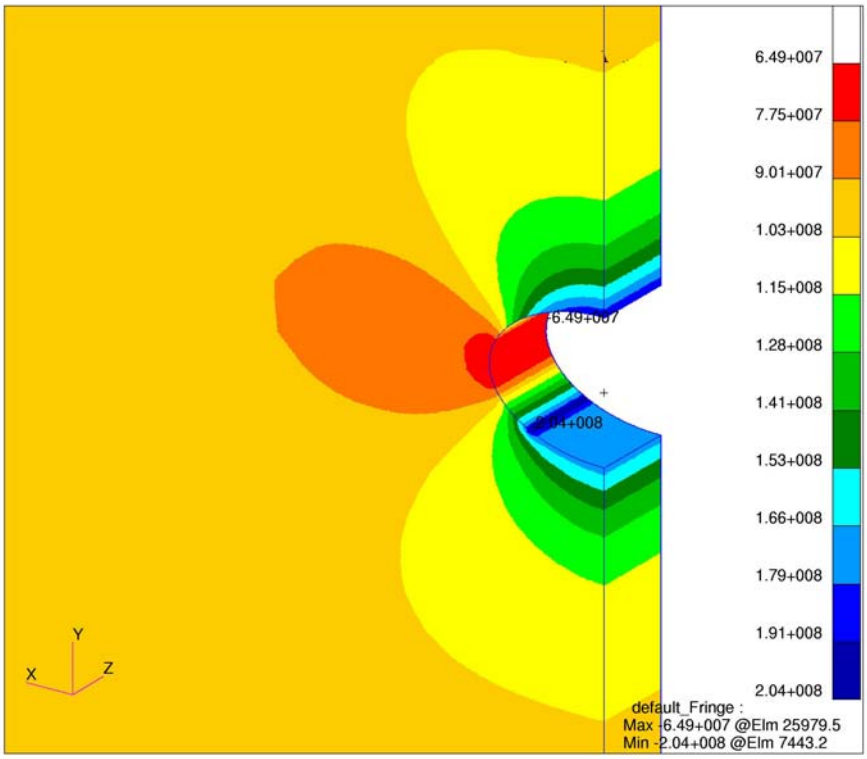

Figure 14b Maximum Compressive Principal Stress – 100 Years

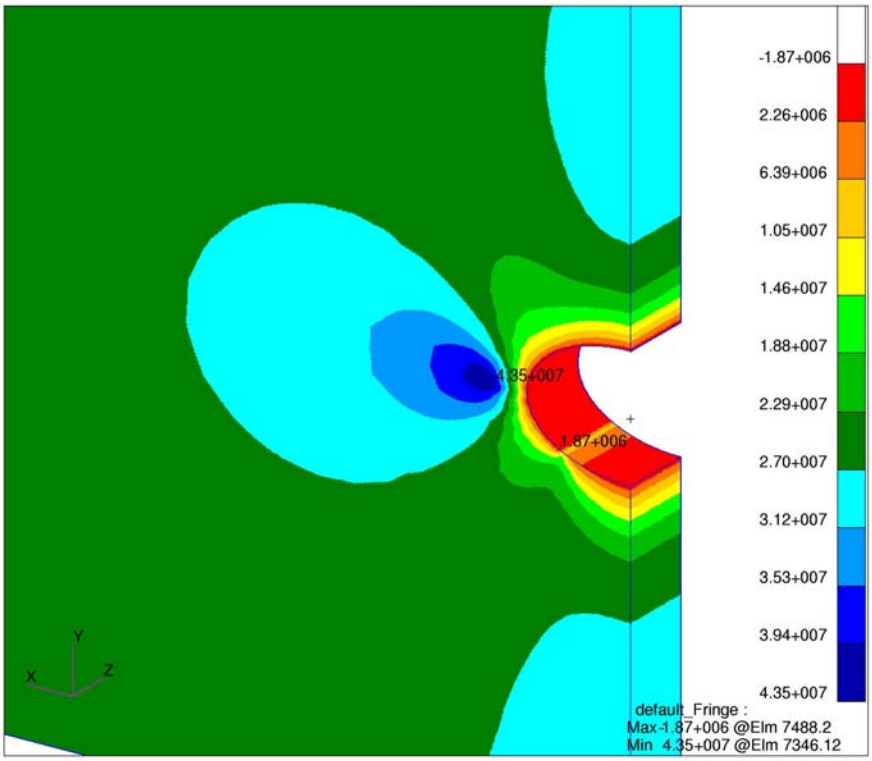

Figure 15a Maximum Principal Stress – 100 Years

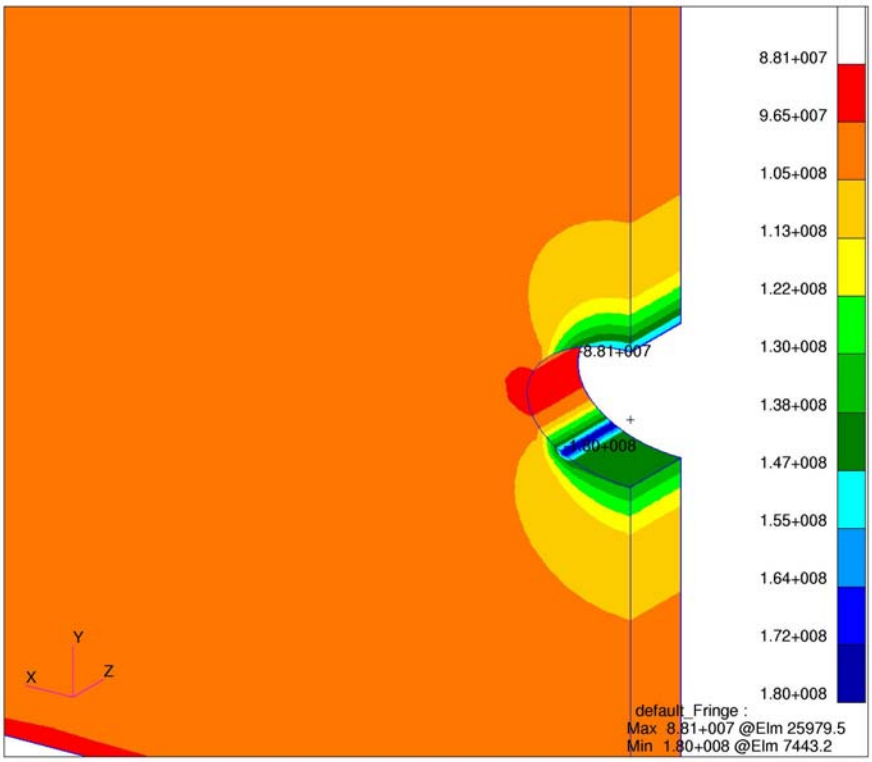

Figure 15b Minimum Principal Stress – 100 Years

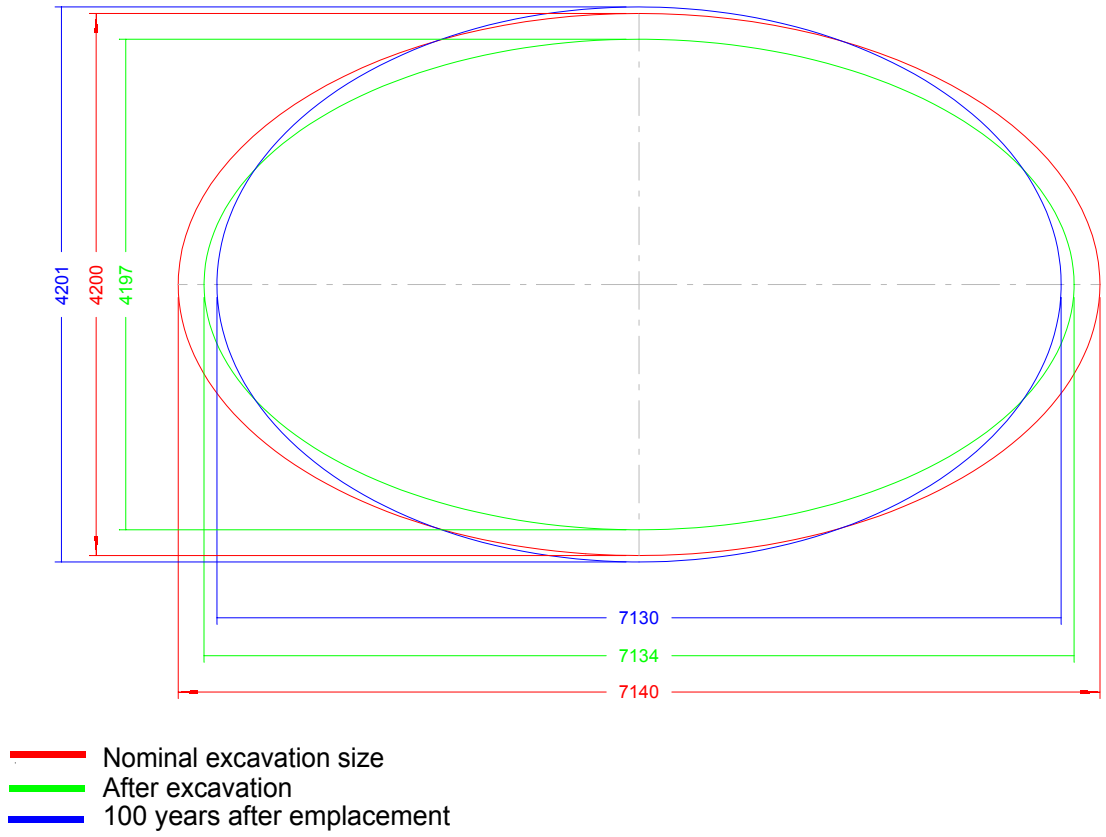

Figure 16 Emplacement Room Displacement

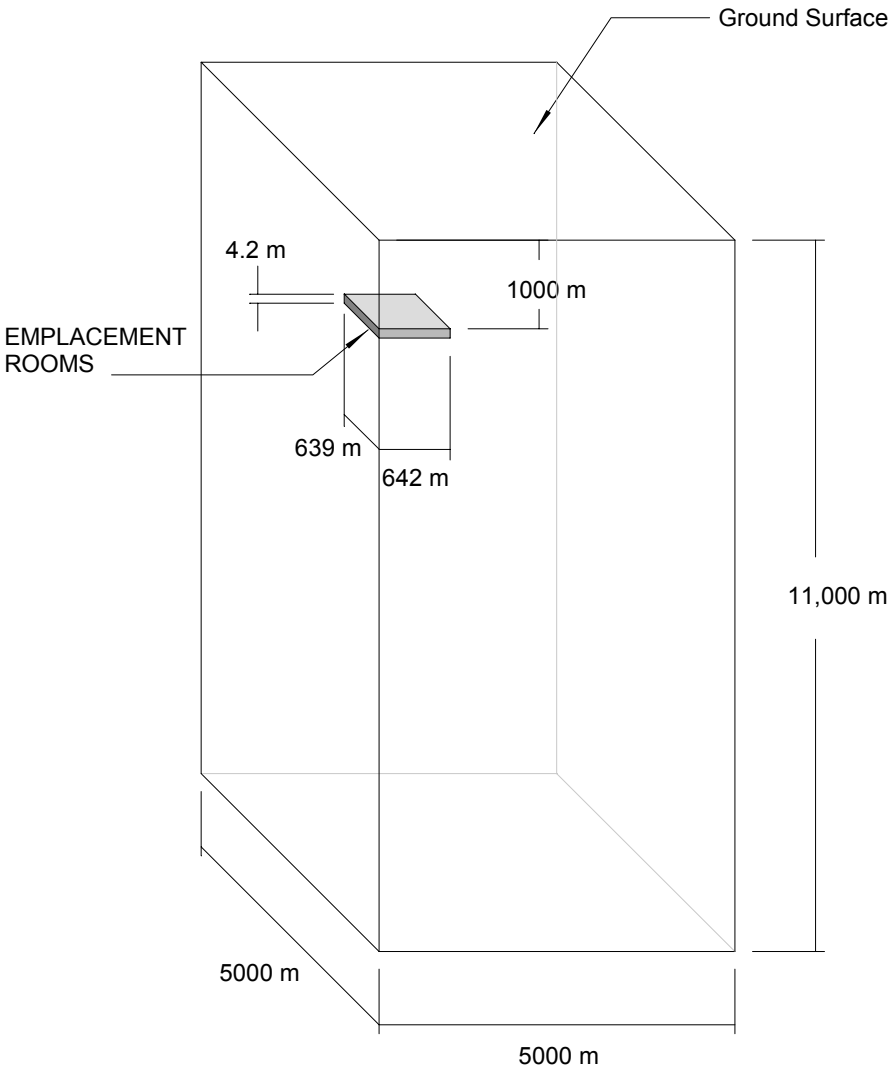

Figure 17. Perspective View of Far-Field Model

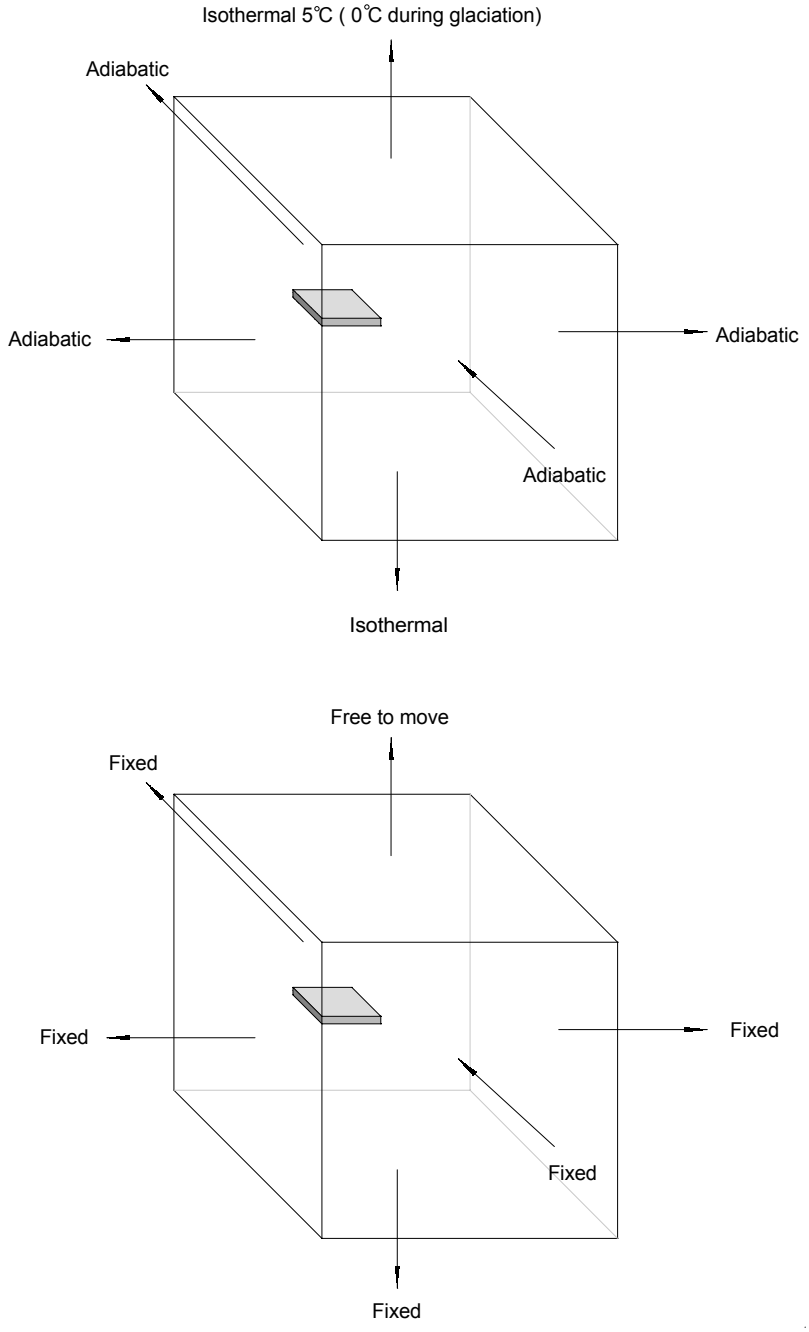

Figure 18. Thermal and Mechanical Boundary Conditions.

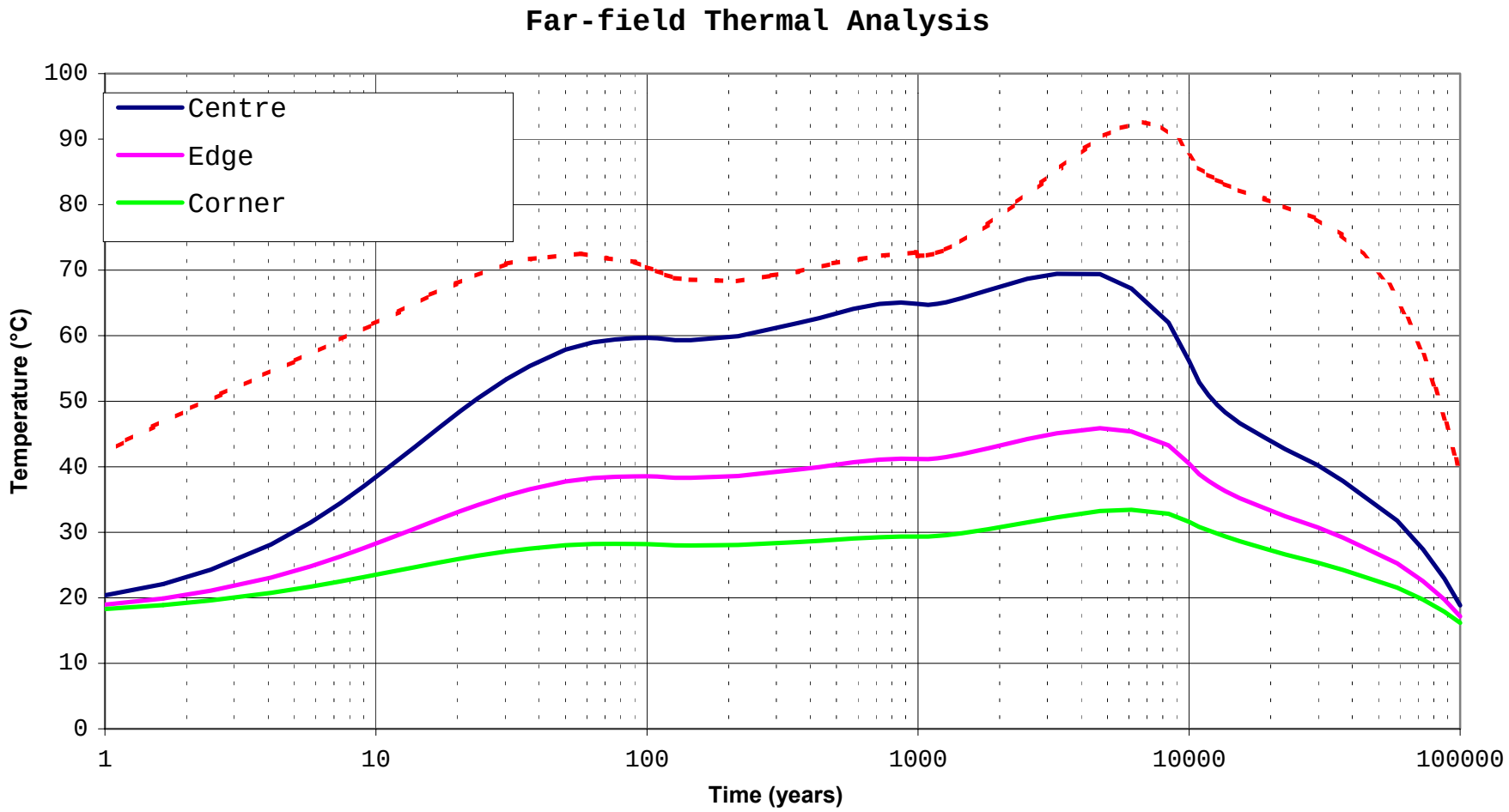

Figure 19 Temperature History.

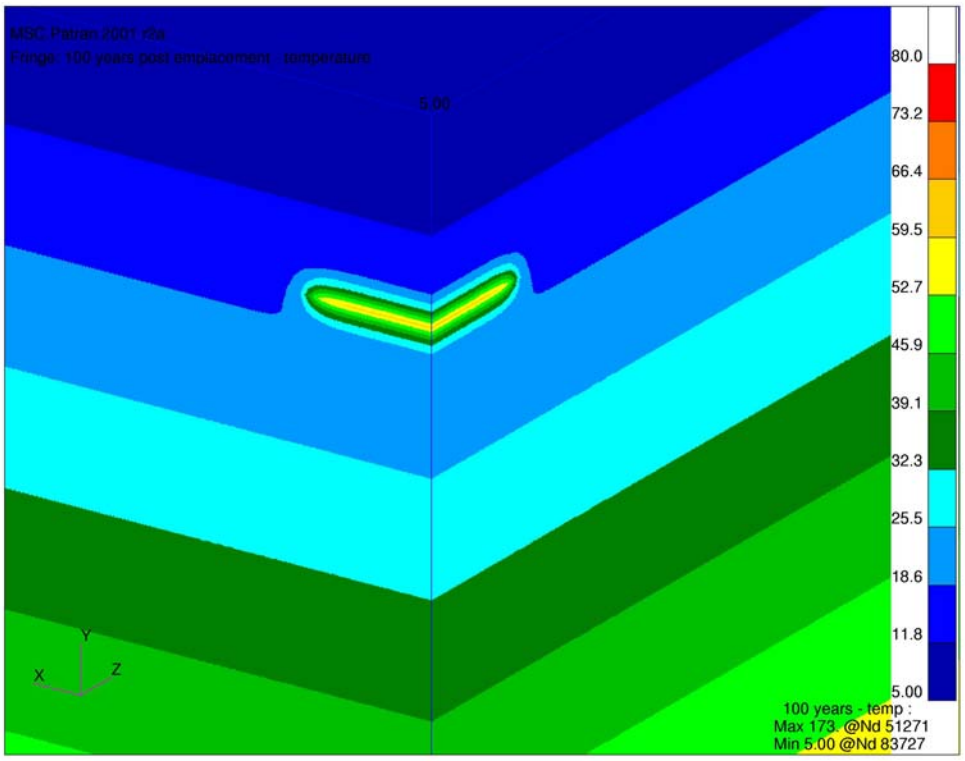

Figure 20a Temperature Profile – 100 Years.

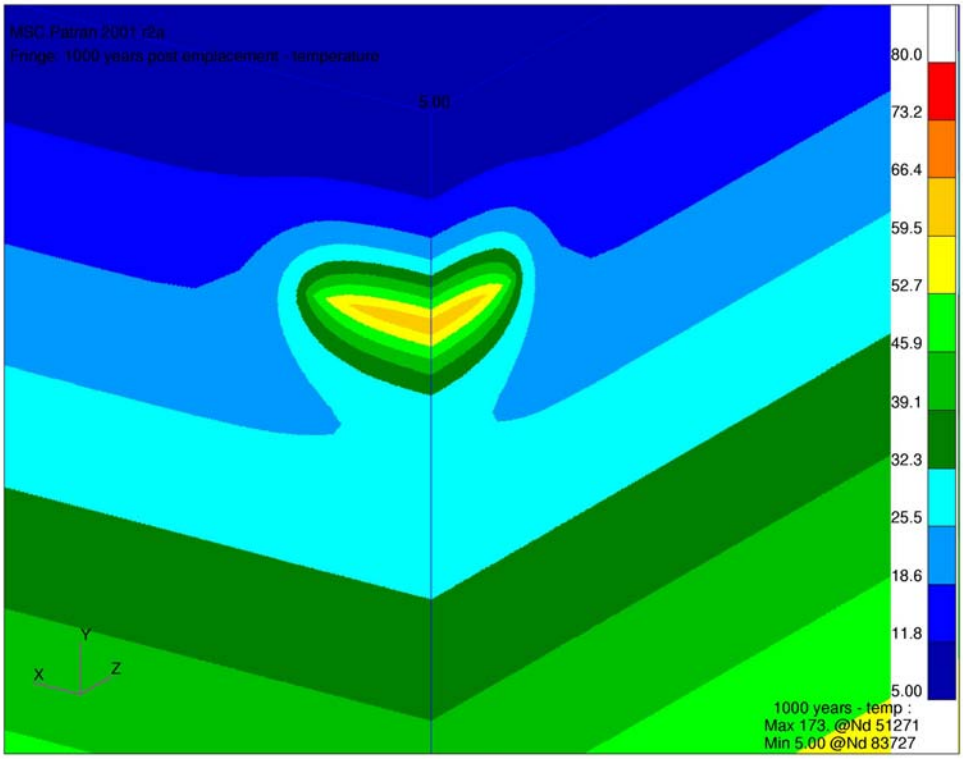

Figure 20b Temperature Profile – 1,000 Years.

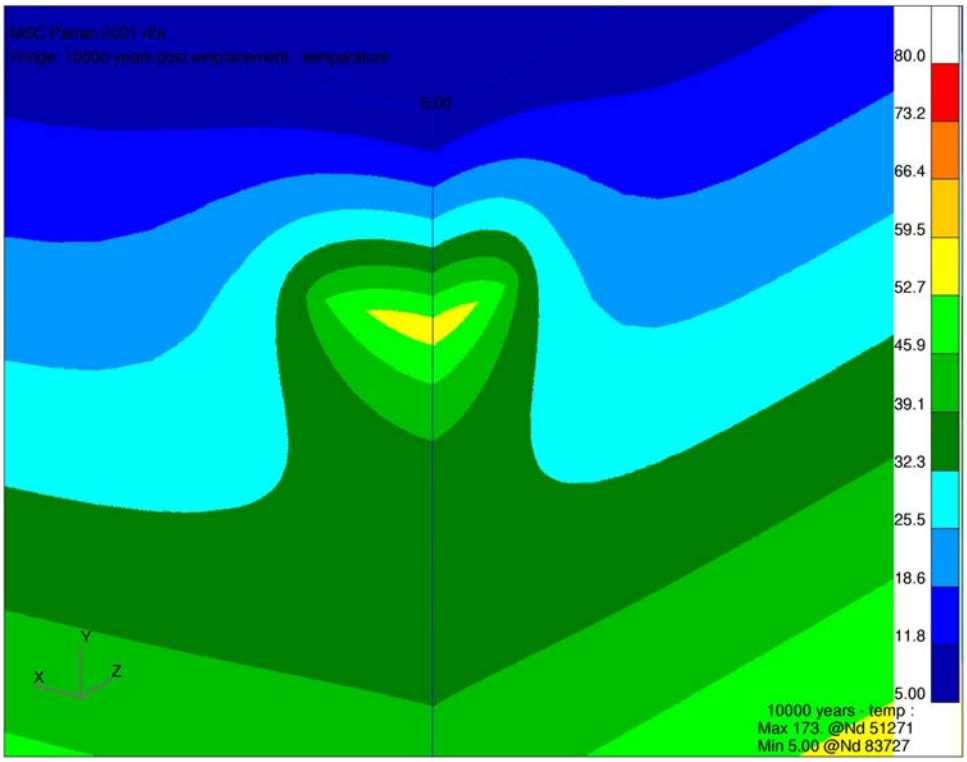

Figure 20c Temperature Profile – 10,000 Years.

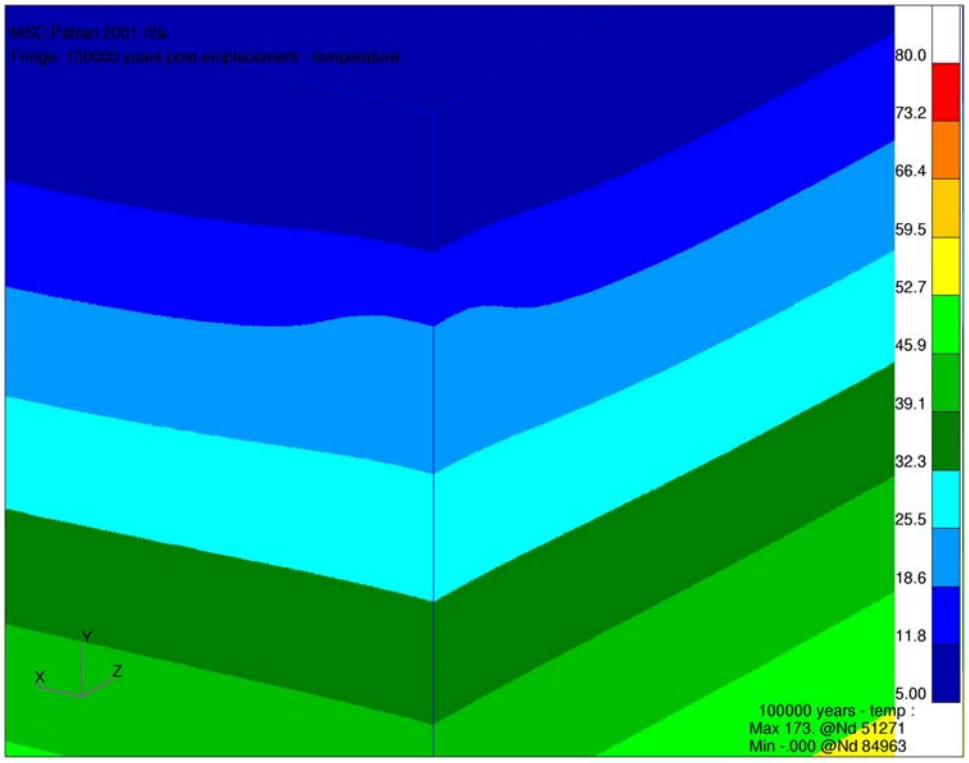

Figure 20d Temperature Profile – 100,000 Years.

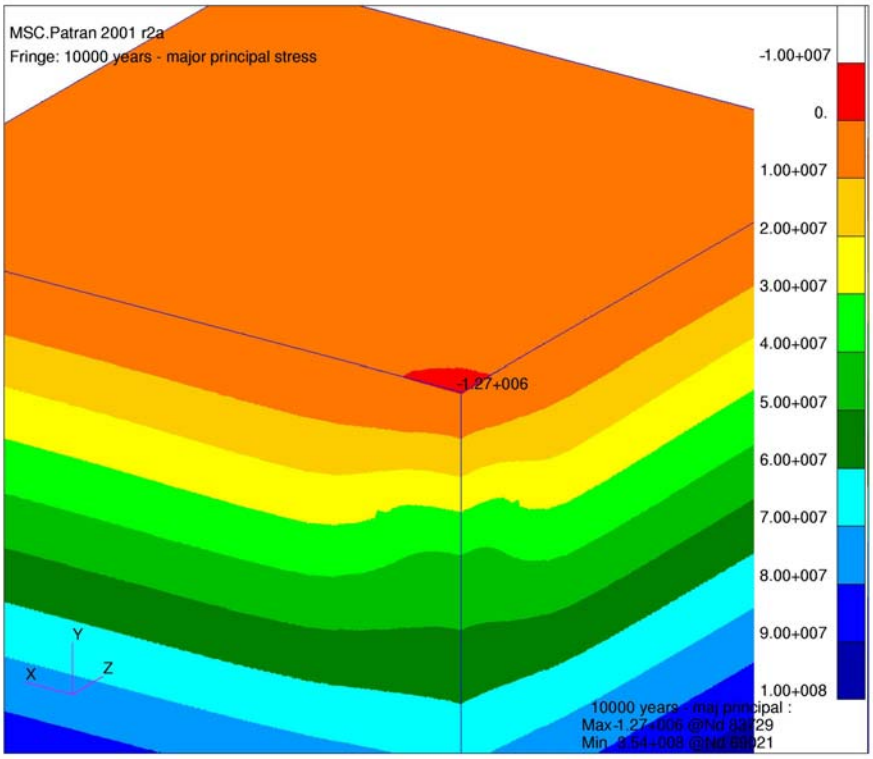

Figure 21 Maximum Tensile Principal Stress – 10,000 Years.

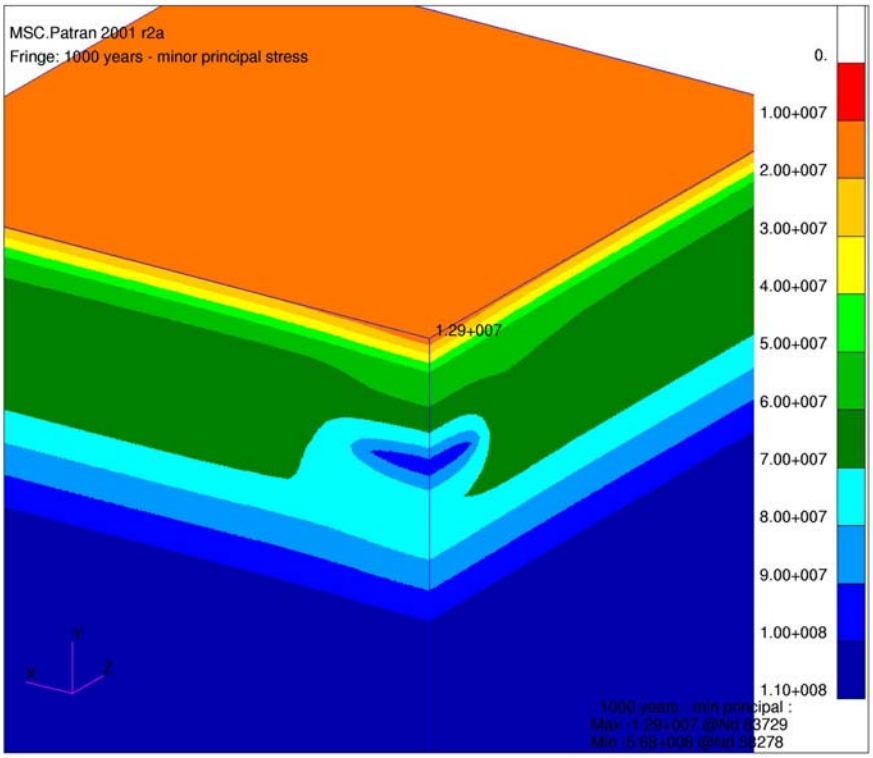

Figure 22 Maximum Compressive Principal Stress – 1,000 Years.

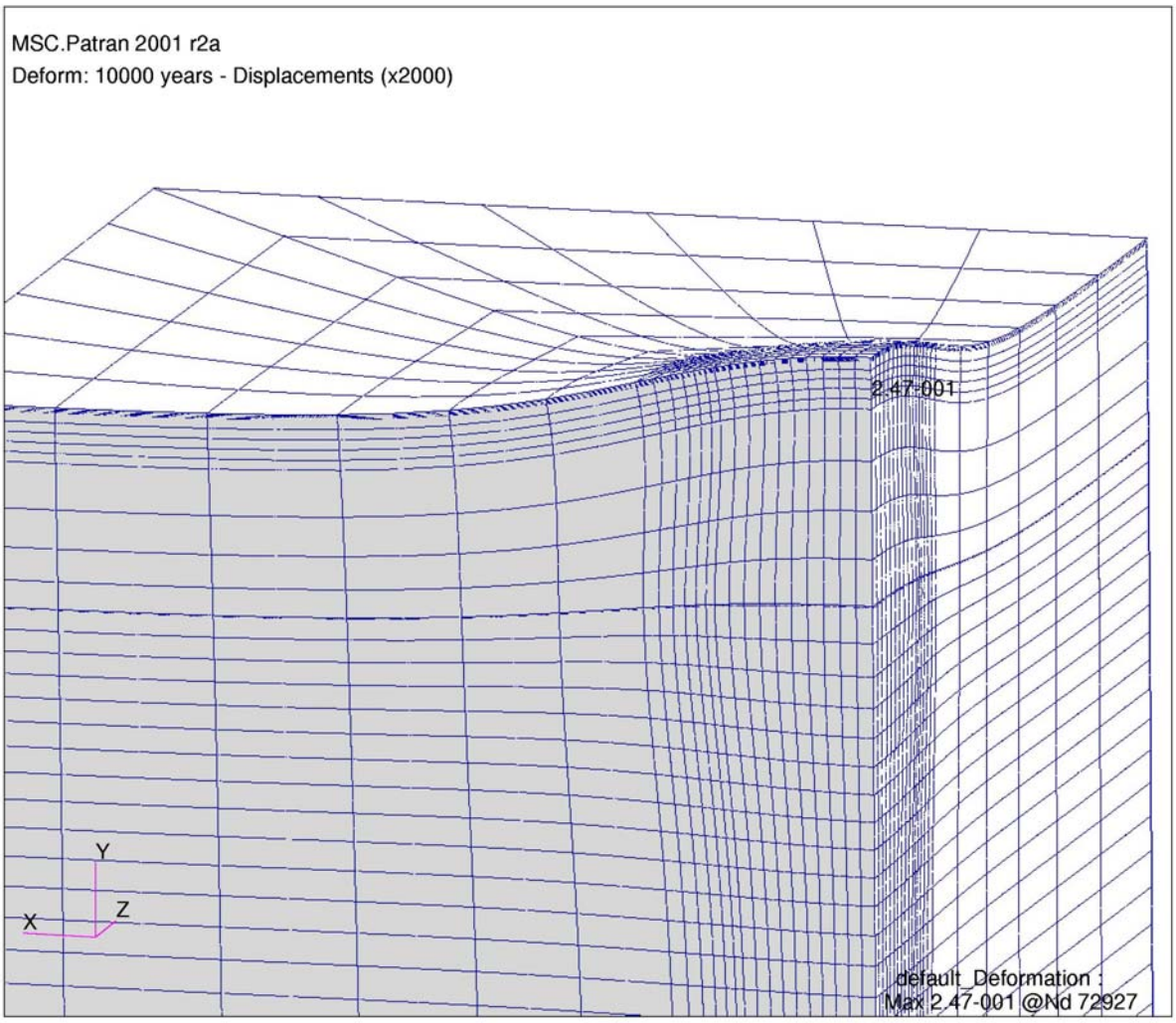

Figure 23 Ground Deformation (x2000) – 10,000 Years.

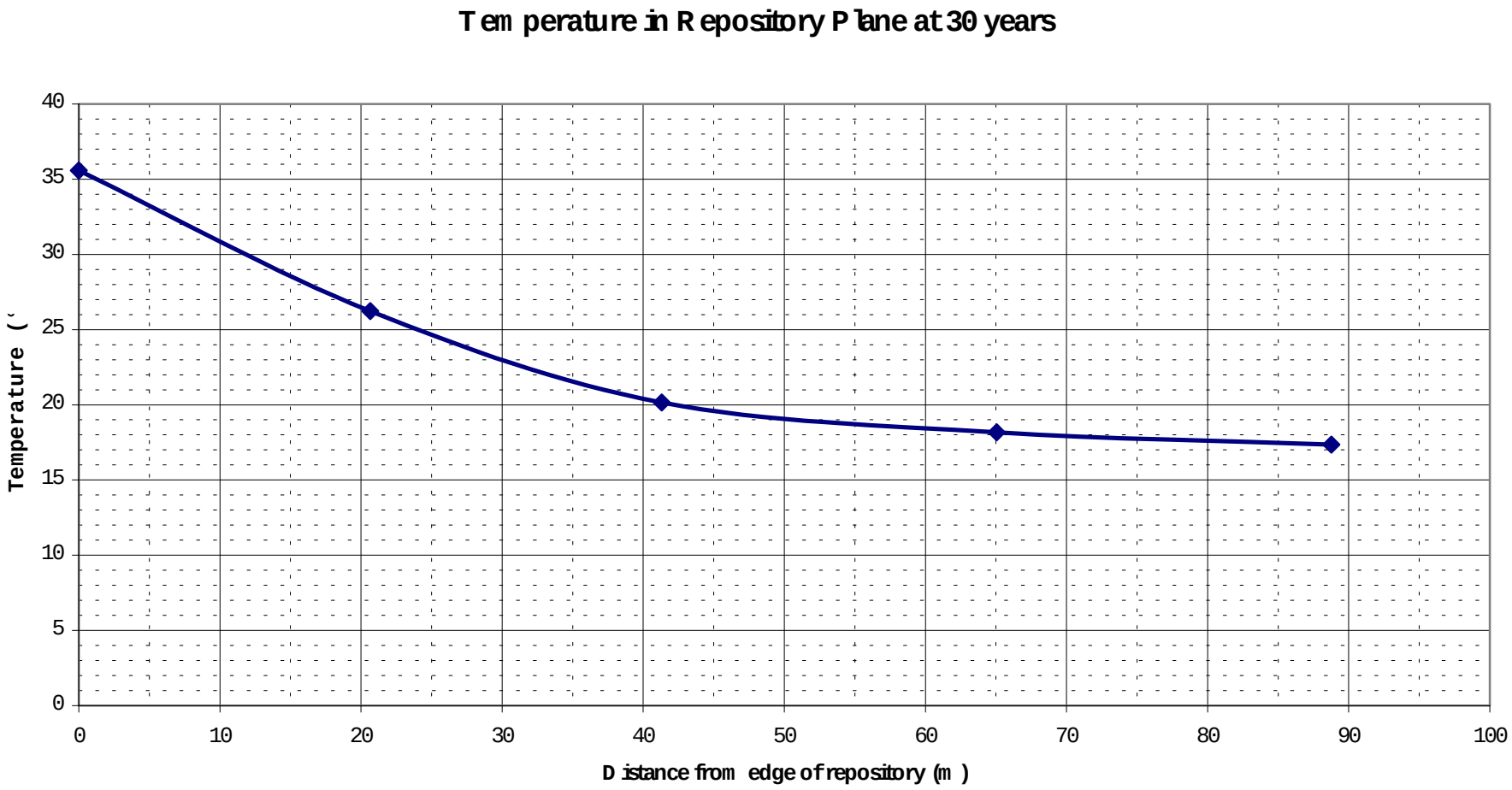

Figure 24 Temperature Profile at Edge of Repository.

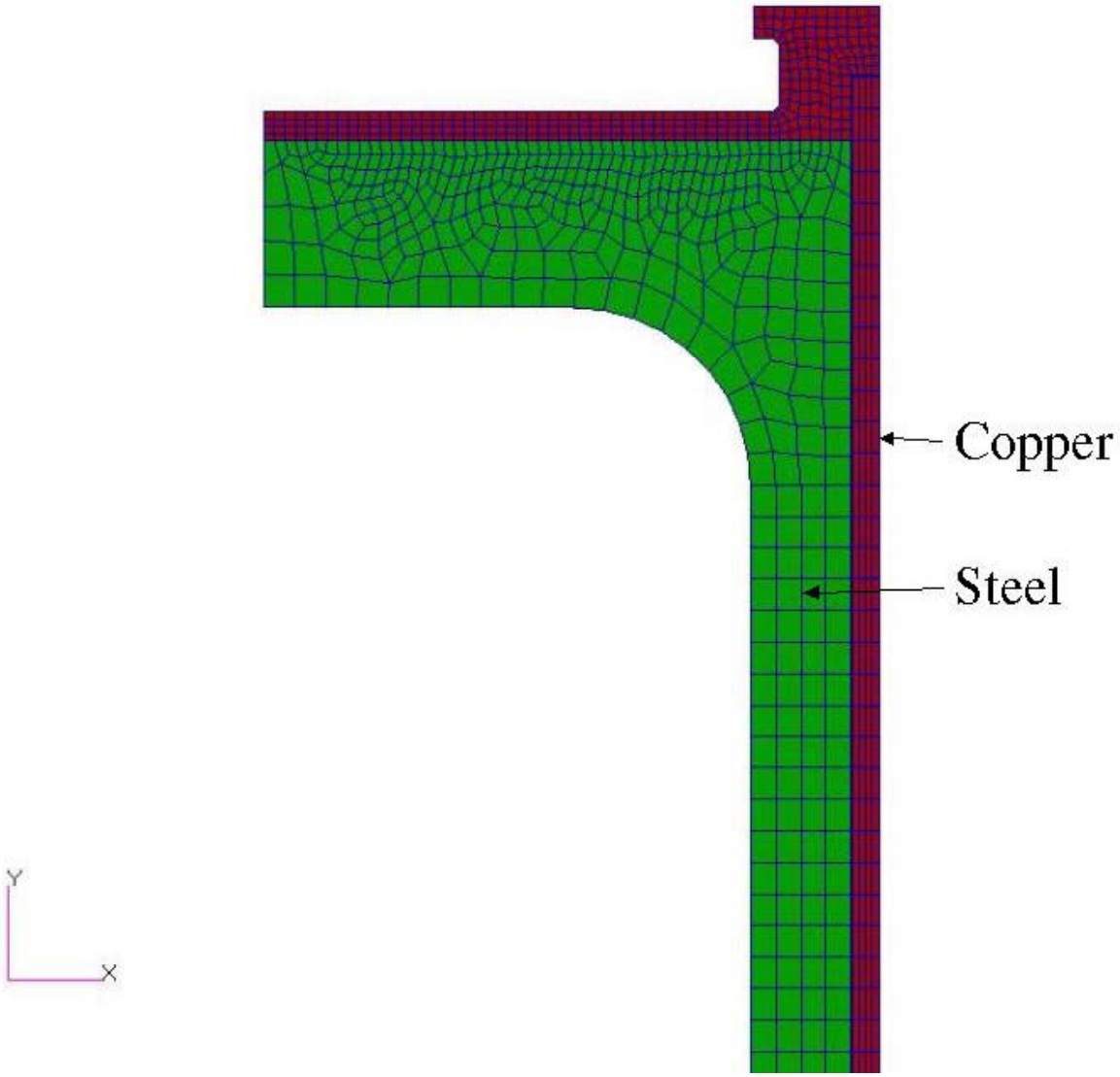

Figure 25 Axisymmetric Model for Pressure Loadcase Analysis.

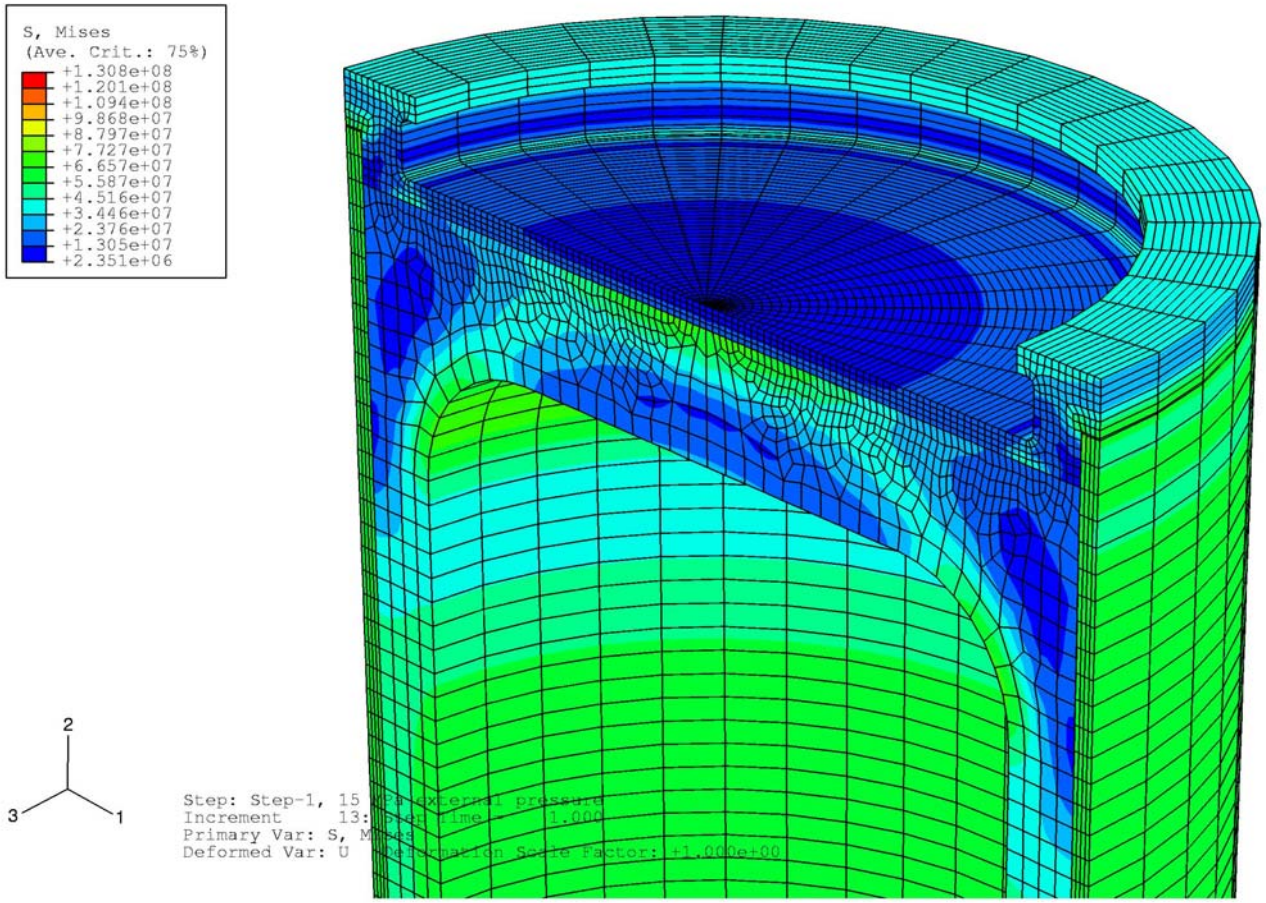

Figure 26a 15 MPa Pressure Loading (Von Mises stress).

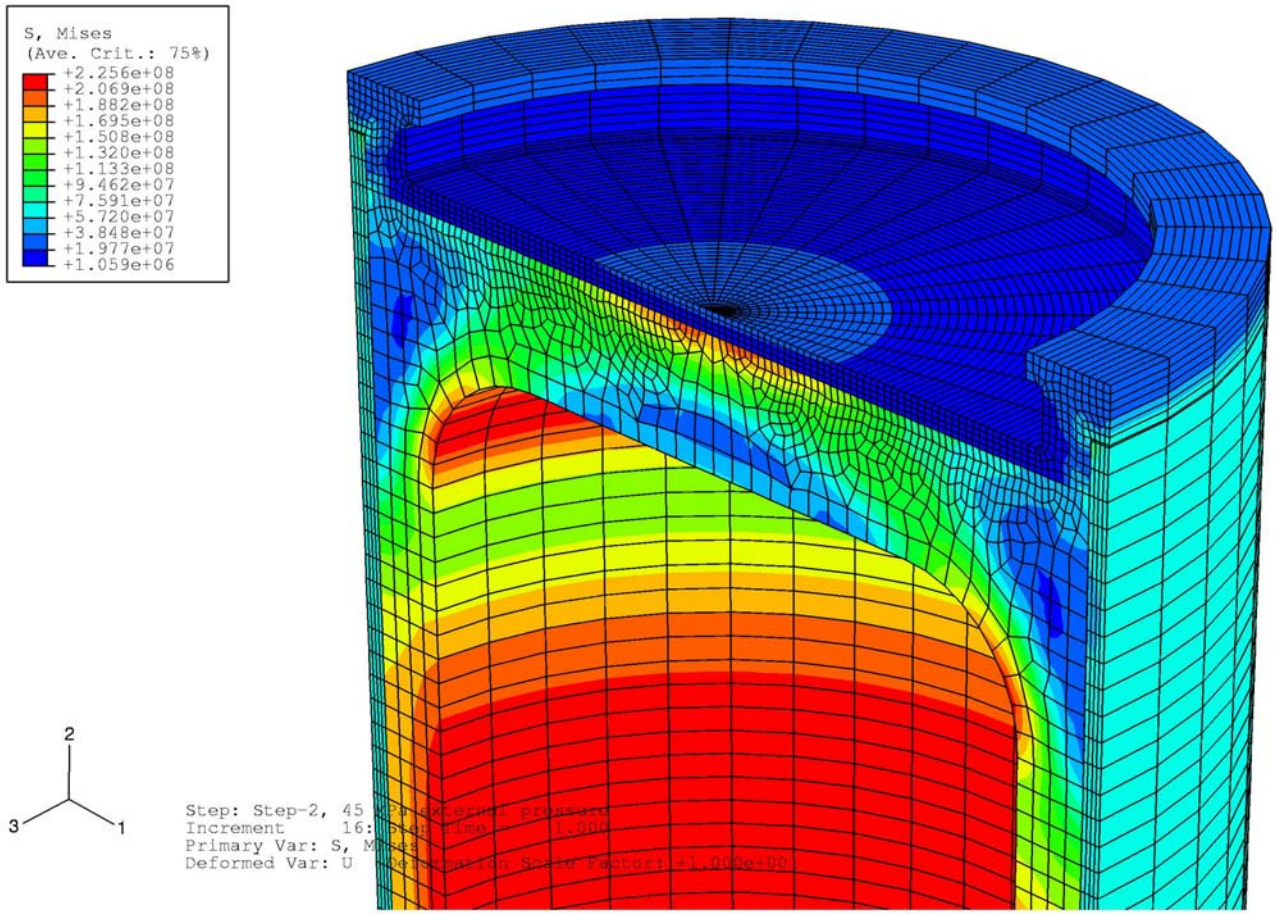

Figure 26b 45 MPa Pressure Loading (Von Mises stress).

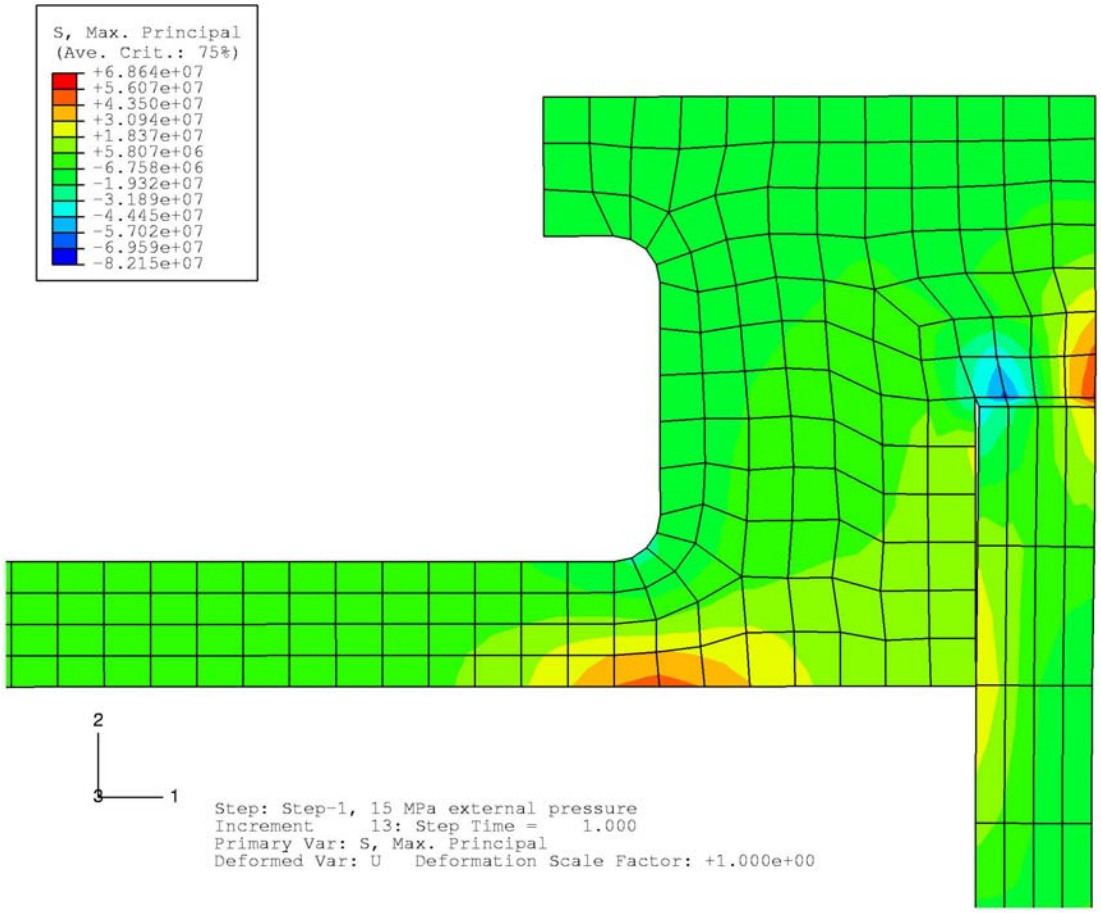

Figure 27a Copper Container Maximum Principal Stress (15 MPa).

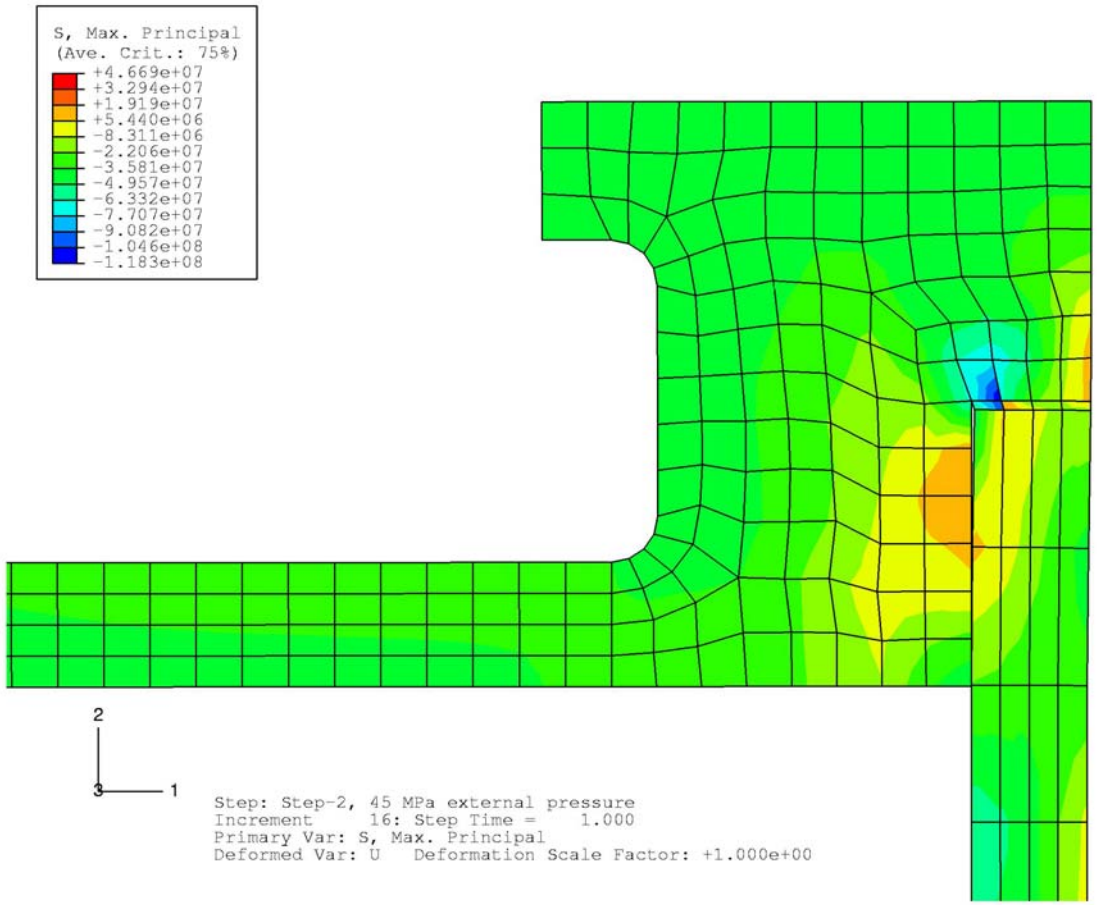

Figure 27b Copper Container Maximum Principal Stress (45 MPa).

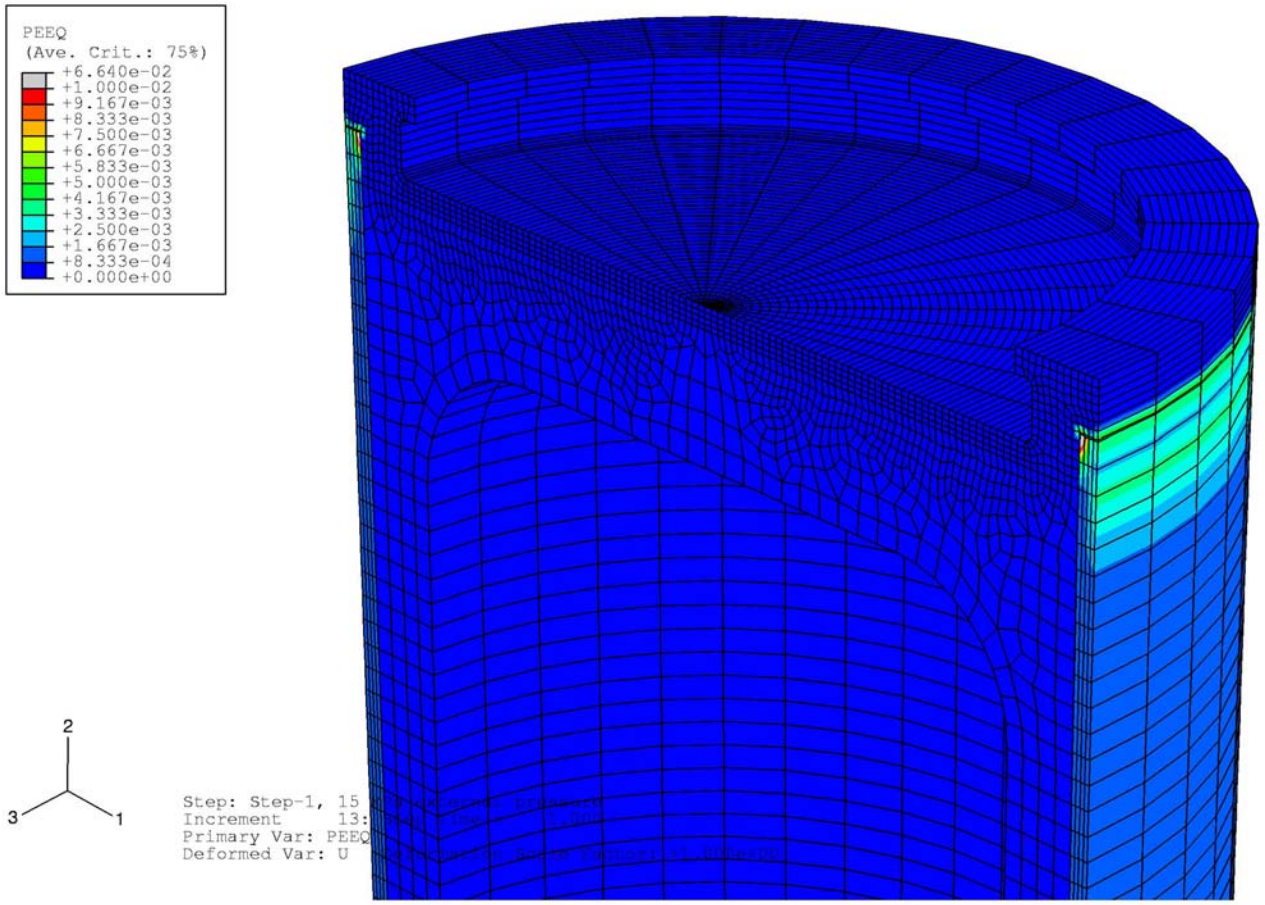

Figure 28a 15 MPa Pressure Loading (strain).

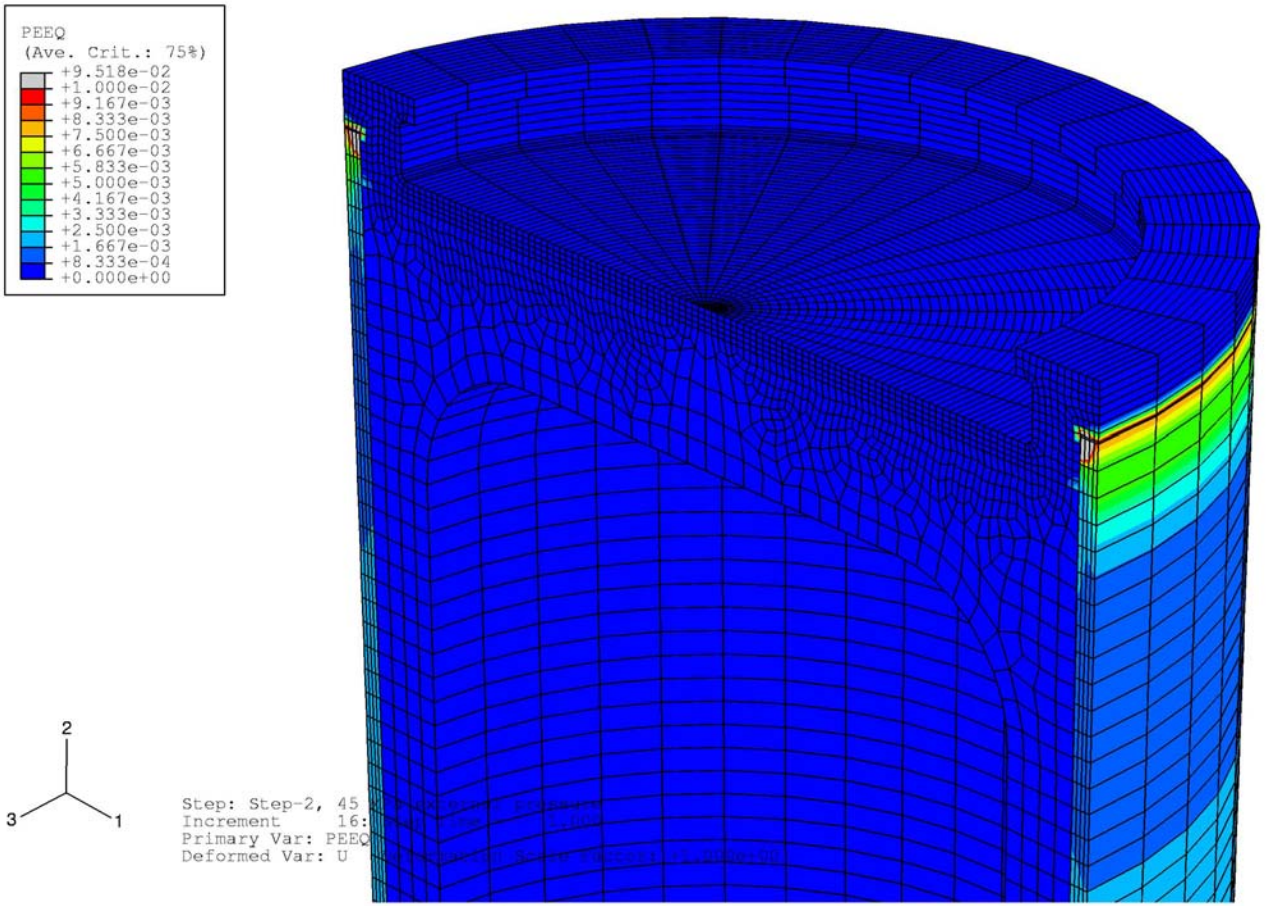

Figure 28b 45 MPa Pressure Loading (strain).

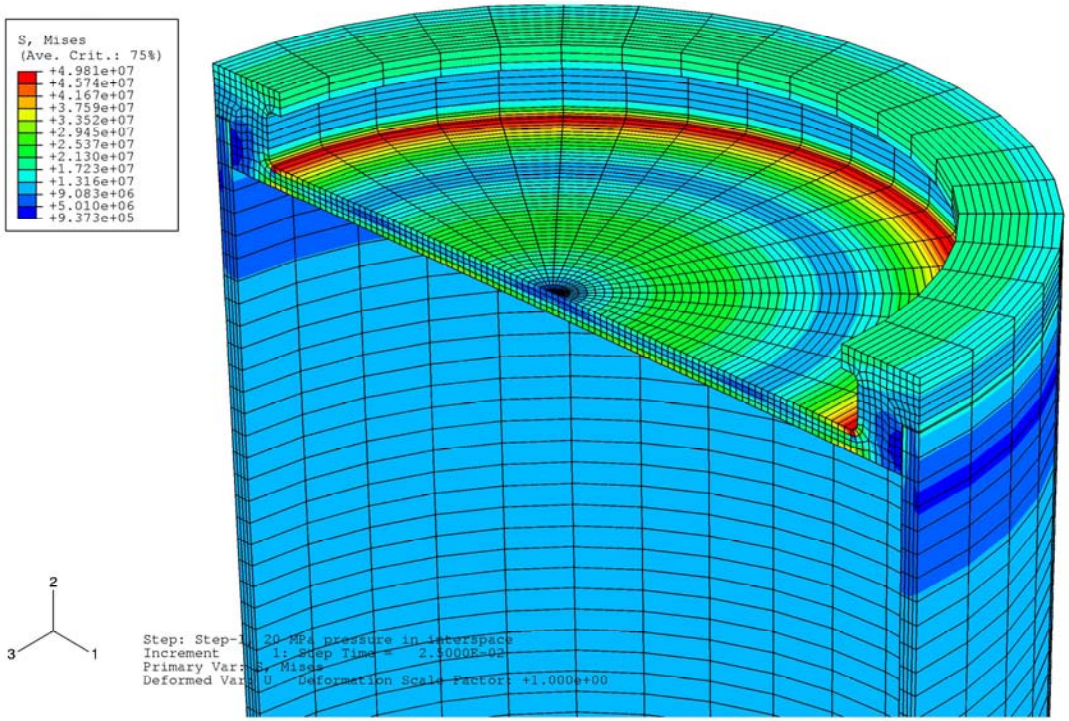

Figure 29. Internal Pressure Case (von Mises stress).

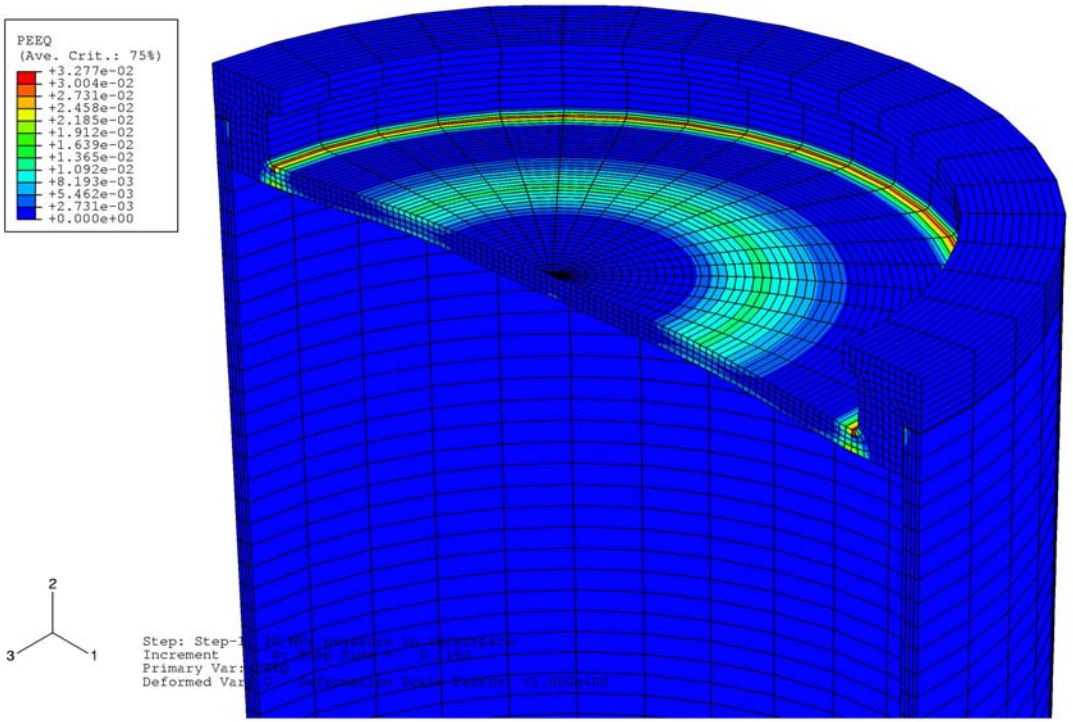

Figure 30. Internal Pressure Case (strain).

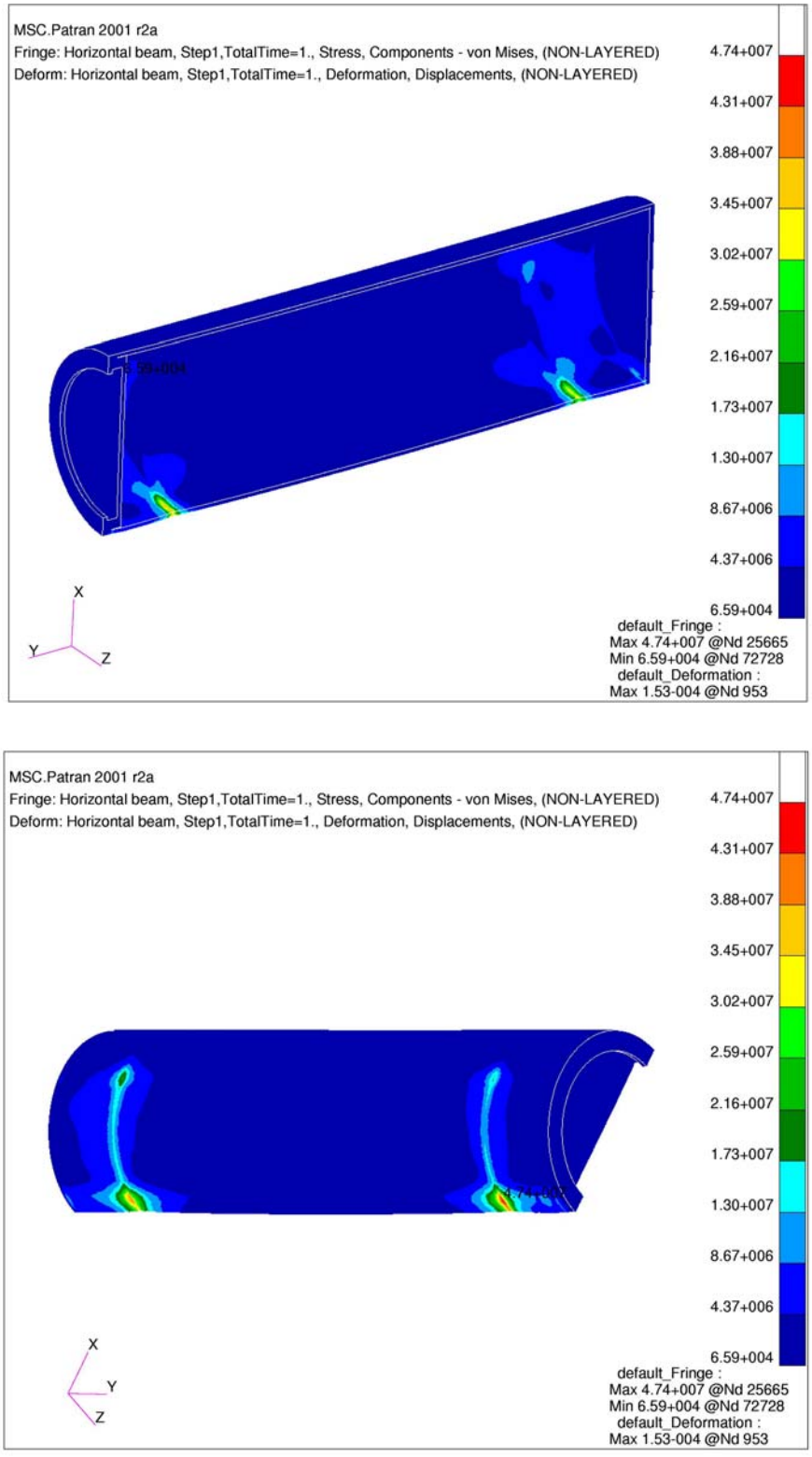

Figure 31. UFC Two-point Lifting Case – von Mises Stress (Copper)

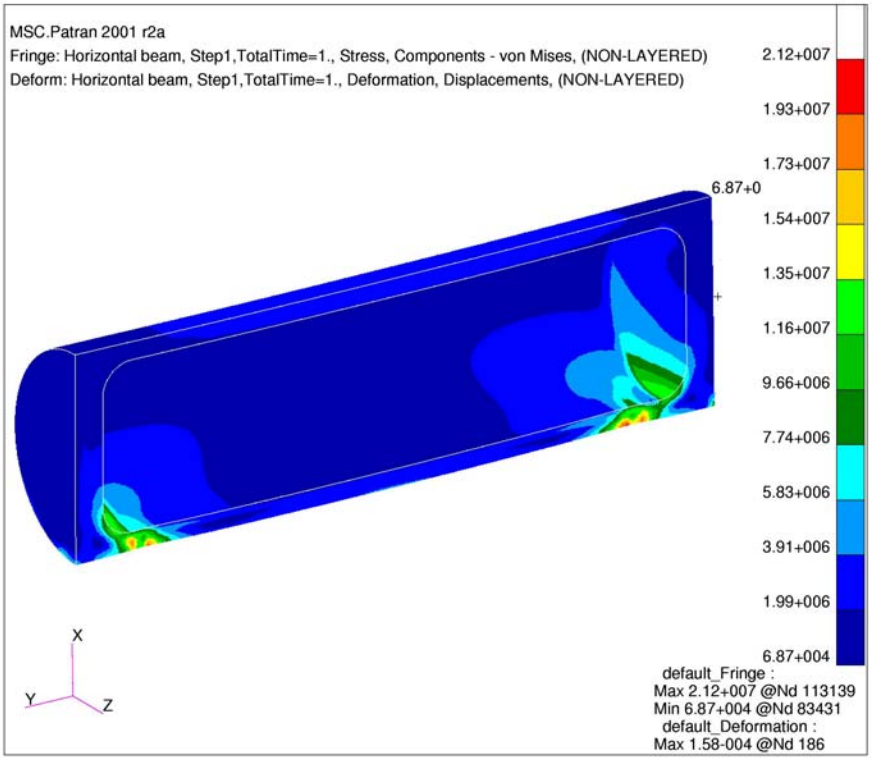

Figure 32. UFC Two-point Lifting Case – von Mises Stress (Steel)

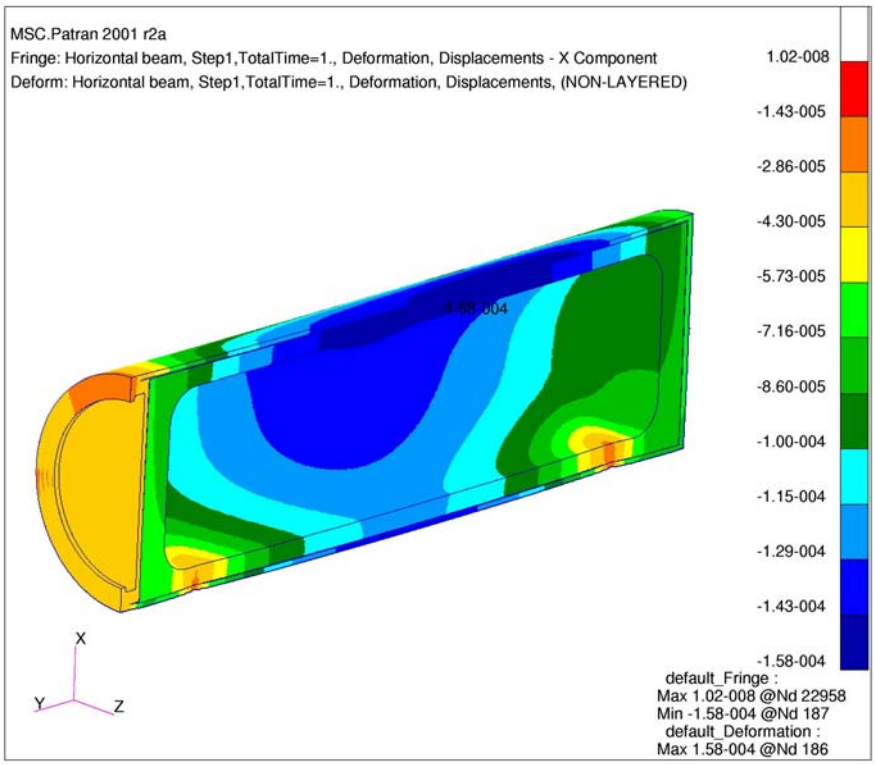

Figure 33. UFC Two-point Lifting Case – Deformation

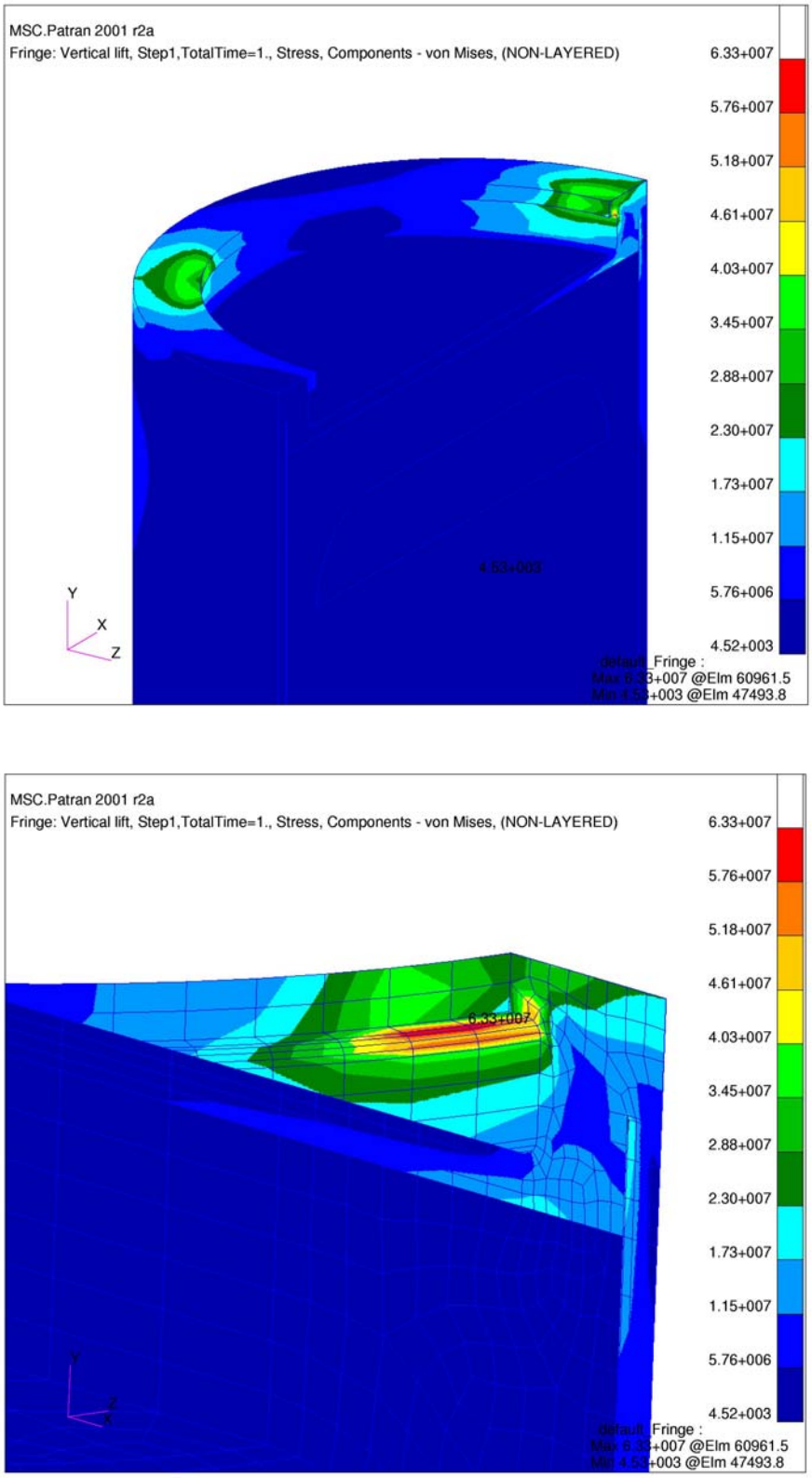

Figure 34. UFC Lifting Case – von Mises Stress

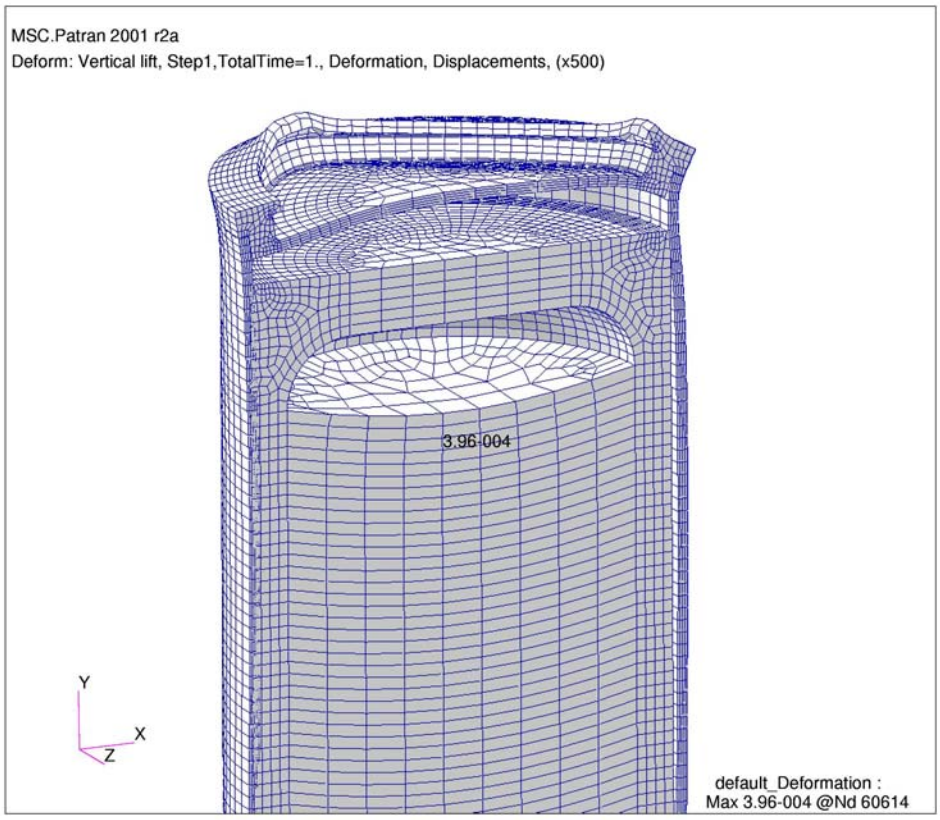

Figure 35. UFC Lifting Case – Deformation

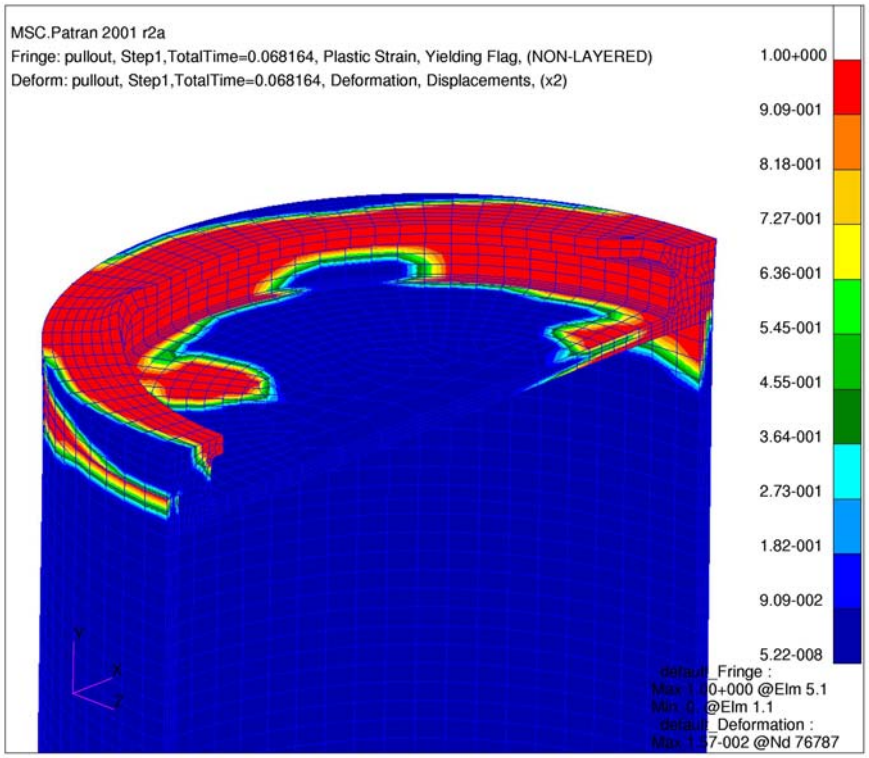

Figure 36. UFC Maximum Load Lifting Case – Yield

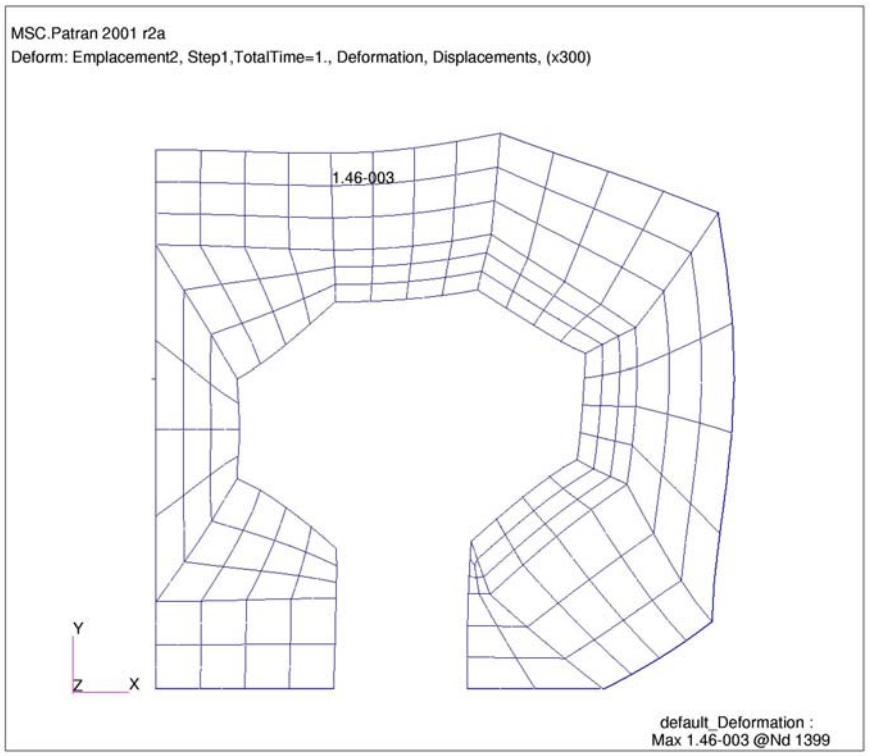

Figure 37. Emplacement Room Deformation – Prior to UFC placement

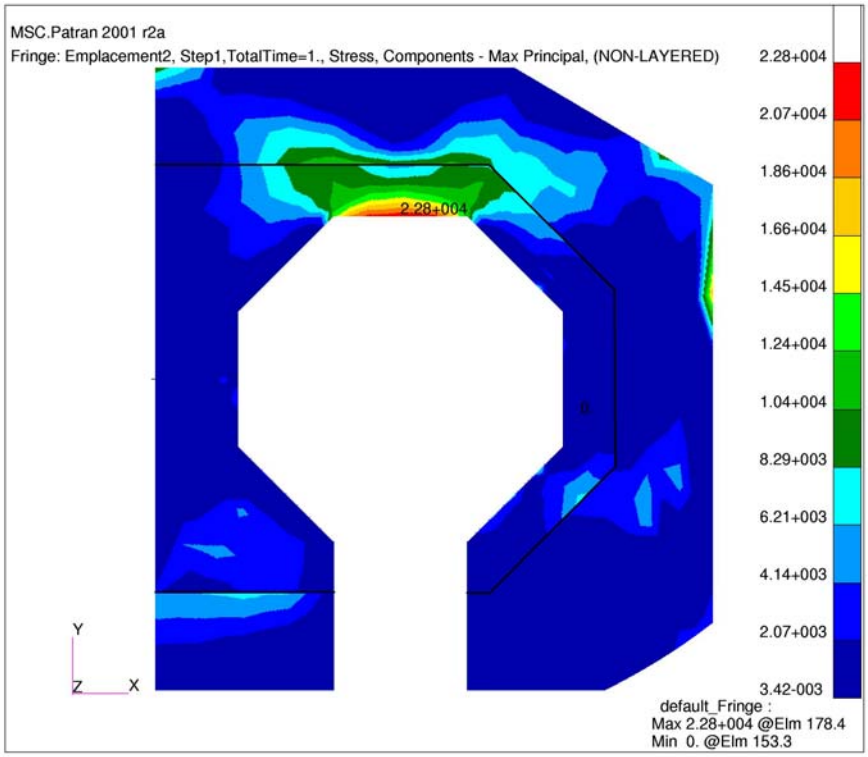

Figure 38. Emplacement Room prior to UFC placement (Maximum principal stress)

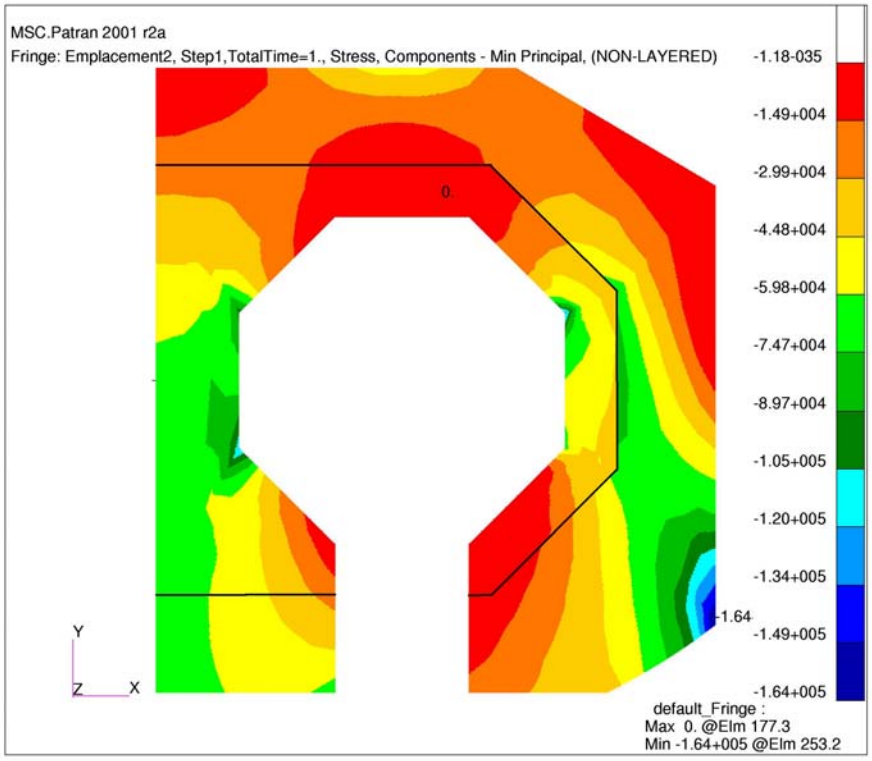

Figure 39. Emplacement Room prior to UFC placement (Minimum principal stress)

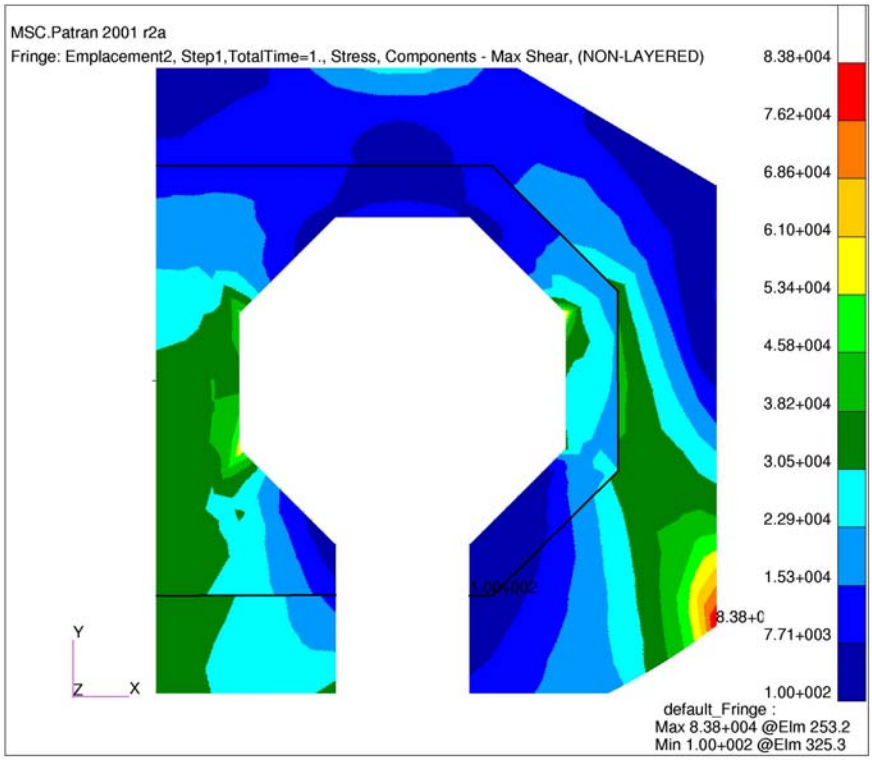

Figure 40. Emplacement Room prior to UFC placement (Maximum shear stress)

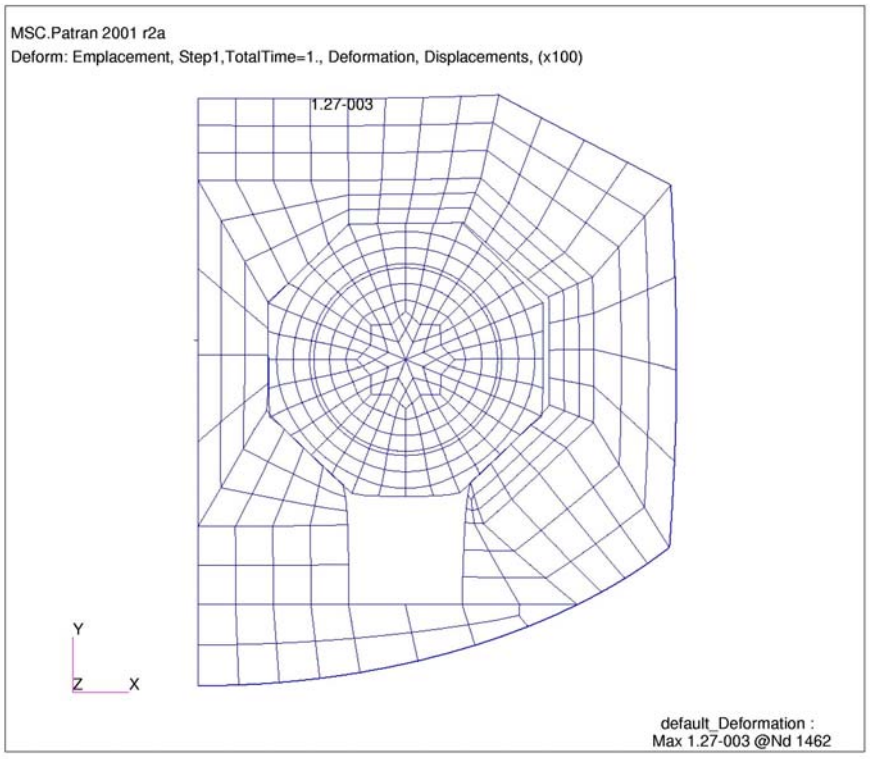

Figure 41. Emplacement Room Deformation after UFC placement

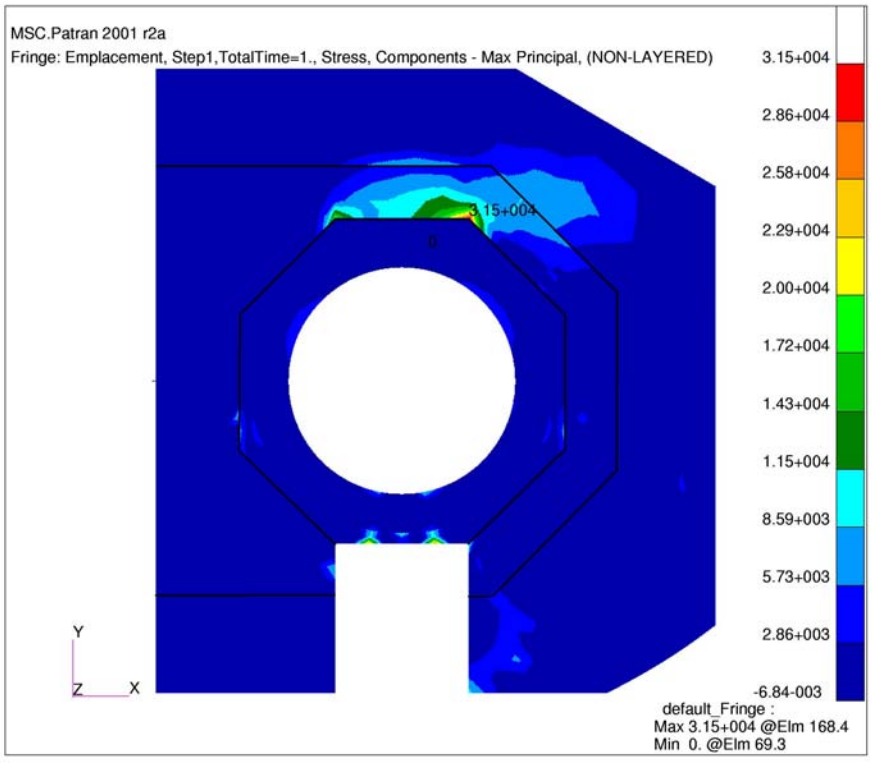

Figure 42. Emplacement Room after UFC placement (Maximum principal stress)

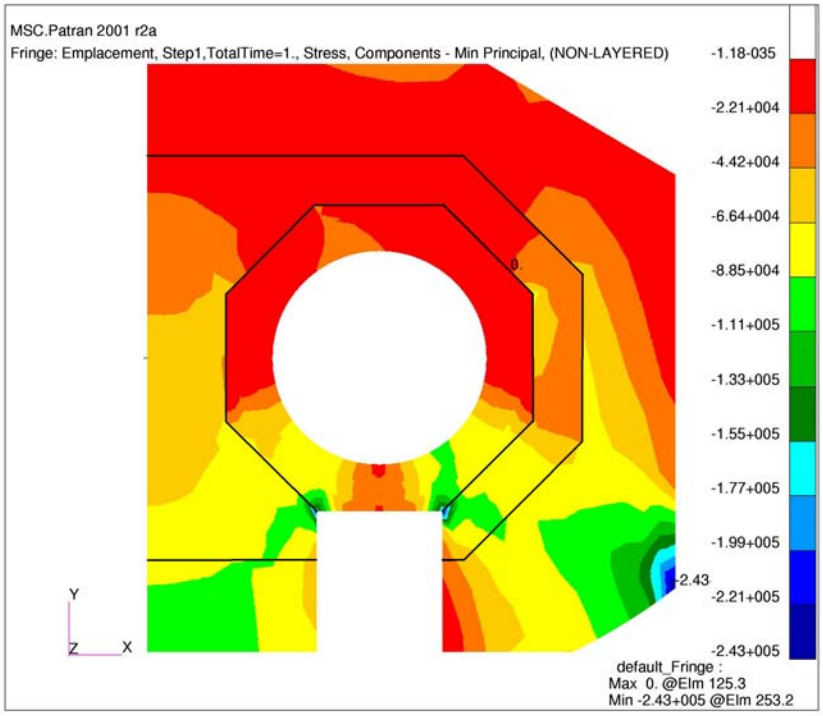

Figure 43. Emplacement Room after UFC placement (Minimum principal stress)

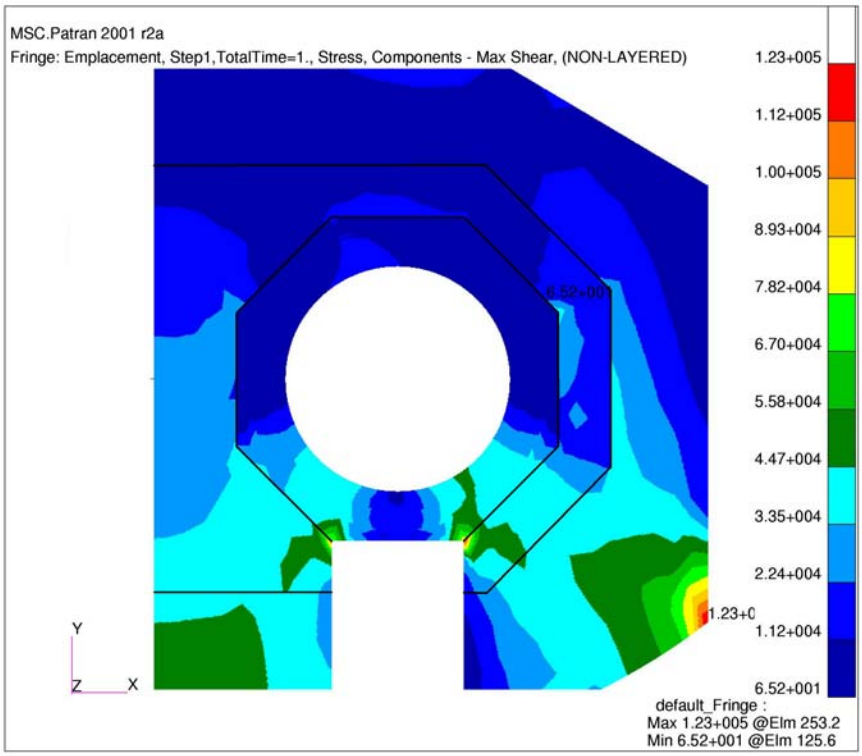

Figure 44. Emplacement Room after UFC placement (Maximum shear stress)